MIRD Pamphlet No. 22 - Radiobiology and Dosimetry of Alpha-Particle Emitters for Targeted Radionuclide Therapy

George Sgouros[1], John C. Roeske[2], Michael R. McDevitt[3], Stig Palm[4], Barry J. Allen[5], Darrell R. Fisher[6], A. Bertrand Brill[7], Hong Song[1], Roger W. Howell[8], Gamal Akabani[9]

[1]Radiology and Radiological Science, Johns Hopkins University, Baltimore MD
[2]Radiation Oncology, Loyola University Medical Center, Maywood IL
[3]Medicine and Radiology, Memorial Sloan-Kettering Cancer Center, New York NY
[4]International Atomic Energy Agency, Vienna, Austria
[5]Centre for Experimental Radiation Oncology, St. George Cancer Centre, Kagarah, Australia
[6]Radioisotopes Program, Pacific Northwest National Laboratory, Richland WA
[7]Department of Radiology, Vanderbilt University, Nashville TN
[8]Division of Radiation Research, Department of Radiology, New Jersey Medical School, University of Medicine and Dentistry of New Jersey, Newark NJ
[9]Food and Drug Administration, Rockville MD

In collaboration with the SNM MIRD Committee:
Wesley E. Bolch, A Bertrand Brill, Darrell R. Fisher, Roger W. Howell, Ruby F. Meredith, George Sgouros (Chairman), Barry W. Wessels, Pat B. Zanzonico

Correspondence and reprint requests to:

George Sgouros, Ph.D.
Department of Radiology and Radiological Science
CRB II 4M61 / 1550 Orleans St
Johns Hopkins University, School of Medicine
Baltimore MD 21231
410 614 0116 (voice); 413 487-3753 (FAX)
gsgouros@jhmi.edu (e-mail)

INDEX

ABSTRACT

The potential of alpha-particle emitters to treat cancer has been recognized since the early 1900s. Advances in the targeted delivery of radionuclides, in radionuclide conjugation chemistry, and in the increased availability of alpha-emitters appropriate for clinical use have recently led to patient trials of alpha-particle-emitter labeled radiopharmaceuticals. Although alpha-emitters have been studied for many decades, their current use in humans for targeted therapy is an important milestone. The objective of this work is to review those aspects of the field that are pertinent to targeted alpha-particle-emitter therapy and to provide guidance and recommendations for human alpha-particle-emitter dosimetry.

A. Introduction

Alpha-particle-emitting radionuclides have been the subject of considerable investigation as cancer therapeutics (1-4), and a number of reviews on this topic have been published (5-9). In the context of targeted therapy, alpha-particle emitters have the advantages of high potency and specificity. These advantages arise from the densely ionizing track and short path length of the emitted positively charged helium nucleus in tissue. The practical implication of these features, as well as, the distinction between alpha-particles and the more widely used beta-particle emitters for targeted radionuclide therapy is that it is possible to sterilize individual tumor cells solely from self-irradiation with alpha-particle emitters. This is generally not possible with beta-particle emitters given achievable antibody specific activity, tumor-cell antigen expression levels and the need to avoid prohibitive toxicity (5). These attributes combine to provide the fundamental strength and rationale for using alpha-particle-emitting radionuclides for cancer therapy. Current approaches to cancer treatment are largely ineffective once the tumor has metastasized and tumor cells are disseminated throughout the body. There is also increasing evidence that not all tumor cells are relevant targets for effective tumor eradication and that sterilization of a putative sub-population of a small number of tumor stem cells may be critical to treatment efficacy (10). The eradication of such disseminated tumor cells, or of a sub-population of tumor stem cells, requires a systemic targeted therapy that is minimally susceptible to chemo- or radio-resistance, that is potent enough to sterilize individual tumor cells and microscopic tumor cell clusters (even at low dose-rate and low oxygen tension) and that exhibits an acceptable toxicity profile (*11*). Alpha-particle emitting radionuclides address this critical need. To accomplish these goals, a reliable, cost-effective source of alpha-particle emitters is needed for research and development, and to support their routine use in clinical practice. Improved chemical labeling and stability will be needed to achieve the desired biodistribution and associated dose distribution necessary for successful therapy with acceptable acute and long-term toxicities. These limitations, have slowed the development and clinical use of alpha-emitter targeted therapy relative to the use of beta- and Auger-electron emitting radionuclides.

The first clinical trial of an alpha-particle emitter in radiolabeled antibody therapy employed ^{213}Bi conjugated to the anti-leukemia antibody, HuM195, and was reported in 1997 (*12,13*), 4 years after ^{213}Bi was first suggested for therapeutic use (*14*). This was followed by a human trial of the anti-tenascin antibody, 81C6, labeled with the alpha-emitter, ^{211}At, in patients with recurrent malignant glioma (*15*). In addition to these two antibody-based trials, a clinical trial of

unconjugated ^{223}Ra against skeletal metastases in patients with breast and prostate cancer was recently completed (*16*). More recently a patient trial of ^{211}At targeting ovarian carcinoma has been initiated (*17*). Future trials of alpha-emitters are anticipated using antibodies labeled with ^{211}At or ^{213}Bi and directed against tumor neovasculature (*18-20*). A conjugation methodology for ^{225}Ac was recently described (*21*), and a Phase I trial of this radionuclide with the anti-leukemia antibody, HuM195, in leukemia patients has recently been initiated (*22*). Table 1 summarizes clinical trials involving alpha-particle-emitting radiopharmaceuticals.

This Report focuses on alpha-emitter dosimetry as it relates to human use in targeted therapy. This introduction is followed by a brief historical review of alpha-emitters (Section B), focusing on early human exposures and highlighting the distinction between the highly toxic and long-lived alpha-emitters first used in humans and the alpha-emitters that have been used clinically or are being projected for clinical use. Section C provides a review of alpha-emitter studies both *in vitro* and *in vivo*. This section highlights the radiobiology of alpha-emitters that is relevant to targeted therapy in humans. Closely related to the radiobiology of alpha-emitters is the concept of Relative Biological Effectiveness (RBE), which is reviewed in Section D. The dosimetry of alpha-emitters has been addressed in a large number of publications. Section E describes the criteria for microdosimetry, the different approaches for performing such calculations, and briefly reviews studies in which such calculations have been performed. Section F provides a survey of alpha-emitters of interest for human use including the properties of individual alpha-emitters and a summary of important pre-clinical and clinical studies. Section G outlines a progression of studies and dosimetry analyses that are recommended for feasibility and toxicity evaluations. Recommendations and conclusions are summarized in Section H.

Therapeutic nuclear medicine is already a highly multidisciplinary field. Therapy with alpha-particle emitters is easily one of the more multidisciplinary endeavor within this enterprise. This review is intended to provide the necessary background including the physics and dosimetry perspective to aid in the design, conduct, and analysis of clinical trials using alpha-emitting radiotherapeutics.

B. Historical Review

Shortly after natural radioactivity was discovered in 1896 by Becquerel, Soddy and Rutherford showed that naturally radioactive substances were mixtures of several isotopes. They separated radium-224 from thorium in 1902. In 1903, Alexander Graham Bell suggested using radium for tumor therapy (*23*). The abundant alpha emissions from ^{224}Ra and its daughters suggested possible medical applications in dermatology for skin lesions and for treatment of rheumatic diseases (*24*). Radium-224 was first used in 1912 for treatment of ankylosing spondylitis (with limited success), and later for tuberculosis (which was not effective).

Bottled radium solutions as the stimulant "Radithor" were prescribed to cure almost any ailment (*25*). Radium appeared to ease the pain associated with inflammation, stiffening, and crookedness of the vertebral column in ankylosing spondylitis patients, and to ease the movement of joints in patients with rheumatoid synovitis.

Death resulted from acute radiation syndrome in early patients administered large oral doses of radium-226 solution, and internal applications were discontinued for a period of time. The intravenous injection of ^{224}Ra against rheumatic disease began again in France in 1922, in England in 1946, and in Germany in 1947. The use of ^{224}Ra in treatment of ankylosing

spondylitis resumed in 1964 in France. Favorable results encouraged further use of radium-224 against rheumatoid arthritis (*26*). Radium-224 is still used for treating adult spondylitic patients in Germany, but current doses are considerably smaller than those given earlier (*27*).

The major late-effects of ^{224}Ra have been bone cancers induced by the bone-surface-seeking radium and radioactive daughter products. A long-term follow-up of radium-226 watch dial painters also showed malignant bone tumors and carcinomas of the mastoids and paranasal sinuses (*28*).

Thorium colloid ("Thorotrast") containing thorium-232 and decay-series daughter products was given as a contrast medium for radiographic examinations (such as cerebral angiography), primarily in Germany, starting as early as about 1920 and continuing into the 1950s. Liver tumors and leukemia have been the most significant late side-effects of thorotrast (*29*).

As noted above, radium-224 was used for a number of ailments in the early 1900s. This early experience, however, did not translate into early use of alpha-emitting radionuclides for targeted radionuclide therapy. Instead, in 1982, 36 years after its initial use in the treatment of thyroid cancer (*30*), iodine-131, a beta-particle/gamma-ray emitter was first used in radioimmunotherapy (*31*). In contrast, the first targeted therapy using an alpha-particle emitter in humans was reported in 1997 (*13*), 94 years after Alexander Graham Bell suggested placing sources of radium “in or near tumors” (*23*). The alpha-particle emitter used in the clinical trial reported in 1997 was ^{213}Bi, a radionuclide that was not identified in the literature as a candidate for therapy until 1993 (*14*). The contrast between the evolution of beta-particle emitter targeted therapy and alpha-particle emitter therapy is instructive in highlighting the differences in human experience between alpha-particle emitting radionuclides and other radionuclides used in targeted therapy. In the case of beta-particle emitters, prior human experience was helpful and generally positive, coming at a time when the potential hazards of radionuclides were better understood. In contrast, early experience with alpha-particle emitters occurred when the hazards were not appreciated, resulting in their casual use and subsequent negative consequences (*25*).

C. Alpha-Particle Radiobiology

Introduction

Interest in alpha-particle emitting radionuclides for cancer therapy is driven by the physical and radiobiological properties of alpha-particles as compared to those of photons and electrons (Fig. 1). The energy deposited along the path of an alpha-particle per unit path length is shown in Figure 2. As shown on the figure, the energy deposition along the path or linear energy transfer (LET) of an alpha-particle can be two to three orders of magnitude greater than the LET of beta-particles emitted by radionuclides such as ^{131}I, and ^{90}Y

One of the first studies demonstrating the biological effects of heavy charged particles was by Raymond Zirkle in 1932 (*32*). He examined the effect of polonium alpha-particles on cell division in fern spores and showed a much greater biological effect when the spore nucleus was placed in the Bragg peak of the alpha-particle track compared to the plateau region of the track (*33*). Much of the subsequent radiobiology of alpha-particles was established in a series of seminal studies performed by Barendsen and co-workers in the 1960’s (*34-42*). These studies first demonstrated the now familiar and accepted features of alpha-particle irradiation that are outlined in the individual sections, below. A subsequent series of studies on the mutation and inactivation of three different mammalian cell types exposed to helium, boron or nitrogen ions

spanning LET values in the range 20 to 470 keV/μm^{-1} was key in evaluating the various biophysical models that had been posited to explain low vs high LET effects (*43-46*). The work was also instrumental in providing both the experimental results and biophysical analysis to help understand the RBE vs LET relationship established by Barendsen. The biophysical analysis in the last paper of the series (*43*) provided compelling theoretical support for the concept of two types of radiation induced cellular inactivation.: 1) that due to the accumulation of multiple events that can be repaired at low doses (*i.e.*, sub-lethal damage) but that saturate the cellular repair mechanisms at higher doses. This type of inactivation yields the characteristic linear-quadratic dose-response curve for low LET radiation, corresponding to a small number, approximately 3-9, (*i.e.*, ~100 to 300 eV) ionizations in a distance of about 3 nm associated with a low probability of producing lethal lesions. The second type of inactivation arises due to a single lethal event for high LET radiation. In this case, a larger number of ionizations, >10, over the 3 nm distance depositing > 300 eV produce lethal lesions with a high probability. It is important, however, to remember that these studies were performed using external beams of alpha-particles in which the incident alpha-particles were generally orthogonal to an alpha-permeable surface upon which the cells were cultured as a monolayer of adherent cells.

As initially demonstrated, experimentally, by Fisher et al. (*47*), and then theoretically by Humm, et al. (*48*), and most recently by Kvinnsland et al. (*49*) the spatial distribution of alpha-particle emitters has an important impact on the absorbed dose distribution and, correspondingly, on the slope of the cell-survival curve. Neti and Howell recently provided experimental evidence of a log-normal cellular uptake of ^{210}Po citrate among a cell population uniformly exposed to the radiochemical and showed that this distribution can substantially alter the cell survival curve (*50*). Although many of the results obtained from the external beam studies, (summarized in Table 2) are generally applicable regardless of the alpha-particle distribution, specific parameters such as the average number of alpha-particle traversals to induce a lethal event or the D_0 value (*i.e.*, the absorbed dose required to reduce cell survival to 0.37) are highly sensitive to experimental factors such as the geometry of the cells, the thickness/diameter of the cell nucleus, the distribution of DNA within the nucleus (*i.e.*, the phase of the cell cycle) and the number and spatial distribution of the alpha-particle sources relative to the target nuclei.

The distinction between DNA DSBs caused by a single high-LET track versus DNA damage caused by multiple low-LET tracks is illustrated in Figure 3. This basic observation underpins almost all of the radiobiology of alpha-particles.

Traversals required for cell kill

The average number of α-particle nuclear traversals required to kill a cell, as measured by the loss of the subsequent ability to form a colony ranges from as low as 1 (*51*) to as high as 20 (*52*). If bystander effects are included, the lower end of the range would include 0. As noted above, the variability in this value when bystander effects are not considered arises because of the high sensitivity of this determination to the geometry of the cell and the nucleus during irradiation and also the LET of the incident alpha-particles and the LET distribution within the nucleus.

Quoting from a publication of Raju, et al. (*53*), "*The notion that a cell will be inactivated by the passage of a single α particle through a cell nucleus prevailed until Lloyd and her associates (52) demonstrated that 10 to 20 5.6 MeV α particles were required to induce one lethal lesion in flattened C3H 10T1/2 cells. Studies by Bird, et al (54) showed that approximately four ^{3}He ions*

were required to pass through the cell nucleus to induce one lethal lesion in V79 cells at the G_1/S-phase border, cells in late S phase required five to eight ^{3}He ions. Todd, et al. (55) investigated the effect of 3.5 MeV α particles on synchronized T-1 cells, and observed that approximately one α particle out of four to five traversing a cell nucleus is effective in inducing one lethal lesion. Roberts and Goodhead (56) estimated that one out of six 3.2 MeV α-particle traversals through a C3H 10T1/2 cell nucleus is lethal. Barendsen (57) concluded that the probability of inactivation per unit track length of high-LET α particles is approximately 0.08 μm^{-1} for both T-1 and C3H 10T1/2 cells consistent with the results of Roberts and Goodhead for C3H10T1/2 cells (56)." In a study comparing high LET effects of Auger vs alpha-particle emitters, Howell and co-workers found that about 9 decays of ^{210}Po were required to reduce cell survival to 37% (D_0) when it was distributed between the cytoplasm and nucleus of V79 cells; the energy deposited in the cell nucleus corresponds to about two complete (maximum chord length) traversals of the cell nucleus (*58*). In a murine lymphoma cell line, approximately 25 cell-bound alpha-particle emitting ^{212}B immunoconjugates were required to reduce clonogenic survival by 90% (*59*). The theoretical efficiency of DSB production when an alpha-particle passes through DNA was examined by Charlton et al. (*60*) and was found to be surprisingly low; approximately 1/8 of 10 MeV alphas passing through a 54-nucleotide section of DNA produce a DSB. One passage in four of 1.2-MeV alphas produces a DSB.

Barendsen's estimate of the inactivation probability per unit track length and Goodhead et al.'s determination of the number of lethal lesions per micrometer track through the nucleus (*43*) suggests another approach for estimating inactivation probability. Along these lines, Charlton and Turner introduced the total alpha-particle path length (or chord length) through the nucleus as a useful parameter (*61*). This was used to derive, λ, the mean free path between lethal events for alpha particles traveling through nuclei. Drawing from an extensive compilation of experimental data, this parameter was found to range from 1.5 to 64.4 μm. As expected, λ, was found to be dependent on the LET (Fig. 4). The use of an inactivation probability per unit track length through the nucleus has also been used in a model describing radiation-induced cellular inactivation and transformation. By incorporating aspects of a state vector model for carcinogenesis (*62*) into the inactivation/transformation model, Crawford-Brown and Hoffman (*63*) have described a model that successfully predicts both cell survival and transformation after irradiation by alphas of different LET at absorbed doses below 1 Gy. This model was used to examine the impact on model predictions of including a correlation between initiation of cellular transformation and cellular inactivation. At absorbed doses greater than 1 Gy a significant difference was observed in the predicted probability that a cell is transformed and survives.

Cell survival curve

Cell survival curves (*i.e.*, surviving fraction, SF, versus absorbed dose, D) for low LET radiation such as X-rays exhibit an initial "shoulder" which is thought to reflect the repair of radiation damage. This type of cell-survival curve can be represented by the linear-quadratic equation:

$$SF = e^{-\alpha D - \beta D^2}, \qquad \text{C.1}$$

with the parameters, α and β, respectively, are equal to the sensitivity per unit dose, D, and per unit dose squared, D^2. As the absorbed dose exceeds a certain threshold level, presumably the dose at which the radiation damage repair rate is reduced relative to the rate of induced damage,

the relationship between surviving fraction and absorbed dose approaches log-linearity. As shown on Fig. 5, the cell survival curve for alpha-particle radiation is log-linear at low as well as high absorbed doses, *i.e.*, it does not exhibit a shoulder region, reflecting the reduced capability of cells to repair alpha-particle damage. The equation describing this is:

$$SF = e^{-D/D_0}, \qquad \text{C.2}$$

with the parameter, D_0, equal to the absorbed dose required to yield a surviving fraction of 37%. It is important to note that the log-linear aspect of cell survival curves following alpha-particle irradiation reflects a reduced repair capacity, not the absence of repair. That alpha-particle damage is repaired has been demonstrated by a number of studies (see next section). It is important to note that repair of damage is not inconsistent with single-event lethality and a log-linear survival curve. The key distinction is whether death is a result of accumulated damage or of a single event. Cell survival curves that exhibit an initial shoulder reflect cell death that results from the accumulation of damage, whereas log-linear cell survival curves reflect cell death arising from a single event, without the need to accumulate damage. In both situations, repair is possible.

Double strand break (DSB) yield and repair

Depending upon the measurement technique used, the reported alpha-particle RBE for initial yield of DNA double-strand breaks (DSBs) relative to ^{60}Co γ-rays has ranged from 0.7 to 4.4. The higher values are obtained using the cell sucrose sedimentation technique whereas elution techniques have tended to give a value closer to 1. (*64*). The presence of DMSO (0.5 mol/dm^{-3}) reduces the initial yield by 50% and 32% for photons and ^{238}Pu α-particles, respectively (*65*). Pulsed-field gel electropheresis analysis of the size distribution of DNA fragments has revealed that the size distribution of fragments obtained following high LET ion (40 kev/μm He ions and >80 kev/μm N ions) irradiation is shifted towards smaller fragments than would be expected from randomly distributed breaks. In contrast, the distribution from ^{60}Co γ radiation is consistent with a random breakage model (*66,67*). This observation suggests that if the measurement technique used to assess DNA DSBs cannot resolve fragments in the 10- to 150-kbp (kilo-base pair) range, then the extent of DSBs will be underestimated for α radiation. This apparent clustering of DSBs has been found to impact the rate and extent of DSB repair. While the repair rate of repairable damage was found to be independent of LET, the fraction not repaired and the fraction repaired very slowly (>22h) both increased with increasing LET. Interestingly, the majority of DSBs were rapidly rejoined (T1/2 ~ 15 min) even after high LET irradiation (*68*). To investigate misrejoining probability in DSB repair, the integrity of a 3.2-MBp restriction fragment has been used to measure the joining of wrong DNA ends following high-and low-LET radiation. The misrejoining frequency for filtered (0.5 mm copper) 320 kVp X-rays delivered at a dose rate of 2-3 Gy/min was non-linearly related to dose, with less probability of misrejoining at low doses than at high doses. In contrast, the dose-dependence of misrejoining frequency was closer to being linear for 7 MeV helium ions (LET = 97 keV/μm), delivered at a dose-rate of 50-100 Gy/min. Misrejoining frequencies for the high-LET particles were generally greater than for X-rays, particularly at lower doses. (*69*).

The experiments outlined above, along with Monte Carlo simulations of track structure and ionization events suggest that there are different types of DSB, differing in their "complexity" or clustering at the level of individual small damaged segments of DNA (*60,70-72*). At high total absorbed doses, both high and low-LET radiation yield a similar number of DSB but a proportion of the DSBs arising from high-LET radiation are highly complex and repair of these either is not possible or occurs very slowly. This is supported by measurements of the repair kinetics for high- versus low-LET DSBs. A hierarchy of DSBs has, therefore, been envisioned in which "simple" DSBs are generated by both high- and low-LET radiations and these are more rapidly repaired. The more complex DSBs are rare for low-LET radiations but frequent for high-LET radiations; these are more slowly repaired. Finally, there are highly complex DSB, arising from more "severe" ionization clusters, a small number of which are only generated by high LET radiation; these are either not repaired at all or are repaired incorrectly and therefore give rise to the biological effects observed from high-LET radiation. This model has been proposed to explain the discrepancy in RBE for DSB versus RBE for biological effects (*73*). In contrast to the popular impression of double and single strand breaks as being two categories of damage, this model suggests that within the DSB category there are different types of DSB damage that are distinguishable by their repair properties. An alternative model that retains the DSB as a single category of damage has also been proposed. In this model, the highly complex DSB is a result of two DSBs in close proximity to each other. Reproductive cell death arises because the resulting repair effort can lead to loss of part of the DNA or to the exchange of DNA between chromosomes (*74*).

It is important to note that because of the low sensitivity of detecting DNA DSBs, all of the experimental studies described above were performed at average absorbed doses ranging from 20 to 400 Gy with most of the results obtained at doses exceeding 50 Gy. These doses are substantially greater than would be expected from targeted radionuclide therapy and, although the initial induction of DSBs was found to be linear with absorbed dose from alpha-particles, it is not clear that the results of these studies apply to the lower absorbed doses and dose rates typical of targeted radionuclide therapy.

Oxygen effect

In addition to dose-rate, the influence of oxygen concentration has long been recognized as an important factor in the response of cells to radiation (*75,76*). Figure 6 demonstrates that this effect is strongly influenced by the LET of the radiation. The Oxygen Enhancement Ratio (OER) or relative radiosensitivity of cells to oxygen concentration is 1 for charged particles with an LET greater than 140 keV/μm (*34*). The initial LET of 4- to 8- MeV alpha-particles typical of the alpha-emitters of interest in targeted alpha-emitter therapy range from 110 to 61 keV/μm. The OER values in this LET range are 1.3 to 2.1. Since the LET of the emitted alpha-particles increases well beyond the 140 keV/μm threshold for OER=1 as the Bragg peak is approached, the ability of alpha-particles to overcome radioresistance due to hypoxia will depend upon the spatial distribution of the alpha emitters relative to the hypoxic region. It is important to note that the potential advantage noted above, is strictly radiobiological. There are studies suggesting that hypoxia may alter the phenotype of the cell via cell signaling pathways associated with increased concentrations of HIF1-alpha, the hypoxia inducible factor, leading to a cell phenotype that is inherently more resistant to radiation and other cytototoxic agents, including chemotherapeutics (*77*). The classical OER effect has been explained as a free radical-mediated effect in which the presence of oxygen "fixes" free radicals which are then able to induced DNA

damage, thereby making repair of the damage more difficult (*78*). In this case, the reduced OER effect with alpha-particle radiation may be explained by the preponderance of oxygen-independent direct DNA damage (versus oxygen-dependent indirect, that is, free radical-mediated DNA damage) characteristic of alpha particles.

Dose-rate

The influence of absorbed dose rate on cell survival for low-LET emissions is well established. As the dose rate is lowered and the exposure time extended, the biological effect of a given dose is generally reduced (*79*). The primary explanation for this effect is that lower dose rates provide a greater time interval for DNA damage repair. Since high-LET damage is not easily repaired, dose rate or even dose fractionation should not impact cellular survival. Barendsen and co-workers examined changes in survival following alpha-particle irradiation over a dose-rate range of 0.5 to 100 rad/min, and no dose-rate effect was observed (*36*).

Dose rates associated with traversal of an alpha-particle through a cell nucleus have been studied. Stevens et al. (*80*) estimated that an alpha particle deposits a dose of the order of 0.2 Gy to a cell nucleus over a time period of approximately one picosecond (ps), the time required for an alpha particle to traverse a nucleus. This gives a dose rate of approximately 10^8 Gy/s, raising the possibility that high-LET effects may be due to the temporal distribution (*i.e.*, increased dose rate) rather than the spatial distribution of ionization events. The question was examined using the High Brightness Picosecond X-Ray Source, developed at the Rutherford Appleton Laboratory (*81*), which delivers an X-ray absorbed dose equivalent to that of one alpha-particle per cell in approximately 10 ps. This low-LET, ultrahigh dose-rate source was used to measure the OER for cell inactivation by ps X-ray pulses. An OER of about 2.5 was found, consistent with that observed for conventional X-ray and gamma-ray sources and confirming that the enhanced biological effects associated with alpha-particle radiation are indeed due to the high spatial density of ionization events.

Oncogenesis

Although not of prime concern in cancer therapy, a much higher incidence of cancer induction is associated with alpha-particle irradiation (*82*). Accordingly the weighting factor for alpha particles is 20, meaning, that a committee review of the relevant experimental and human data has determined that per unit absorbed dose, alpha-particles are associated with a 20-fold greater risk of cancer induction as compared to a similar absorbed dose of photons or beta particles (*83*). A review of human and animal data related to cancer risk estimates has called the value of 20 into question for bone cancer and leukemia risk, particularly at low absorbed doses (*84*). Consideration of dose to target cells on bone surfaces as opposed to the average bone dose gives an RBE for bone cancer risk of 3 to 12. The authors note that these estimates may also change since there is evidence that bone cancer risk may be best assessed by calculating dose to a 50-µm layer of marrow adjacent to the endosteal bone surface as opposed to a single 10-µm layer as currently assumed. Likewise, a factor of 2 to 3 is more consistent with the experimental data for leukemia induction. It is important to note that all of these estimates are based on alpha-particle emitters not projected for use in targeted alpha-emitter therapy. The few studies that have been performed to examine carcinogenesis of the short-lived alpha-emitters that are of interest in targeted alpha-emitter therapy have all been performed using ^{211}At. Neoplastic changes, predominately papillary carcinomas in various organs were seen in a few animals but not more

than what was expected for untreated mice. Brown and Mitchell (*85*) reported a 13% incidence of plasmocytoma in tumour-bearing mice of the same strain 13-21 months after the treatment with 200-750 kBq of 6-[^{211}At]-astato-MNDP. The frequency of low-grade B-cell non-Hodgkim lymphoma was high but similar to that of the control population. A high incidence of pituitary adenomas and mammary tumours has been seen in rats treated with ^{211}At (*86,87*). These tumors, however, were partially attributed to secondary, hormonal effects associated with a hormonal imbalance resulting from thyroid or ovarian tissue compromise.

Bystander effect

The bystander effect may be loosely defined as a biological alteration (*e.g.*, apoptosis, chromosomal damage or genetic mutation) in a population of cells not exposed to or traversed by ionizing particles that arises when: 1. these cells are in proximity to cells that have been irradiated or 2. are exposed to the cell culture medium of irradiated cells. A broader definition has also been suggested that includes abscopal effects – "the detection of responses in unirradiated cells that can reasonably be assumed to have occurred as a result of exposure of other cells to radiation" (*88*). These effects occur in organs or parts of organs which are remote from the original radiation field. Examples include effects on a contralateral lung when only one lung is irradiated or effects on the whole lung when only a portion of the lung is irradiated (*89,90*). Although the bystander effect is widely considered to be a new observation, reports that the inactivation of biological entities may be brought about equally by ionizations produced within the entity or by the ionization of the surrounding medium have existed since the 1920s (*91*) and observations of clastogenic factors in plasma from radiotherapy patients were first reported in the 1950s (*88,92*). The current high level of interest in bystander effects was sparked by a report by Nagasawa and Little in 1992 (*93*). They found that, using a very low fluence alpha particle microbeam, more cells had sister chromatic exchanges than was predicted by cell traversal probability calculations. Since then, most studies have demonstrated, that high-LET but not low-LET radiation-induced bystander effects are dependent on intracellular interaction and functioning gap junctions (*94-98*). The effect has also been shown to depend upon the dose delivered to the hit cells. This is illustrated in Figure 7 which shows that when 10% of the cells in a dish are hit with an exact number of alpha particles (average LET = 90 keV/μm), the survival of the cells not hit in the dish is reduced, and the reduction in survival depends upon the number of hits experienced by the hit cells (*99*).

In an elegant study examining both high and low LET-bystander, Boyed and co-workers (*100*), demonstrated high-LET bystander effects that did not depend upon direct intracellular interaction. They transfected two human tumor cell lines with the noraderanline transporter (NAT) gene needed for cellular MIBG uptake. Cells were irradiated by incubation with ^{131}I-(low LET β-emitter), ^{123}I- (potentially high LET Auger-emitter), or ^{211}At-(high LET alpha-emitter) labeled MIBG. Unirradited cells were incubated in the medium from transfected cells that had taken up radiolabeled MIBG. Both the donor and recipient cells were tested for clonogenic survival after radiolabeled MIBG and external beam irradiation of the donor cells. This approach made it possible to use as controls the wild-type cell lines that had not been transfected and that did not concentrate MIBG. Using this system they demonstrated that over the dose-range 0-9 Gy, external beam radiation of donor cells caused 30 to 40% clonogenic cell kill in recipient cultures. This potency was maintained but not increased by higher dosage. In contrast, no corresponding saturation of bystander (recipient) cell kill was observed after treatment with ^{131}I-MIBG at activity concentrations which led to 97% kill in donor cells.

Cellular uptake of ^{123}I-MIBG and ^{211}At-MABG induced increasing recipient cell kill up to levels that resulted in direct (donor cell) kill of 35 to 70% of clonogens. Thereafter, the administration of higher activity concentrations of these high-LET emitters was inversely related to the kill of recipient cells. Over the range of activity concentrations examined, neither direct nor indirect kill was observed in cultures of cells not expressing the NAT, and thus incapable of MIBG uptake. The investigators concluded that potent toxins are generated specifically by cells that concentrate radiohalogenated MIBG and that these may be LET dependent and distinct from those elicited by conventional radiotherapy. Using the same basic model, experiments, in spheroids demonstrated spheroid sterilization when only 5% of the cells making up the spheroid expressed NAT; were also performed with spheroids, wherein greater than expected spheroid kill was observed in spheroids with a fraction of the cells transfected. In this system, ^{211}At-MABG was more potent in bystander kill than ^{131}I-MIBG (*101*)

Three-dimensional cell culture systems have also been used to investigate the impact that different fractions of irradiated cells have on cell cluster survival. Bystander effects are observed when survival of all cells making up the cluster is less than that predicted from the fraction of self-irradiated cells (*102-104*). These studies have been confined, however, to beta-particle and Auger-electron emitters. A number of excellent and comprehensive reviews on this subject have been published (*88,97,105,106*) and the reader is referred to these for more on this topic. The remainder of this section will focus on the implications of the bystander effect for radionuclide therapy with alpha-emitting radionuclides.

Bystander effect, ***in vivo***

To date, no studies have been published that examined bystander effects *in vivo* using alpha-particle emitting radionuclides that have been discussed as candidates for radionuclide therapy (*i.e.*, that are the subject of this review). Re-analysis of alpha-emitter studies examining the hot particle hypothesis provide evidence for alpha-particle induced bystander effects, *in vivo*, in Chinese hamsters using ^{239}Pu oxide particles (*106,107*). In these studies, particles of different sizes were injected and lodged in the liver to deliver a range of different local doses while the total average liver absorbed dose was kept constant. Plutonium-239 citrate and the small ^{239}Pu oxide particles distribute uniformly throughout the liver volume, a large fraction of the cells, therefore, experienced an alpha traversal and energy deposition. In contrast, with the largest particles less than 1% of the total cells were likely to have experienced alpha-particle traversals. The incidence of both chromosome aberrations and cancer was dependent only on the total mean absorbed dose to the liver and not on the distribution or on the number of cells irradiated. The authors concluded from these studies that the mass of the total organ volume was the relevant target when estimating absorbed dose for assessment of risk associated with stochastic effects. Although these studies were performed to examine the "hot particle hypothesis" postulated by Tamplin and Cochran (*108*), the results also suggest a bystander effect in that alpha-particle irradiation of a sub-population of cells within an organ affects the organ as a whole. Studies are required to determine whether these conclusions apply to the higher dose rates that are delivered by therapeutic administration of alpha-emitters such as ^{213}Bi and ^{211}At, and to biological endpoints related to the acute effects (*e.g.*, toxicity) that are of primary concern in cancer therapy.

Fractionation

The fundamental rationale for fractionation in external-beam radiotherapy is based upon the differential repair capacity of most normal organs compared to most tumors. This is expressed in terms of early versus late responding tissues, corresponding to high versus low α/β ratios (*109*). Fractionation tends to spare normal organs without a reduced efficacy against tumors. As shown on Figure 8, this is not the case with high-LET radiation (*36*). Cultured cells derived from human kidneys showed the same surviving fraction for a single total absorbed dose of alpha-particle radiation or the same total dose delivered in two equal fractions, separated by 12 hours. Using the same cell line, similar results have been observed when the total dose was delivered in three equal fractions at 4, 8 and 12 hours after cell plating (*35*). Extension of the biologically effective dose (BED) formalism to account for RBE effects has also demonstrated that fractionation is theoretically not likely to confer a normal tissue-sparing effect for high-LET radiations (*110*). Similar conclusions may be drawn for the chronic, exponentially decreasing dose rates delivered by internally administered alpha-particle emitters.

Radiomodulation

Few examples of agents that can modulate alpha-particle radiation induced damage have been reported. In the early 1960s, Barendsen and coworkers compared the radioprotective effects of cysteamine and glycerol (*35*). The surviving fraction of T_1 (human kidney-derived) cells increased by a factor of 3.7 for 250-kVp X-irradiation and only 1.2 for ^{210}Po alpha-particle radiation. Similar results were observed with glycerol; cell survival was increased by 2.0 and 1.2, for 250-kVp X-rays and ^{210}Po alpha-particles, respectively. Qualitatively consistent but quantitatively different results have been obtained with the radiosensitizer, Wortmannin (WM). This irreversible and potent inhibitor of DNA-dependent protein kinase (DNA-PK), is involved in the non-homologous end joining (NHEJ) DNA repair pathway invoked in the repair of DNA double-strand breaks (*111*). In V79 Chinese hamster cells, WM led to a 3 to 4-fold increase in genotoxic damage, as measured by the induction of micronuclei. High LET irradiation, as delivered by a boron neutron -capture reaction, leading to the release of alpha-particles with an average energy of 2.3 MeV, yielded an increase in micronucleus induction of ~2-fold. This suggests that the more complex double-strand damage induced by high-LET radiation is a substrate of the NHEJ pathway (*112,113*). *In vivo* studies in mouse testes have shown that soybean oil, S-(2-aminoethyl)isothiouronium bromide hydrobromide (AET), and cysteamine afford some protection against the cytotoxic effects of 5.3-MeV alpha particles emitted by ^{210}Po (*114-117*). When spermatogonial cell survival was used as the biological endpoint, dose modification factors of 2.2, 2.4, and 2.6 were obtained, respectively. No modification of the spermatogonial response to alpha particles was observed when dimethyl sulfoxide or vitamin C were used (*118,119*).

That DNA damage and its repair are at the core of alpha-emitter radiobiological effects is supported by many years of experimental and theoretical work. It is important, however, to keep in mind that all of the foundation work regarding the radiobiology of alpha-emitters was performed well before modern molecular biology came into existence. In light of the remarkable and far-reaching gains in our understanding of the molecular mechanisms involved in cancer genesis, the cellular response to radiation, and DNA single and double-strand break repair, a re-examination of alpha particle radiobiology, using modern tools is warranted.

D. Relative Biological Effectiveness (RBE)

Introduction

The biological effect of ionizing radiation is influenced by the absorbed dose, the dose rate and the quality of radiation. The radiation quality is characterized by the spatial distribution of the energy imparted and by the density of ionizations per unit path length, referred to as 'linear energy transfer' (LET) or stopping power of a charged particle (*32,83*). Depending upon the effect considered, greater ionization density along a track will increase the probability of inducing a biological effect. Compared to electrons and beta-particles, alpha-particles exhibit a very high density of ionization events along their track (*120*). Electrons and beta particles that are emitted by radionuclides generally range in energy from several MeV to as low as several keV with corresponding LET values ranging from about 0.1 to 1 keV/μm (beta particles actually are characterized by a spectrum of energies; the bottom end of the spectrum is zero). The exception to these is Auger electrons which have energies as low as several eV and corresponding LET values as high as 25 keV/μm. Alpha particles emitted by radionuclides range in energy from 2 to 10 MeV with initial LET values ranging from 60 to 110 keV/μm. A given tissue absorbed dose resulting from alpha-particles, therefore, is likely to yield considerably greater biological effects (again depending upon the effect being considered) than the same absorbed dose delivered by typical electrons or beta particles. To account for differences in energy deposition pattern exhibited by different quality radiations, the concept of relative biological effectiveness or RBE has been established. An authoritative review of this concept, its derivation and appropriate application has been published by the ICRP (ICRP 92 (*83*), ICRP 58 (*121*)) and the reader is encouraged to consult this source for additional information. In radiobiology, RBE equals the ratio of absorbed doses of two types of radiation that produce the same specified biological effect.

RBE defined

RBE is calculated as the absorbed dose of a reference radiation (*e.g.*, X-rays, γ-rays, beta-particles), $D_r(x)$, required to produce a biological effect, *x*, divided by the absorbed dose of the test radiation, $D_t(x)$, required to produce the same biological effect:

$$RBE(x) = \frac{D_r(x)}{D_t(x)} \qquad \text{D.1}$$

RBE is thus an experimentally determined value defined for a particular biological effect and therefore for a particular biological system. The experimentally determined value can be influenced by the following: 1. The variability of the biological system. 2. The methodology used for calculating the absorbed dose of the two radiation types. 3. Since, as described above, the RBE is related to the pattern of ionizing energy deposition along a particle track, the RBE for a particular radiation type will also depend upon the initial emission energy of the particle (*i.e.*, how close the particle is to the end of it's track – the Bragg Peak). 4. If the reference radiation yields a dose-response relationship that is not log-linear for the biological system examined, the RBE value will depend upon the specific biological quantitative endpoint selected (*e.g.,* D_{50}, D_{37} ($=D_0$), D_{10}, etc. which determines whether the comparison falls in the shoulder or in the log-linear region of a dose-response or survival curve), 5) the type of biological endpoint (*e.g.*,

survival, mutation), and 6) the dose rates of the test and reference radiations. The first of these relates to the variability of the model system across different laboratories. The issue has been examined for studies, *in vitro* (*122*). The second of these, the methodology used for dosimetry should, ideally, not be on the list. The methodology used should provide the true absorbed dose value or specific energy distribution (Cf. Section E) to the relevant biological target for both the test and reference radiations. In practice, however, this is a challenge even for studies, *in vitro* (*123*). In the setting of human alpha-particle emitter dosimetry, consistency and reproducibility will be as important if not more important than accuracy. This issue is discussed in greater detail in the recommendations for dosimetry section, below. The third item listed, above, has been examined by Charlton, *et al*. (*124*) and Howell, *et al*. (*125*). In the studies by Howell, *et al.*, a uniform distribution of decays was assumed to calcuate the D_0 for seven alpha-emitting isotopes covering a wide range of initial energies. Using the D_0 obtained for X-rays for the cell line used in the alpha-emitter calculations, a linear relationship between RBE and initial alpha-particle energy was obtained over an initial alpha energy ranging from 5 to 8.5 MeV. The straight line was given by $RBE = 2.9\text{-}0.167E_i$, where E_i is the initial alpha-particle energy in MeV. As shown below, this is an approximate scaling of the equation derived from *in vivo* experimental data by Howell, et al. (*125*). In addition to effects related to the Bragg peak, non-uniform biodistribution of the alpha-emitters also leads to microdosimetric effects that impact RBE and the slope of the cell-survival curve (*47-49*).

Strictly speaking, the test radiation should be delivered in an identical manner as the reference radiation (*e.g.*, chronic, acute, etc.). However, acute externally administered x- and γ-rays are often used as the reference radiation when RBE values are determined for internally administered radionuclides. Given the often sizeable difference in biological responses to acute versus chronic low-LET radiation, the dose rate at which the reference radiation is delivered can impact the resulting RBE (*126*). The dose-rate pattern delivered by radiopharmaceuticals are generally well represented by multicomponent exponential functions. Howell et al. have delivered such patterns with external beams of ^{137}Cs γ-rays (*127*). This approach was utilized to study the bone marrow response to exponentially decreasing dose rates of ^{137}Cs γ-rays (*128*). The response of granulocyte-macrophage colony forming cells in the marrow to decreasing dose rates with half-times ranging from 62 h to ∞ (*i.e.* constant dose rate) were studied and compared with the response to acute exposures. Mean lethal doses for chonic irradiation were up to 40% higher than those for acute exposures. Thus, care must be taken when comparing RBE values based on different reference radiations.

Based upon a review of experimental literature, an RBE value of between 3 and 5 was recommended for cell killing by a panel convened by the Department of Energy in 1996 (*129*)). Since human studies using alpha-particle emitters have yet to be analyzed for deterministic effects, an RBE of 5 was recommended for projecting the possible deterministic biological effects associated with an estimated alpha-particle absorbed dose.

RBE vs LET

The classic relationship between LET and RBE for cell inactivation (*38*) is shown in Figure 9. The figure shows a maximum at an LET of 110 keV/μm close to the LET of alpha particles emitted by radionuclides. The drop in RBE at higher LET values has been interpreted to reflect overkill. If one assumes that a certain amount of damage is required in a particular target volume to inactivate a cell, then there will be an optimal LET that will deposit an amount of energy that

is sufficient to cause that amount of damage. Once the required energy has been reached, the additional energy that is deposited as a consequence of further increases in LET is "wasted." Note that the figure also shows the dependence of RBE on biological end-point with each of the individual curves corresponds to a different level of cell survival.

RBE, in vivo

A biodistribution, dosimetry and comparative efficacy study of intravenously injected ^{211}At performed by Harrison and Royle (*130*), examined the relative effectiveness of ^{211}At and 250-kVp X-rays (0.72 Gy/min) on reducing testes mass and sperm number in mice. At 28 days after injection of ^{211}At or exposure to X-rays, an RBE of 4 was reported for testes mass reduction and 5 for sperm number reduction.

Using a well-characterized mouse testis model with testicular sperm head survival as the biological end-point, the RBE, *in vivo*, of alpha-particle emitting radionuclides administered intratesticularly has been measured relative to acute external 60- or 120-kVp X-rays (~ 0.1 Gy/min), (*116,125,131*). RBE estimates for several alpha-emitters are summarized in Table 3 and plotted in Figure 10. These data were used to derive an empirical relationship between the RBE and initial alpha-particle energy, *in vivo*, for this model:

$$RBE_\alpha = 9.14 - 0.510E_\alpha;\ 3 < E_\alpha < 9\ \text{MeV}. \qquad \text{D.2}$$

This equation was used to derive an RBE for ^{223}Ra when it is in equilibrium with its alpha- and beta-emitting daughters. The calculated value of 5.6, obtained by weighted sum of RBEs for the individual emissions, was in agreement with the experimental RBE value of 5.4 (*125*).

RBE values, *in vivo*, for ^{211}At and ^{213}Bi radioimmunotherapy have been reported. Behr, *et al.* found an RBE of approximately 1 for ^{213}Bi- vs ^{90}Y-labeled Fab' antibody in nude mice when the biological end point was the maximum tolerated dose with the bone marrow being the dose-limiting organ (*132*). The absorbed dose to blood was used to derive the RBE. Blood absorbed dose was calculated using a mathematical model that accounted for beta and gamma cross-fire in the mouse (*133*). When the biological end-point in this same human colon cancer xenograft (GW39) model was anti-tumor efficacy, determined as the time for tumor volume quadruplication, an RBE of 2 to 3 was observed at tumor doses greater than 10 Gy and in excess of 14 at tumor doses less than that (*i.e.*, in the "shoulder" region of the dose-response curve).

In a recent report by Elgqvist, et al., the myelotoxicity in nude mice of intact MX35 antibody labeled with ^{211}At was compared with ^{99m}Tc-labeled antibody and with whole-body ^{60}Co irradiation (*134*). Bone marrow dosimetry was performed by Monte Carlo simulation using an anatomical model developed by Muthuswamy, et al (*135*) and an electron point-kernel (*136*) or ICRU stopping powers (*137*) for electron and alpha-particle energy deposition, respectively. The energy deposited within marrow sites was calculated by integrating over the track length within the marrow. The photon contribution from ^{99m}Tc was added as a whole-body dose. Leukocyte suppression was used as the biological end-point. RBE± SD values of 3.4 ± 0.6 and 5.0 ± 0.9 were obtained when ^{211}At was compared with ^{99m}Tc and whole-body ^{60}Co irradiation, respectively.

The RBE for tumor growth inhibition of ^{211}At-labeled F(ab')$_2$ fragments of the MX35 antibody was obtained in nude mice bearing subcutaneous xenografts of the human ovarian cancer cell line, OVCAR-3 (*138*). Growth inhibition was taken as the average normalized tumor volume

over a 15-day period starting at day 8, post-treatment. This was plotted against absorbed dose and the D_0 value for ^{211}At treatment was compared with that for whole-body ^{60}Co irradiation (~2 Gy/hr). The tumor absorbed dose was estimated as the product of the tumor cumulated activity concentration and the total alpha-particle energy per disintegration. An RBE of 4.8 ± 0.7 was reported.

The RBE of alpha- relative to beta-emitter radioimmunotherapy has also been examined in leukemia patients treated with the HuM195 (anti-CD33) antibody. Data from phase I trials of ^{90}Y-HuM195 and ^{213}Bi-HuM195 were used to examine the relationship between mean absorbed dose and nadir duration of peripheral leukocyte counts (ND) or % reduction in marrow blasts (RMB). Regions of interest around vertebral bodies T11-L5 were used to assess marrow uptake and pharmacokinetics; ^{111}In was used as an imaging surrogate for ^{90}Y. These data were integrated over time, then divided by the estimated volume of marrow in T11-L5 and multiplied by the total beta- and alpha-particle energy released per disintegration of ^{90}Y or ^{213}Bi to yield red marrow absorbed dose. The dose contribution of beta-particle emissions from ^{213}Bi is 7%, the photon contribution is substantially lower, both were considered negligible in the analysis. RMB was obtained from histopathological scoring of bone marrow biopsies collected before and after treatment. Absorbed dose-versus-response comparisons for both myelotoxicity and tumor-burden reduction did not yield a statistically significant difference between ^{90}Y and ^{213}Bi (ND: p=0.6; RMB; p=0.08), giving an RBE of approximately 1 for both (*139*).

The RBE values reported for radioimmunotherapy studies *in vivo* are summarized in Table 4. In addition to showing a wide variability in RBE, the table also shows diversity in the biological end-points and the reference radiations used. Such diversity in model systems makes it difficult to draw general conclusions and to extrapolate animal studies to the human. In all cases, including the results shown in Table 3, uniform activity distribution was assumed and the average absorbed dose was estimated. Given the administered activities and the total estimated absorbed doses delivered, estimation of average absorbed dose as opposed to specific energy distribution reflects the assumption that the stochastic relative deviation of the local dose from the mean is not likely to exceed 20% (see section on criterion for adopting microdosimetry). Additional studies are required, however, to evaluate this for non-target tissue (such as for toxicity evaluation).

An important question for alpha-particle-emitter radionuclide therapy is the degree to which RBE values, obtained in pre-clinical biological systems are applicable to predicting tumor response or toxicity in humans. This question is closely related to the ability to perform accurate alpha-particle dosimetry in humans. To date, there is only a small number of reported human trials using alpha-particle emitters and these have not been rigorously examined to evaluate RBE. Since RBE is strictly defined relative to a reference radiation that is delivered in the same manner, it is not likely that human data will yield RBE values in the strict sense. Rather a comparison to historical results with external beam radiation or with beta-emitting radionuclides will have to suffice. Together with the dependency of RBE on the alpha-particle energy, the biological effect being considered, and the dose calculation methodology, analysis of patient results for estimation of RBEs will likely yield consistent results only if a standard approach to alpha-particle-emitter dosimetry is adopted.

RBE, Q, and w_R

The discussion thus far has focused on RBE. RBE is occasionally confused with quality factors, Q, and radiation weighting factors, w_R. This confusion reflects the historical evolution of RBE which was originally defined as Relative Biological Efficiency and intended to apply to both radiobiology (deterministic effects) and protection (stochastic effects). As currently recommended by the ICRP, however, RBE is not to be used directly in radiation protection but only as a starting quantity to derive the radiation weighting factor w_R which replaced the quality factor Q in the most recent ICRP recommendations (*140,141*). The RBE values used to arrive at w_R relate to stochastic endpoints such as cancer induction, rather than deterministic endpoints such as normal tissue toxicity and tumor cell sterilization in cancer therapy patients. As noted earlier, the ICRP radiation weighting factor for alpha particles is 20. This value, intended only for stochastic effects caused by alpha particle irradiation, is based on animal experiments and from analysis of historical alpha-emitter exposures. In contrast to RBE values, weighting factors are not directly measured values but rather are consensus recommendations of the International Commission on Radiological Protection (*142*).

The radiation weighting factor w_R, is a unit-less factor that converts average absorbed dose (in units of gray (Gy)) to equivalent dose in an organ or tissue. The SI units for equivalent dose are referred to by the special name, sievert (Sv). The Sv is is not a unit in the conventional sense, but rather, is intended to indicate that the absorbed dose value has been adjusted to reflect a biological risk that is associated with *stochastic effects*. Although the Sv is often used in the context of deterministic effects, this is not strictly correct since the ICRP has stipulated that it should only be used to designate the risk of incurring stochastic biological effects such as cancer. While the ICRP has reported on RBE for deterministic effects (RBE_M), no special name has been chosen by the ICRP for the product of absorbed dose and a factor such as RBE that specifically reflects similar scaling for a deterministic effect (*121*).

E. Alpha-Particle Dosimetry

Introduction

Radiation dosimetry offers a means for standardizing and comparing the efficacy of different radiation-based treatments. It provides a logical basis for understanding the effects that various radiation qualities have on biological matter. For alpha particle emitters, accurate dosimetry calculations require knowledge of the activity distribution as a function of time at the cellular and subcellular level (*143*). Furthermore, an accurate representation of the geometry at this level is also required. For *in vitro* experiments (*i.e.*, cell survival studies), the activity distribution is straightforward, consisting of uptake on the surface or within the cell, along with a known fraction in the surrounding solution. In these experiments, the cell and nucleus can be approximated as concentric spheres the dimensions of which can be easily measured. However, for clinical applications, these idealizations give way to complex activity and tissue geometries. In these cases, modelling the three-dimensional geometry of a spheroid (*144,145*) or using microscopic data from tissue biopsy samples (*146*) can provide information on the target geometry. Determining the activity distribution, however, remains difficult. Autoradiography (*147*) may provide a snapshot of the activity distribution at one instance in time. However, the determination of the activity as a function of time may require mathematical modeling (*148-150*)

of the carrier molecules as they diffuse through tissue and bind to markers on cell surfaces. Ideally, such modelling should be validated using animal model measurements, *in vivo*.

Case for microdosimetry

There are two methods for calculating the energy deposited by individual alpha particles. One method uses the MIRD formalism to calculate the average dose to the target (cell nucleus) for a variety of source compartments (cell surface, cytoplasm and nucleus). Extensive tables have been produced for various combinations of alpha-particle emitting radionuclides and cellular geometries (*151,152*). The basis for using mean absorbed dose is related to the biological properties of low-LET radiations such that a large number, often several thousands, of statistically independent radiation deposition events in a single cell nucleus is required to induce a demonstrable biological effect. In such a case, the statistical variation of the energy imparted to different cell nuclei is minimal. In contrast, for high-LET irradiation, such as alpha-particles, the effect of even a single event in the cell nucleus is so great that the mean absorbed dose can be a misleading index of biological effect. This is due to several reasons. Foremost is that the number of alpha particles that traverse a cell nucleus is often very few and therefore stochastic variations become important. In addition, the path of the alpha particle through the cell nucleus is also critical. An alpha particle that crosses directly through a cell nucleus will deposit a large amount of energy, while one that merely grazes the surface will deposit little or no energy. Thus, a second method for alpha particle dosimetry – microdosimetry – takes into account the stochastic nature of energy deposited in small targets. The fundamental quantities in classical microdosimetry are specific energy (energy per unit mass) and lineal energy (energy per unit path length through the target) (*153*). Microdosimetry was originally proposed by Rossi (*154*) to understand the stochastic nature of energy deposited in matter by external ionizing radiation. It has subsequently been adapted to the case of internally deposited alpha particle emitters (*155-157*).

Microdosimetric techniques

Microdosimetric spectra may be calculated using either analytical or Monte Carlo methods (*158*). Analytical methods use convolutions (via Fourier transforms) of the single-event spectrum to calculate multi-event distributions (*154*). The single-event spectrum represents the pattern of specific energy depositions for exactly one alpha-particle hit. Kellerer developed a method to efficiently determine the multiple-event spectrum through the use of Fourier transforms (*159*). While analytical codes are computationally efficient, they are often limited to simple source-target geometries as the single-event spectrum must be known for each source-target configuration. Monte Carlo codes offer greater flexibility than analytical methods, and can simulate a wide variety of geometries and source configurations. Idealizations are often made to simplify the coding and reduce calculation time. In nearly all Monte Carlo codes, alpha particles are assumed to travel in straight lines. This approximation is valid for alpha particles having energies less than 10 MeV (*153*). In addition, the range of delta rays (energetic electrons originating from the alpha-particle track that cause secondary ionizations in the vicinity of the track) and the width of the alpha-particle track (~ 100 nm) are often ignored since the targets that are studied (*i.e.*, cell nucleus) are much larger than these dimensions (*160*). The rate of alpha-particle energy loss is characterized by the stopping power. These data for a variety of media can be obtained from the literature (*137,161-163*). Inherent in the stopping-power formulation is the continuous slowing-down approximation (CSDA). As the name implies, this approximation

assumes that alpha particles lose energy continuously as they traverse matter. Thus, the calculated specific energy imparted depends on the choice of stopping powers used.

Criterion for adopting microdosimetry

The rationale for microdosimetry was outlined by Kellerer and Chmelevsky (*164*). They suggested that the stochastic variations of energy deposited within the target must be taken into account when the relative deviation of the local dose exceeds 20%. For example, a small cell nucleus with a diameter of 5 μm irradiated by alpha particles would require an average dose of at least 100 Gy in order for the relative deviations to be less than the 20% threshold. Thus, the necessity for microdosimetric methods will depend on the source distribution, the target size and shape and the expected mean dose. For small average doses (such as those expected by non-targeted tissues) microdosimetry may be important in characterizing the pattern of energy deposition and in understanding how this relates to clinical outcomes. However, in tumor, where the mean dose may be large, a microdosimetric treatment may not be necessary.

Microdosimetry implementation techniques

While microdosimetry has increased our understanding of stochastic patterns of energy deposition by alpha particles in both simple and complex geometries and has made it possible to explain observations made *in vitro,* application to clinical practice has been limited because time-dependent activity distributions at the sub-cellular level are complex and not well characterized *in vivo*. Roeske and Stinchcomb (*165,166*) described a technique for determining dosimetric parameters that are important in alpha-particle dosimetry. These parameters consist of the average dose, standard deviation of specific energy, and the fraction of cells receiving zero hits. The individual values are determined using tables of the "S" value, and the first and second moments of the single-event spectra. The average dose is determined by multiplying the "S" value by the cumulated activity within the source compartment. Dividing the average dose by the first moment of the single-event spectrum yields the average number of hits. Subsequently, the fraction of cells receiving zero hits (or any number of hits) can be determined by using the average number of hits and the Poisson distribution. The standard deviation is the product of the average number of hits and the second moment of the single-event spectrum. Individual moments may be determined using either analytical methods or Monte Carlo calculations. Stinchcomb and Roeske (*167*) have produced tables of the "S" value, and the individual moments for a number of geometries and source configurations appropriate for alpha particle therapy. These tables were also used in the analysis of cell survival following alpha-particle irradiation (*167*).

Applications of microdosimetry

Early applications of microdosimetry were performed to assess the probability of cancer induction following exposure to alpha-emitters. These exposures were generally not intended for therapeutic purposes and carcinogenesis was of concern. In one such application, the specific energy distributions for plutonium oxide in dog lung were calculated. The calculations accounted for the size distribution of the inhaled aerosol and the associated deposition probabilities in the lung for various particle sizes. The distribution of target sites, the probability of an alpha particle intersecting a target site and the range, energy loss, straggling characteristics and delta-ray production of alpha-particle tracks was also considered. The analysis provided an improved understanding of the relationship between dose, as described by microdosimetric

specific energy spectra, and response, as measured by the incidence of lung tumors in beagle dogs (*168*).

In radioimmunotherapy (RIT), microdosimetry has been used in a number of alpha-particle applications. These applications can be broadly characterized as theoretical studies of simple cellular geometries, experimental analysis of cell survival following alpha-particle irradiation, and the microdosimetry of realistic geometries such as multicellular spheroids and bone marrow. The work in each of these categories will be discussed separately.

Roesch (*155*) described one approach for calculating microdosimetric spectra. Fisher (*47*) subsequently applied this approach to a number of geometries that have therapeutic application including sources distributed on and within individual cells, sources distributed within spherical clusters of cells, and sources located in cylinders (i.e, blood vessels) that deposited energy within spherical cell nuclei a short distance away. These calculations showed the number of alpha-particle emissions originating from cell-surfaces that would be needed to inactivate cancer cells with high efficiency. The basic geometries that described the spatial distribution of alpha-emitters relative to the spatial distribution of target spheres have served as the basis of those used in several theoretical studies. In one such study, Humm (*169*) used a Monte Carlo method with a model of cell survival to estimate the surviving fraction of cells located outside of a capillary and cells located within a tumor with uniformly distributed ^{211}At. Although the mean dose was similar for these two types of geometries, there was a significant variation in the expected cell survival due to the differences in the specific energy spectra. In particular, the fraction of cells receiving no alpha-particle hits increased with distance from the capillary (due to the short range of the alpha particles). The surviving fraction versus mean specific energy was bi-exponential. That is, for low doses, the slope of this curve was similar to that of a uniformly irradiated tumor. However, with increasing doses, the curve was less steep and asymptotically approached a value corresponding to the fraction of non-hit cells. Building upon the previous analysis, Humm and Chin (*48*) analyzed how specific energy spectra are affected by cell nucleus size, binding fraction, cell volume fraction and nonuniform binding. Their results indicated that nonuniform distributions of alpha-particle emitters can result in expected survival curves that deviate significantly from the classical mono-exponential curves produced by a uniform, external source of alpha particles. In these studies, although the inherent cell sensitivity (z_o) was held constant, the slope of the cell survival curve as a function of absorbed dose to the medium was highly dependent upon the source configuration. Furthermore, simulations in which cells were more uniformly irradiated resulted in steeper cell survival curves than those in which the distribution of alpha emitters was highly heterogeneous. The effects of cell size and shape on expected cell survival were further studied by Stinchcomb and Roeske (*170*). In their analysis, the cell and nucleus were assigned various shapes ranging from spheres to ellipsoids where the ratio of the major-to-minor axis was varied from 1 to 5 while the volume of the nucleus was held constant. Separately, the dimensions of the nucleus were varied while the shape was held constant. Calculations of specific energy spectra and resulting cell survival demonstrated that the expected surviving fraction was not a strong function of the target shape, provided the volume was fixed. However, significant variations in cell survival were observed as the volume of the nucleus was varied. More recently, Aubineau-Laniece and colleagues developed a Monte Carlo code to simulate cylindrical geometries as a model for bronchial airway bifurcations (*171*). In a series of reports on alpha particles from radon progeny, Fakir and co-workers (*172-174*) demonstrated that for uniform surface emissions, there were significant variations in cellular energy deposition.

Larger variations in the hit frequencies and energy deposited were observed when a nonuniform distribution of activity was also considered. Palm et al (*175*) examined the microdosimetric effects of daughter products from ^{211}At. Separate simulations were performed assuming the daughter products decayed at the site of ^{211}At emission or that they diffused away from the site. Based on an analysis of experimental data, the ^{210}Po daughter product seemed to diffuse from the decay site, decreasing the energy deposited in the cell nucleus by a factor of 2. All of these studies illustrate the need to accurately model the source/target geometry. Moreover, approximations, such as using mean values may impact both the specific-energy spectrum and subsequent calculation of cell survival (*49*).

Application to cellular clusters

Single-cell survival analyses following alpha-particle irradiation has also been extended to multicellular clusters. Charlton (*145*) described a multicellular spheroid model and simulated alpha-particle energy deposition events within individual cell nuclei. A cell survival model that takes into account the effects of varying LET (*61*) was combined with the distribution of alpha-particle tracks throughout cells within the spheroid. Simulating a uniform source distribution (average 1 decay/cell, 50% cell packing), this analysis demonstrated that cell survival decreased significantly (from 57% to 37%) as the spheroid diameter increased from 75 to 225 μm. The number of hits per cell also increased in larger spheroids when longer-ranged alpha-particle emitters were considered. Cell survival subsequently decreased from 46% to 26% in 200-μm diameter spheroids as the packing fraction was increased from 40% to 70% (also with, 1 decay/cell). The decrease in cell survival was due to the increased crossfire dose as the packing fraction was increased. In a separate simulation, the total number of decays per spheroid was kept constant while a small fraction of cells (20%) was assumed not to take up any activity. This process simulated the effects of cells that lacked a specific targeting moiety. It is interesting to note that the unlabeled fraction did not significantly alter the expected cell survival. In these studies, the specific energy distribution is highly nonuniform and varies with depth below the spheroid surface. Thus, a single dose or specific-energy distribution is not representative of that through the entire tumor. By combining the specific-energy distribution with cell survival models, it is possible to gain insight into those factors which will influence the therapeutic efficacy of a particular targeting approach. However most of these cell survival models do not take into account second-order processes such as the bystander effect which may play an important role in modeling cellular clusters and micrometastases. Refinement of these models is currently an active area of research (*94,176*).

Application to the bone marrow

Bone marrow is often the dose-limiting organ in RIT. The dosimetry of bone marrow is difficult due to its complex geometry as well as the presence of tissue inhomogeneities. Thus, idealized models, as have been utilized in the previous studies, must be replaced by more realistic geometries. The work to date on estimating specific energy spectra for bone marrow has focused largely on using histological samples obtained from humans or animal models. Akabani and Zaltusky (*146*) obtained histological samples of beagle bone marrow, and manually measured chord length distributions. Using a Monte Carlo program, they calculated the single-event specific energy distribution for sources both in the extracellular fluid and on the surface of red marrow cells. These single-event distributions were combined with a model of cell survival. This analysis demonstrated that activity concentrated on the cell surface resulted in significantly

greater cell killing than does activity in the extracellular fluid. The effect of LET on the survival of human haemotopoietic stem cells in various geometries was studied by Charlton et al. (*124*). These geometries were determined from human marrow samples obtained from cadavers. Microdosimetric spectra and cell survival were calculated for three different source/target geometries: a) isolated cells labeled on their surfaces; b) a non-targeted distribution of decays in an extended volume; and c) non-targeted decays in marrow with 36% of the marrow volume occupied by fat. Two different radionuclides, ^{149}Tb and ^{211}At, were considered. These simulations indicated that for targeted decays ^{149}Tb was 5 times more effective than ^{211}At when compared on a hit-by-hit basis. This enhancement was due to the lower energy of ^{149}Tb resulting in a higher LET of the incident alpha particles. They also concluded that cell survival was a function of the position of the decay relative to the cell nucleus. Using a similar model as Charlton (*124*), Utteridge et al. (*177*) considered the risk of developing secondary malignancies (*i.e.*, leukemia) from alpha particles. This risk may be important in evaluating the future therapeutic application of alpha particles in patients who have an excellent prognosis. Three alpha-emitting radionuclides were considered based on the particle's relative range (short, medium and long). In this analysis, the authors calculated the fraction of cells that are hit and would survive (as these would potentially cause secondary malignancies). They determined that the lowest fraction occurred for low energies and the highest fraction occurred for the highest energy alpha-particle emitter.

F. Alpha-Particle Emitters of Interest for Human Use

This section provides a survey of alpha-particle emitters of interest for human use including the properties of individual alpha-emitters and a summary of important pre-clinical and clinical studies. The section focuses on those alpha emitters that have emerged in the last two decades as possible candidates for targeted cancer therapy. Radium-224 ($T_{1/2}$ = 3.66 d; 5.7 MeV alpha-emitter), a historically important radionuclide that is still used clinically, does not fall under this category but is briefly described for completeness.

From the mid 1940s until 1990, ^{224}Ra-radium chloride was used for treatment of different bone and joint diseases mainly in Germany. Starting in 2000, pure ^{224}Ra-radium chloride was again made available in Germany for treatment, by intravenous administraton, of ankylosing spondylitis (AS). Total activities of 10 MBq (10 administrations of 1 MBq over 10 weeks) were approved.

Lassmann et al. (*27*) examined the dosimetry of this treatment schedule. Dosimetry was performed according to the model proposed by the International Commission on Radiological Protection (ICRP) (*178*). A maximum bone-surface absorbed dose of 4.4 Gy was estimated. The excess absolute risk associated with this treatment was estimated to be 0.2% for malignant bone tumors; and 0.4% for leukemia.

Astatine-211 (^{211}At)

Radionuclide properties

Astatine-211 has a half-life of 7.2 hours. It decays with 58.3% probability through the electron capture process to ^{211}Po, which has a half-life of 0.52 s, and decays by emitting a 7.45 MeV alpha-particle to stable ^{207}Pb. As a consequence of the electron-capture process, polonium K X-rays are emitted that permit external imaging, the two most abundant of these X-rays have energies of 77 and 80 keV with yields of 0.1 and 0.2 per disintegration (*179*) (12 and 20% of all

photon emissions (*180*)), respectively. In 1% of the ^{211}Po decays, the emitted alpha-particle will have a different initial energy (6.57 or 6.89 MeV). The other branch (41.7%) involves the direct emission of a 5.87 MeV alpha-particle, leaving a relatively long-lived ($T_{½}$=32.9 y) ^{207}Bi daughter. The long half-life of this daughter is not problematic because less than 0.001 ^{207}Bi decays occur for every ^{211}At decay (*3*).

Astatine-211 is mainly produced via the ^{209}Bi(α,2n)^{211}At nuclear reaction using cyclotron beam irradiation ($22.0 \leq E_\alpha \leq 28.5$ MeV) utilizing external or internal targets (*181,182*). Isolation of the nuclide can be achieved either through solvent extraction or by dry-distillation of the irradiated target material. The technique most commonly used to convert ^{211}At to a chemically useful form is dry-distillation, and several different kinds of apparatus and procedures have been reported (*183-186*).

Pre-clinical studies

Shortly after the first production of astatine (*187*), made possible by the completion of the 60-inch Berkeley cyclotron, the first report on the distribution of the new element in the thyroid glands of normal and thyrotoxic guinea pigs was published. In that study, ^{131}I was used for comparison. Much of the special dosimetry required for internal alpha-particle radiotherapy was clear at this early stage. The report states: "*The density of ionising radiation produced by these alpha-particles is over two hundred-fold greater than that resulting from the radio-iodine beta-rays. This means that, since the range of the alpha-particles is so short, the thyroid cells which accumulate element 85 in the largest quantities would suffer the brunt of its radiation. The action of radio-iodine in the thyroid gland would be much more diffuse because of the longer range of the beta-rays. Therefore, there would be a considerable radiation effect upon the thyroid cells lying at a distance from those areas in which relatively large quantities of radio-iodine have been concentrated* (*188*)".

Fourteen years later, Hamilton *et al.* (*189*) provided complete biodistribution data on all organs of rats for both astatine and radio-iodine (*i.e.*, ^{131}I). Two monkeys were used for the assessment of astatine uptake in the thyroid gland following intraperitoneal injection. An additional 3 monkeys were injected with astatine into the anterior chamber of the eyes in order to study the biological effect of this radionuclide. The latter study was motivated by interest in the possibility of internal irradiation of retention cysts on the anterior chamber of the eye. All experiments showed a high degree of accumulation of astatine in the thyroid gland. Early reports estimated a lethal whole-body dose in rats of approximately 1.1 Gy. More recent reports have stated whole-body LD_{10} values in mice of 0.5 Gy (BALB/c nu/nu) and 1.0 Gy ($B6CF_1$) (*190*).

A number of ^{211}At formulations have been investigated for biological use. The biodistribution and resulting biological effects of these have been previously reviewed by Zalutsky and Vaidyanathan, (*3*) and readers are encouraged to consult this highly authoritative review. A summary of the various ^{211}At compounds follows.

As noted above, [^{211}At]astatide was the earliest form of ^{211}At investigated. Astatine is directly below iodine in the periodic table, accordingly, the proclivitity of astatide for the thyroid is second only to that of iodide itself. The retention of astatide in other tissues is consistently higher than that of iodide with astatide uptake in macrophage-bearing organs such as the liver and spleen an order of magnitude higher than that of iodide. The toxicity of IV-administered

[^{211}At]astatide was investigated in mice (*190*). The LD_{10} in $B6C3F_1$ mice was 28 kBq/g body weight; near the LD_{10}, mild changes in the heart, liver and stomach were observed in animals followed for 1 year (*3,190*). In athymic mice bearing subcutaneous human follicular thyroid carcinoma 11-28% of the injected dose per gram accumulated in the tumor.

To overcome the normal-organ uptake of [^{211}At]astatide, ^{211}At-labeled particulates have been investigated for intracavitary application. Bloomer *et al*. (*191*) examined the efficacy of ^{211}At-tellurium colloid for the treatment of malignant ovarian cancer ascites in mice. Mice were cured with intraperitoneal administered activities of 925 to 1850 kBq. At these activities, mild morbidity was manifested as weight loss. Cured animals, observed for 200 days, exhibited no visible radiation effects. Histological sections of major organs showed no evidence of tumor and were unremarkable except for the thyroid. The thyroids of treated mice, when found, were fibrotic and granular. Radiocolloid activities in excess of 2775 kBq were uniformly fatal in 5 to 7 days. These results were compared to ^{90}Y and ^{32}P particulates, for which activities of 7440 to 5550 kBq prolonged median survival but did not result in cures (*1*). The ^{211}At-tellurium colloid was rather unstable, with 20% of ^{211}At released after 2-h incubation in fetal calf serum (*1*). Alternative particulate systems have been investigated to overcome the poor stability of this colloid (*192,193*).

Naphthoquinone derivatives labeled with ^{211}At have been investigated for targeted tumor therapy. Naphthoquinone diphosphates selectively accumulate in some tumors due to cell-membrane associated alkaline phosphatase activity (*194*). Intravenous administration of 6-[^{211}At]astato-2-methyl-1,4-naphthoquinol diphosphate (6-[^{211}At]astato-MNDP) led to cure rates of 45 to 65% at admnistered activities of 55-300kBq in a subcutaneous CMT-93 murine rectal adenocarcinoma model (*195*). As demonstrated by alpha-particle autoradiography, in tumor cells, a significant fraction of the labeled compound was taken up in the cell nuclei of tumor cells (*196*). To address the concern of secondary malignancies with high-LET targeted radiotherapeutics, Brown *et al.* (*85*) performed a histopathological evaluation of the late tissue effects in more than a hundred C57B1/10 mice that had been cured of their CMT-93 tumors following the admnistration of upto 750 kBq 6-[^{211}At]astato-MNDP. Abnormalities were seen primarily in mice receiving more than 300 kBq. The most common of these were lymphoma, plasmacytoma and chronic pulmonary fibrosis. At activity levels in the therapeutic dose range (55-300 kBq), the incidence of significant late radiation effects was less than 15%.

Pre-clinical studies investigating melanoma targeting using ^{211}At-methylene blue (MTB) analogs have demonstrated a 5-fold greater uptake of 4-[^{211}At]astato-MTB in pigmented B16 murine melanoma cells compared to amelanotic cells (*197,198*). The therapeutic effectiveness, *in vivo*, was determined by a lung colony-forming assay combined with a search for metastases to organs other than lungs. Athymic mice were IV-injected with a suspension of HX34 human melanoma cells. The number of surviving tumor colonies found in the lungs of ^{211}At-treated animals was approximately 95% lower than that in controls. The reduction was similar for both 1.67 and 3.33 MBq 4-[^{211}At]astato-MTB but was highly dependent on the cell number injected and the time-interval between tumor cell innoculation and 4-[^{211}At]astato-MTB injection (*199*). In a subsequent study, therapeutic effectiveness was evaluated by the growth rate of subcutaneously implanted human melanoma xenografts and the onset and size of lymph node metastases; efficacy against a highly pigmented cell line, HX118 was compared with HX34, a poorly

pigmented cell line. Growth delay was highly dependent upon the intial tumor diameter and the cell line targeted. Growth delays of 65 and 7 days were obtained for HX118 and HX34 (0.5 to 0.6 mm diameter) tumors, respectively (*200*). As these studies were performed in athymic mice which do not have melanin in the skin or in their normal ocular and cerebral stuctures, tumor targeting in the presence of melanin-positive normal structures could not be evaluated.

To expand upon the efficacy of the thymidine analog, 5-[^{125}I]iodo-2'-deoxyuridine (IUdR) against cells in S-phase to cells adjacent to those targeted that may not be in S-phase, an astatinated analogue of IUdR, [^{211}At]AUdR, was developed (*201*). Studies performed, *in vitro*, demonstrated [^{211}At]AUdR uptake in tumor cells similar to that of IUdR. Clonogenic assays demonstrated remarkable cytotoxicity of [^{211}At]AUdR; reduction in survival to 37% was achieved with less than 3 ^{211}At atoms bound per cell. The yield of DNA DSB was 10 times greater for [^{211}At]AUdR compared to [^{125}I]IUdR (*202*). The instability, *in vivo*, of [^{211}At]AUdR (*201*) has led to the investigation of other compounds that can be labeled with ^{211}At and incorporated into cellular DNA. The ^{211}At analogue of [$^{125/131}$I]FIAU, [^{211}At]FAAU was produced but also demonstrated poor stability, *in vivo* (*203*).

An astatinated analogue of the radioiodine-labeled compound *meta*-iodobenzylguanidine (MIBG) has been developed (*204,205*). [^{131}I]MIBG is used for the diagnosis and treatment of neuroendocrine tumors. In a clonogenic survival assay the activity concentration of [^{211}At]MABG required to reduce cell survival, *in vitro*, to 37% was more than 1000-fold less than that of no-carrier-added [^{131}I]MIBG (384 vs 0.215 kBq/ml); the D_0 for [^{211}At]MABG was equivalent to 6 to 7 atoms/cell. The importance of specific targeting was confirmed by the observation that [^{211}At]astatide was 80-fold less effective than the MABG construct (*206*). Mouse biodistribution studies with [^{211}At]MABG demonstrated peak tumor accumulation slightly greater than that of [^{131}I]MIBG. Similar specific uptake of these two labeled agents was observed in the heart and adrenal glands; these two tissues exhibit uptake of MIBG due to an active process. Pre-treatment with unlabeled MIBG increased tumor uptake of [^{211}At]MABG by 150% while reducing heart uptake by 30% (*204,207*). Fluoro-substituted analogues to increase tumor retention have been synthesized and increased tumor uptake has been demonstrated *in vitro*; greater normal organ uptake was also observed, however (*208,209*).

The shorter range and greater potency of alpha-particles would be expected to reduce marrow toxicity relative to beta-emitters in the targeting of bony metastases (*146*). To examine the potential of ^{211}At to relieve pain and slow tumor progression in bony metastases, ^{211}At-labeled bisphosphonates have been developed (*210*). The distribution of ^{211}At-labeled bisphosphonates in normal mice was similar to that of iodine analogues. Bone surface to bone marrow absorbed dose ratios for these conjugates were approximately 3 times greater than for ^{131}I-labeled conjugates. Co-injection or pre-injection of unlabeled bisphosphonates reduced normal organ accumulation without compromising bone accumulation (*211*).

As noted above, ^{211}At has been examined in a wide variety of formulations for targeted therapy in humans. The greatest effort in terms of radiochemistry and pre-clinical studies has been in ^{211}At immunoconjugates. The majority of this work has been performed by the Zalutsky lab at Duke University. More recently, the group at Göteborg, Sweden has also contributed pre-

clinical ^{211}At immunoconjugate studies; both groups have initiated clinical studies of ^{211}At (see below).

Although astatine is directly below iodine in the periodic table, the tyrosine halogenation approach to radiolabeling of proteins (*e.g.*, antibodies) does not work with ^{211}At (*212,213*) and an alternative chemistry (N-succinimidyl 3-[^{211}At]astatobenzoate (SAB)) for antibody conjugation was developed by Zalutsky and co-workers (*214-216*). The cytotoxicity of ^{211}At-labeled antibodies has been studied for single cells in suspension, small groups of cells grown as a monolayer, and against spheroids (multicellular spherical clusters of cells). The D_0 was sensitive to the cellular configuration. Against single cells, the specific ^{211}At-labeled antibody was 80 times more potent than ^{211}At-labeled bovine serum albumin (^{211}At-BSA) control in reducing clonogenic survival with a D_0 equivalent to an average of 40 atoms per cell; against monolayer cells, specific antibody was 4 times more cytotoxic than ^{211}At-BSA (*217*). The ^{211}At-labeled chimeric antibody 81C6, reactive with the extracellular matrix antigen tenascin was effective in reducing the doubling time of human glioma spheroids with radii greater than the range of ^{211}At alpha-particles (*218*).

Targeting and biodistribution studies of ^{211}At-labeled Mel-14 antibody F(ab')$_2$ fragments, reactive with a glioma and melanoma-associated antigen, have been performed (*219*). Tumor retention of ^{211}At in an athymic subcutaneous D-54 MG human glioma xenograft model was essentially identical to that of ^{131}I at all times after injection except 24 h, at which time ^{211}At had decayed to 10% of the administered activity. The level of ^{211}At in normal tissues such as stomach, spleen and lungs, however, was greater than that of ^{131}I.

To increase the cellular retention of ^{211}At following antibody internalization and lysosomal catabolism, a labeling method, using N-succinimidyl 5-[^{211}At]astato-3-pyridinecarboxylate ([^{211}At]SAPC), that yields positively charged astatopyridine-substituted catabolites was developed. This labeling approach demonstrated greater retention in tumor cells using an antibody against a tumor-associated mutant EGF receptor (*220,221*).

The biodistribution, toxicity and efficacy of the anti-tenascin antibody, 81C6, labeled with ^{211}At were evaluated. In an athymic human glioma xenograft model, tumor accumulation of ^{211}At-chimeric 81C6 reached 20% injected activity per gram at 16 h and persisted at this level for the remaining 48 h data collection period; uptake in normal organs was approximately the same as for the ^{131}I labeled antibody (*222*). The toxicity and LD_{10} of intravenously administered ^{211}At-chimeric 81C6 antibody was established in the $B6C3F_1$ mouse strain (*223*). The LD_{10} was 45.7 kBq/g and 101.5 kBq/g in male and female mice, respectively. Perivascular fibrosis of the intraventricular septum of the heart, bone marrow suppression, spermatic maturation delay, splenic white pulp atrophy and reduction in thyroid mass were observed in some of the long-term survivors that had received the highest administered activity. The toxicity of the IV-administered antibody was about half of that observed for IV administered [^{211}At]astatide (*190*). The efficacy of ^{211}At-murine 81C6 antibody was investigated in an athymic rat model of neoplastic meningitis (*224*). No difference in survival was observed between intrathecally injected saline and 444 kBq ^{211}At-45.6 irrelevant Ab controls. At the same level of activity, 3 of 9 mice were cured (300 day survival, no evidence of disease) following intrathecal

administration of the specific antibody; six of ten mice were cured following treatment with 666 kBq; no therapeutic effect was observed with ^{131}I labeled antibody (*225*).

Astatine-211 has been used for evaluating the therapeutic efficacy, toxicity, and radiation dosimetry in the treatment of disseminated micro-metastatic ovarian cancer in nude mice. The therapeutic efficacy for animals as well as the mean absorbed dose in tumors was studied in different settings for both intact and fragmented mAbs (MX35, MX35 F(ab)′$_2$, or MOv18) (*226,227*). Animals were inoculated with ~1×10^7 OVCAR-3 cells. At 1, 3, 4, 5, or 7 weeks after inoculation, the animals were intraperitoneally treated with 0.4–1.2 MBq ^{211}At-MX35 or with 25–400 kBq ^{211}At-MX35 F(ab')$_2$. Eight weeks after treatment the animals were sacrificed and the tumor-free fraction (TFF), *i.e.*, percent of animals with no macro- and microscopic tumors and no ascites, was determined. The mean TFF was 64% after treatment of 0.4–1.2 MBq ^{211}At-MX35. The mean absorbed dose was >6 Gy for tumor radius (r_{tumor}) <71 μm. A significant increase in the TFF was observed between 50 (TFF = 22%) and 100 kBq (TFF = 50%) ^{211}At-MX35 F(ab')$_2$. This was confirmed by a model of the metastatic cure probability. The TFF was 95% for $r_{tumor} \leq 30$ μm when 400 kBq ^{211}At-MX35 F(ab')$_2$ was intraperitoneally injected. The TFF was significantly higher at later time points (*i.e.*, at 4, 5, or 7 wk after inoculation) for ^{211}At-MX35 F(ab')$_2$ compared to ^{211}At-Rituximab F(ab')$_2$ irrelevant mAb, explained by a high mean absorbed dose (>22 Gy) to the tumors.

The therapeutic efficacy and myelotoxicity was also studied for 50, 400, or 800 kBq intraperitoneally injected ^{211}At-MX35 F(ab')$_2$, administered as single or fractionated treatments (*228*). The TFF was 17%, 39%, and 56% for 50, 400, and 800 kBq injected, respectively. The TFF was 22%, 28%, and 41% for 3×17, 3×133, and 3×267 kBq injected (4 d between each treatment), respectively. No significant difference between single and fractionated treatment was noticed (P >0.5). Alleviation in the myelotoxicity was noticed for the fractionated treatment compared to the single treatment in terms of a decreased suppression from 46% to 19%, and delayed nadir from days 4 to 11 of the WBC counts.

The myelotoxicity and the relative biological effectiveness (RBE) for alpha-particles were studied in both tumor- and non-tumor bearing mice (*138*). For determining the RBE on tumors, growth inhibition (GI) after irradiation was studied with subcutaneous xenografts of the human ovarian cancer cell line NIH:OVCAR-3 implanted in nude mice. The animals received an intravenous injection of ^{211}At-labeled monoclonal antibody MX35 F(ab')$_2$ at different levels of radioactivity (0.33, 0.65, and 0.90 MBq). Control mice received unlabeled MX35 F(ab')$_2$ only. External irradiation of the tumors was performed with ^{60}Co. The RBE was found to be 4.8 ± 0.7.

For determining the RBE on non-tumor bearing mice, animals were injected intraperitoneally or intravenously with ^{211}At- or ^{99m}Tc-mAbs. Myelotoxicity was measured as suppression of white blood cell (WBC) counts. Whole-body retention was measured with a NaI(Tl)-well detector and the absorbed dose to the bone marrow was calculated, for alpha-particles, electrons, and gammas. The biodistribution of ^{211}At- and ^{99m}Tc-mAbs was also measured. A nadir of the WBC counts at 4–7 days after injection was observed. A mean value for the bone marrow-to-blood ratio of 0.58 was observed for the ^{211}At-mAbs. The *in vivo* RBE for alpha-particles was 3.4 ± 0.6 in relation to electrons from ^{99m}Tc and 5.0 ± 0.9 in relation to external ^{60}Co irradiation.

Clinical studies

In 1954, a study on the accumulation of ^{211}At in the thyroid gland in patients suffering from various disorders of that organ was reported (*229*). In 1990, at the Carl Gustav Carus University Hospital in Dresden, Germany, Doberenz and co-workers injected 200 MBq ^{211}At-labeled human serum albumin microspheres into the lingual artery of a patient with incurable recurrent carcinoma of the tongue. Complete tumor necrosis was achieved in the region supplied by the lingual artery, the necrosis eventually spread to the entire tongue and the tumor reappeared in the palate. Excluding a slight depression of thyroid function, clinical follow-up and paraclinical observation did not show any adverse reactions or side effects that could be related to ^{211}At microspheres. (*230*).

The first targeted radiotherapeutic labeled with ^{211}At, evaluated as part of a clinical trial, was initiated in the late '90s at Duke University using ^{211}At-chimeric 81C6 antibody. The ^{211}At-labeled antibody was administered into the surgically created tumor resection cavity of patients with recurrent malignant brain tumors (*231*). Seventeen patients have been treated with single does of 10 mg ch81C6 labeled with escalating activities of ^{211}At, ranging from 74 to 370 MBq. Leakage of ^{211}At from the cavity was determined by imaging and serial blood counting. An average of 96% of all ^{211}At decays occurred within the cavity. The activity in the blood pool was 0.032 and 0.26 percent of the injected activity at 2 and 24 h, respectively. The estimated absorbed dose to the tumor cavity margin was 2986 Gy; the absorbed dose to normal brain, liver, spleen and bone marrow was less than 10 Gy. Median survival in these recurrent brain cancer patients was increased from the historically expected 25 to 30 weeks to 54 weeks. As of the last review of these data in 2004, two patients with recurrent glioblastoma were alive 151 and 153 weeks after ^{211}At-labeled chimeric 81C6 therapy (*232*). More recently, a paper summarizing clinical experience with ^{211}At-ch81C6 has been published (*15*).

In February 2005, a phase I trial of ^{211}At-MX35 F(ab')$_2$ in patients with ovarian carcinoma was started at the Göteborg University in Göteborg, Sweden for study of toxicity at escalating activities and pharmacokinetics for absorbed dose assessment. To-date, six (of a planned total of 9) have been treated (*17*). All patients had undergone a second-line chemotherapy with good remission. At laparoscopy, two days before the therapy, a peritoneal catheter was inserted and the peritoneal cavity was inspected. Peritoneal scintigraphy was made with 2L of ^{99m}Tc LyoMAA to study the fluid distribution in peritoneum. ~500 MBq ^{211}At was labeled to the antibody. 50 MBq (3 patients) or 100 MBq (2 patients) in 2L was infused via the peritoneal catheter. Gamma camera whole body scan was made at 1, 6, 12 and 24h (occasionally up to 48h) and SPECT at 3 - 6h. Samples of blood, urine and peritoneal fluid were collected at 1 - 48h. The specific activity of labeled MX35 F(ab´)$_2$ was ~150 MBq/mg, the radiochemical purity and the immunoreactive fraction ~97 %. The 24h and 48h urinary excretion of ^{211}At was (mean values; physical decay corrected) 2% and 7%, respectively. Uptake in thyroid at 24h was 1%. No other organ uptake was detected. Absorbed doses were 0.08 mGy/MBq to bone marrow, 15 mGy/MBq to unblocked thyroid, and 8 mGy/MBq to the peritoneal surface. No adverse effects were observed.

Bismuth-212 (^{212}Bi)

Radionuclide properties

Bismuth-212 is a naturally occurring radionuclide and is part of the Thorium-232 ($t_{1/2}$ = 1.4 x 10^{10} years) decay chain. ^{212}Bi has a half life of 1.01 hrs, and decays through two branches (*233*). Approximately 64% of the decays occur by beta emission (E_{max} = 2.3 MeV) to ^{212}Po which subsequently decays via an 8.78 MeV alpha particle. The remaining fraction decays via alpha particle emission (E = 6.08 MeV) to ^{208}Tl ($t_{1/2}$ = 3.1 min) which is followed by the emission of a beta particle. Both branches of the decay scheme terminate with ^{208}Pb (stable). Because of the multiple beta emissions that occur with the ^{212}Bi decay, crossfire may result thus irradiating unlabeled cells or cells located a short distance from the decay site. In addition, ^{208}Tl, a daughter of ^{212}Bi with a 3-min half-life, emits an energetic gamma (E = 2.6 MeV, 99.8%), which requires heavy generator shielding. Bismuth-212 can be produced in clinical quantities from a ^{224}Ra generator ($t_{1/2}$ = 3.66 days) (*234*). This generator was subsequently modified by employing ^{224}Ra as a source for ^{212}Pb ($t_{1/2}$ = 10.6 h) (*235*). By sorbing the ^{212}Pb on a lead selective chromatographic medium, high purity ^{212}Bi can be generated as the daughter product of ^{212}Pb. Despite the short half life of ^{212}Bi, multiple milkings of this generator may be used to deliver therapeutic doses over several fractions.

Pre-clinical studies

One of the earliest investigations of ^{212}Bi in radioimmunotherapy employed a monoclonal antibody, anti-Tac, directed against the human interleukin 2 (IL-2) receptor (*236*). Antibody specific activities of 37 to 1480 kBq/μg were achieved. Targeting of the ^{212}Bi-labeled antibody to the IL-2 positive adult T-cell leukemia cells was demonstrated, *in vitro*. Activity levels of 18.5 kBq/ml, corresponding to 12 cGy to 10^5 cells in 1 ml volume, reduced the proliferative capacity of the target cells by more than 98%; cytotoxicity was diminished by blocking using excess unlabeled specific antibody or when an isotype-matched irrelevant antibody was used instead of the specific antibody. Macklis et al. subsequently demonstrated that intraperitoneal (i.p.) injection of ^{212}Bi-labeled IgM antibody was, successful in eliminating ascities and curing mice of their disease (*2*). Mice, previously inoculated i.p. with Thy 1.2+ EL-4 tumor cells were administered ^{212}Bi labeled to a specific and non-specific antibody. Gamma camera imaging demonstrated high splenic uptake approximately 2 hrs post-injection. Administration of the antibody via the i.p route limited the amount of activity in the blood to less than 8% at the same time point. Evaluation of therapeutic efficacy demonstrated that control animals died within 20 days, those treated with a non-specific antibody died within 33 days, and approximately 80% of those treated with anti-Thy 1.2 IgM were cured at a dose level of 5.55-8.51 MBq (150-230 μCi). However, at high dose levels (14.8 MBq), one of two animals died due to acute toxicity. Biodistribution studies in the same model system showed a significant accumulation of ^{212}Bi in the kidneys two hours after i.p. injection. Approximately 30% of the remaining activity at that time point was associated with the kidneys and bladder, thus indicating the need for stable chelates. Accordingly, considerable effort has been directed toward the development of ^{212}Bi chelation complexes that are stable *in vivo*. These studies identified the *trans*-cyclohexyldiethylenetriaminepentaacetic acid (CHXA-DTPA) chelate as providing the most stable, antibody-radiometal conjugate *in vivo*. (*237-242*).

Using this chelate, Huneke, *et al.* (*243*) assessed the specificity, toxicity and efficacy of ^{212}Bi-mediated radioimmunotherapy, in vivo, using a virally (Rauscher leukemia virus) induced

murine erythroleukemia animal model. Administration of 5.55 MBq ^{213}Bi-labeled specific antibody yielded a median survival approximately twice that of untreated controls (118 days *versus* 63 d; $p<0.01$). Since the virus was not eliminated in these studies, all mice eventually succumbed to the virally-induced leukemia. Hartmann *et al.* (*244*) evaluated the use of ^{212}Bi conjugated to humanized anti-Tac monoclonal antibody. The antibody was administered via the i.p and i.v routes three days after nude mice were inoculated with tumor cells. For the i.p administration, doses of 5.55-7.4 MBq prevented tumor occurrence in 75% of the animals. In animals injected via the i.v route, tumor prevention following s.c. tumor inoculation occurred in only 30% of the mice. In addition, the authors also evaluated the efficacy of treating large tumors. Doses of up to 7.4 MBq failed to induce tumor regression. Closer examination revealed that only 5-6% of the injected activity per gram was present in the tumor at 2 hrs post-injection (approximately 2 half lives). Thus, the lack of a response was not surprising. Furthermore, marrow suppression was observed at activities of greater than 7.4 MBq. Bisumth-212 has been studied by Rotmensch et al (*245*) for treating ovarian cancer. The biodistribution and toxicity of ^{212}Bi oxychloride was evaluated in rabbits and efficacy was studied in mice. For toxicity studies, 3 groups of rabbits were injected with graduated doses of ^{212}Bi, imaged and sacrificed at 0.5, 1 and 3 hours post-injection. Imaging studies showed that ^{212}Bi was uniformly distributed throughout the peritoneal cavity. After three hours, 76-84% of the available activity remained in the peritoneal cavity. Most of the remaining activity was in the carcass with a small amount in the blood, bone marrow, GI tract and other organs. Up to 2.22 GBq (60 mCi) of activity was well-tolerated in rabbits with only transient thrombocytopenia and leukopenia. All counts recovered within one week after reaching their nadir. Doses of greater than 2.96 GBq were fatal. For an administration of 1.85 GBq, the authors estimated the dose to the peritoneal fluid as 4873 cGy with the highest normal tissue doses to the GI tract, kidneys and ovaries (approximately 50 cGy). The dose estimated to marrow (2.4 cGy) did not correlate with observed toxicity indicating that microscopic evaluation of the activity distribution in marrow may be required. In the evaluation of therapeutic efficacy, 3.33 MBq of ^{212}Bi in tumor-bearing mice produced a median survival of 82 days compared to 20 days in the control group. Up to 40% of the mice were cured of disease. The highest normal tissue doses were estimated to the kidneys and GI tract. Based on the results of the work cited above, it appears that ^{212}Bi would be advantageous for treating small, micrometastatic disease confined to a specific compartment.

Macklis et al (*246*) evaluated the hematoxicity of bismuth produced by low level exposure. Results obtained, *in vivo*, indicated that ^{212}Bi could induce hematosuppression thus making this radionuclide a candidate for preparation of patients for bone marrow transplantation.

Hassfjell et al. (*247,248*) considered the use of ^{212}Bi DOTMP for the treatment of bone metastases. While beta-particle emitters have been used for this treatment, alpha particles offer a theoretical advantage in that their short range would treat tumor cells while limiting the dose to bone marrow. In studies with mice injected through the tail vein, they reported that ^{212}Bi DOTMP is rapidly taken up in the bone matrix with a fast clearance from blood and other organs. The maximum uptake of 26% ID/g was noted in the femur at 15 min post-injection. In addition, the complex was shown to be stable with a significantly smaller quantity of activity taken up by the kidneys.

Due to the 1-h half-life of ^{212}Bi, the majority of studies with this alpha-particle emitter have been in situations that allow rapid targeting of the ^{212}Bi-labeled agent. To increase the targeting potential to less easily accessible targets, the 10.6 h half-life parent, ^{212}Pb, has been examined as an *in vivo* generator for ^{212}Bi delivery. In this approach, the ^{212}Pb is conjugated to the targeting agent. Miao et al. (*249*) examined this strategy for delivering ^{212}Bi to melanoma, a highly radioresistant tumor. The melanoma targeting peptide, 1,4,7,10-tetraazacyclodecane-1,4,7,10-tetraacetic acid (DOTA)-Re(Arg^{11})CCMSH, a melanotropin analogue, was radiolabeled with ^{212}Pb. Biodistribution and therapy performed in the B16/F1 melanoma-bearing C57 mouse flank tumor model exhibited rapid tumor uptake and extended retention of the labeled peptide, coupled with rapid whole body disappearance. Radiation dose delivered to the tumor was estimated to be 1.65cGy/kBq (61 rad/μCi) ^{212}Pb administered; the estimated absorbed dose to the kidneys was 0.97 cGy/kBq ^{212}Pb administered. ^{212}Pb decays to ^{212}Bi by beta emission (average energy of 101 keV). The dose calculations accounted for cross-organ beta dose from ^{212}Pb using a dosimetry model of the mouse (*250*); alpha energy from ^{212}Bi decay was assumed to be locally deposited. Treatment of melanoma-bearing mice with 1.85, 3.70, and 7.40 MBq of ^{212}Pb[DOTA]-Re(Arg^{11})CCMSH extended their mean survival to 22, 28, and 49.8 days, respectively, compared with the14.6-day mean survival of the placebo control group. Forty-five percent of the mice receiving 7.4 MBq doses survived the study disease-free. Treatment of B16/F1 murine melanoma-bearing mice with ^{212}Pb[DOTA]-Re(Arg^{11})CCMSH significantly decreased tumor growth rates resulting in extended mean survival times, and in many cases, complete remission of disease.

In summary, animal experiments with ^{212}Bi have yielded several important results. First, stable chelates are needed to ensure minimum uptake by the kidneys and other organs. Second, ^{212}Bi appears suitable for the treatment of micrometastatic disease such as ovarian cancer or bony metastases. Bismuth-212 is limited in the treatment of larger tumors due to its short half life and range. Finally, as in other forms of radioimmunotherapy, hematotoxicity may be the limiting toxicity. Because of the high energy gammas associated with ^{212}Bi decay, a large volume of bone marrow may be irradiated particularly in regional therapy situations. Further, studies are needed to assess the biodistribution on the microscopic level to ascertain the dosimetric cause of observed toxicities.

Bismuth-213 (^{213}Bi)

Radionuclide properties

Bismuth-213 was the first alpha-particle emitting radionuclide to be used in a clinical trial of alpha-particle radioimmunotherapy (*13,251*). It was proposed as a cancer therapeutic by Geerlings, et al. (*14*) and developed for clinical implementation by the Scheinberg Lab at Memorial Sloan-Kettering Cancer Center. Bismuth-213 decays with a 45.6 min. half-life via a branched scheme that leads to the emission of two alpha particles, with energies of approximately 6 and 8 MeV and yields of 2 and 98%, respectively. Three beta particles are also emitted with energies of 444, 659, and 198 keV, having yields of 98, 2 and 100%, respectively. The last of these betas is emitted by ^{209}Pb which has a half-life of 3.25 h and decays to stable ^{209}Bi. Bismuth-213 also emits a gamma ray photon at an energy of 440 keV and a yield of 16.5%. This photon has been used to perform patient imaging and dosimetry (*252*). Importantly, ^{213}Bi decay does not lead to a significant emission of highly energetic (>1 to 2 MeV) photons and, therefore, the requirement for lead shielding associated with the use of this

isotope of bismuth is substantially reduced compared with the requirement associated with ^{212}Bi. The reduced requirement for shielding, the availability of a clinical generator system (*253*), and the development of rapid and stable conjugation methodologies (*254-256*) have been key factors in the relatively rapid clinical implementation of ^{213}Bi-labeled antibody therapy of leukemia and the widespread study of this radionuclide for therapy of other cancers (see summary below).

Pre-clinical studies

Using a lung metastatsis model with an antibody that targets normal lung vasculature, delivering up to 50% of the injected activity to the lungs, Kennel, et al (*19,257-259*), found that intravenous injection of 0.925 to 7.4 MBq (25 to 200 μCi) significantly extended the life span of treated animals over that of controls (up to 98 ±56 days vs 13.6 ± 1.8 days). Consistent with the non-specific targeting approach used in this model, necropsy and histologic evaluation of treated animals showed delayed lung fibrosis; all cured animals eventually succumbed to lung damage (*258*). The same model was also used to demonstrate that^{131}I, ^{90}Y and ^{211}At, although therapeutic, were generally not as optimal as ^{213}Bi. In the case of the beta emitters, ^{131}I and ^{90}Y, this was due to increased toxicity associated with the long range of the beta emitters (*18,260*). Astatine-211 was not as effective because of its lower dose-rate, relative to ^{213}Bi. Behr, et al, (*132*) examined ^{213}Bi- vs. ^{90}Y-labeled Fab targeting of liver metastases and demonstrated histologically confirmed cure in 95% of animals treated with the MTD activity level of 25.9 MBq ^{213}Bi-Fab in lysine pre-treated mice; in the same model, the cure rate following MTD (9.25 MBq) administration of ^{90}Y-Fab was 20%. IgG targeting was not examined in these studies and, due to rapid uptake of Fab in the kidneys, chronic renal toxicity was observed in treated mice that did not receive lysine protection. Other studies have also shown efficacy against metastases (*261-263*). These results obtained, *in vivo*, have also been supported by spheroid studies, *in vitro* (*264,265*). In contrast to the efficacy observed against metastases, targeting of sub-cutaneous tumors using single-chain variable region constructs and dimers thereof (*266*) or a DOTA-biotin pre-targeting approach (*267*) did not yield encouraging therapeutic results, either because a specific therapeutic effect was not demonstrated (scFv) or because of high renal toxicity (DOTA-biotin).

Locoregional targeting of tumor cells by administration of targeted ^{213}Bi into the intraperitoneal cavity has been examined by several investigators. Using an antibody, d9MAb, against a characteristic E-cadherin mutation found in diffuse-type gastric cancer, localization of ^{213}Bi to tumor cells exhibiting the mutation was observed in an IP tumor model (*268*). Median survival was prolonged by 62 days when 0.37 MBq ^{213}Bi-d9MAb were IP-administered 1 and 8 days after IP tumor inoculation (*269*). Cell kill experiments, *in vitro*, using this model system demonstrated that cell death was not due to a caspase 3-dependent pathway suggesting a non-apoptotic cell death mechanism (*270*). Using an IP xenograft model obtained by IP administration of colorectal carcinoma cells, Brechbiel and co-workers demonstrated a 23 and 39 day increase in median survival following IP administration of 18.5 and 27.8 MBq ^{213}Bi-Herceptin Ab, respectively, 3 days after tumor inoculation (*271*). The same group found dose-dependent delay in the growth of sub-cutaneously inoculated colorectal carcinoma cells following IP injection of ^{213}Bi-labeled HuCC49ΔCH2, a CH2-domain deleted construct of the humanized CC49 antibody (anti-TAG-72) (*272*). Efficacy of ^{213}Bi-labeled antibody has also been demonstrated in a B-cell lymphoma xenograft model. IP injection of 4.03 MBq ^{213}Bi-LL1 (anti-CD47) antibody 2 days after i.v. tumor inoculation led to apparent cure (182 days) in 6 of 9 treated mice (*273*).

In addition to the preclinical studies in melanoma (*274-276*) which have led to patient trials of ^{213}Bi-9.2.27 antibody, the group at the St. George Hospital in Kogarah, Australia has performed pre-clinical studies in ovarian (*277*), prostate (*262*), pancreatic (*278,279*), and breast cancer (*280*). Studies have been performed using four different ^{213}Bi labeled constructs: C595, an anti-mucin antibody, Herceptin, anti-HER2/neu antibody, BLCA-38, anti-prostate and bladder cancer antibody and PAI2, a human recombinant plasminogen activator inhibitor, type 2 (47 kD) that is reactive with membrane-bound urokinase plasminogen activator (uPA) (*262,280*) In ovarian cancer, the OVCAR-3 cell line was used to show concentration dependent cytotoxicity of ^{213}Bi-labeled PAI2 and C595 against monolayer and spheroid culture (*281*). In prostate cancer, targeting of three different human prostate cancer cell lines using a combination of ^{213}Bi-antibodies and ^{213}Bi-PAI2 gave D_0 values of 0.56, 0.63 and 1.0 MBq/ml for the cell lines PC-3, DU 145 and LNCaP-LN3, respectively (*282*). In a nude mouse xenograft model of prostate cancer, a single, 947 MBq/kg ip administration of ^{213}Bi-PAI2, given 3 days after subcutaneous inoculation with PC-3 tumor cells showed a 22 day delay in observable tumor formation, relative to untreated controls. Five equal administrations over 5 successive days starting at 3 days after inoculation for a total administered activity of 1421 MBq/kg resulted in complete control over the 13 week study period. The same administration protocol at 6, 12 and 18 days after tumor inoculation resulted in statistically significant growth inhibition relative to controls ($p = 0.008$, 0.03 and 0.02, respectively) (*283*). Bismuth-213-labeled PAI2 was also evaluated in a pre-vascularized subcutaneous model of pancreatic cancer. A single local injection of ~222MBq/kg 2 days post-cell inoculation completely inhibited tumor growth over 12 weeks. Tumor growth delays of 7 and 14 days were observed when 111 and 222 MBq/kg were administered, intraperitoneally, 2 days after tumor inoculation. High renal localization of ^{213}Bi-PAI2 was noted to be dose-limiting. In the same animal model, the anti-MUC1 antibody, C595, yielded similar results (*284*). Using a similar pre-vascularized model of breast cancer a single local injection of 0.925 MBq ^{213}Bi-PAI2 at 2-4 day after inoculation yielded complete growth inhibition in 23 of 40 treated mice. When the local injection was delayed to 7 and 14 days after inoculation, 2/8 and 1/8 mice showed complete growth inhibition; the remainder exhibited statistically significant growth delay relative to untreated mice. Intraperitoneal injection of 0.93, 1.85, 3.70 MBq ^{213}Bi-PAI2 at 2 days after inoculation yielded substantial growth inhibition that lasted approximately 35 days post-innoculation.

Efficacy of the anti-PSMA antibody J591 labeled with ^{213}Bi, has been examined in LNCaP cells grown in monolayer culture, as spheroids and in a xenograft nude mouse model, *in vivo* (*264,285*). An LD_{50} of 8.1 kBq/ml at a specific activity of 2.4 TBq/g was found for monolayer culture. The time course of spheroid volume reductions was found to be sensitive to the initial spheroid volume. J591 labeled with 0.9 MBq/ml ^{213}Bi resulted in a 3-log reduction in spheroid volume on day 33, relative to control, for spheroids with an initial diameter of 130 μm; 1.8 MBq/ml were required to achieve a similar response for spheroids with an initial diameter of 180 μm. Equivalent spheroid responses were observed after 12 Gy of acute external beam photon irradiation. Monte Carlo-based microdosimetric analyses of the ^{213}Bi decay distribution in individual spheroids of 130-μm diameter yielded an average α-particle dose of 3.7 Gy to the spheroids, resulting in a relative biological effectiveness factor of 3.2 relative to photon irradiation. At 2 days after intramuscular injection of LNCaP cells in matrigel, IV administration of 2.96 MBq in equally divided doses over 4 days led to a 21-day improvement in median survival relative to non-specific, labeled control Ab therapy.

Targeting of ^{213}Bi using the somatostatin analogue [DOTA^0,Tyr^3] octreotide (DOTATOC) against pancreatic cancer has also been examined in a rat model of pancreatic cancer. Tumor growth inhibition was observed in both small (0.75 mm^3) and large (1720 mm^3) volume tumors following IV administration of 12.6 and 22.2 MBq ^{212}Bi-DOTATOC, respectively. Nephrotoxicity was generally minimal. One out of 4 rats that received 22 MBq exhibited mild interstitial nephritis lesions. Rats receiving less than 13 MBq exhibitied nephritis lesions that were characterized as minimal; no significant changes in creatinine clearance were observed in any of the rats (*286*).

A three-step pre-targeting technique using a humanized anti-Tac antibody-streptavidin conjugate (HAT-SA) in which the HAT-SA is administered initially and allowed to target. This is followed by a clearing agent to remove HAT-SA that is not tumor-bound and then a ^{213}Bi-DOTA-biotin conjugate is administered to deliver the radioactivity to the previously targeted sites. Efficacy of this approach was evaluated in an immunodeficient murine model of human T-cell leukemia. Median survival was increased by 47.5 and 29.9 days following 9.25 MBq ^{213}Bi-DOTA-biotin administered according to a pre-targeting protocol in small and large tumor burden groups, respectively (*287*).

The use of ^{213}Bi labeled anti-CD45 or anti-T cell receptor αβ (TCRαβ) antibody as an alternative to total-body irradiation in the preparative regimen for nonmyeloablative allogeneic hematopoietic cell transplantation has been examined in a canine model (*288,289*). A greater than 30 week follow-up demonstrated that 51.8 to 77.7 MBq/kg ^{213}Bi-anti-CD45 or 74 to 100 MBq/kg ^{213}Bi-anti-TCRαβ resulted in stable engraftment of matched donor marrow. No signs of graft-versus-host disease or other toxicities were noted; mild and transient elevation of liver enzymes was observed in 4 of 15 dogs.

Song et al. investigated the efficacy of an antibody (7.16.4) against the rat variant of HER-2/neu, labeled with the alpha-particle emitter ^{213}Bi to treat widespread metastases in a rat/neu transgenic mouse model of metastatic mammary carcinoma (*290*). The model manifests wide-spread dissemination of tumor cells leading to osteolytic bone lesions and liver metastases, common sites of clinical metastases (*291*). The maximum tolerated dose was 4.44 MBq of ^{213}Bi-7.16.4. The kinetics of marrow suppression and subsequent recovery were determined. Three days after left cardiac ventricular injection of 10^5 rat HER-2/neu-expressing syngeneic tumor cells, neu-N mice were treated with (a) 4.44 MBq ^{213}Bi-7.16.4, (b) 3.33 MBq ^{213}Bi-7.16.4, (c) 4.44 MBq ^{213}Bi-Rituximab (unreactive control), and (d) unlabeled 7.16.4. Treatment with 4.44 MBq ^{213}Bi-7.16.4 increased median survival time to 41 days compared with 28 days for the untreated controls ($P < 0.0001$); corresponding median survival times for groups b, c, and d were 36 ($P < 0.001$), 31 ($P < 0.01$), and 33 ($P = 0.05$) days, respectively. Median survival relative to controls was not significantly improved in mice injected with 10-fold less cells or with multiple courses of treatment. Alpha-emitter ^{213}Bi-labeled monoclonal antibody targeting the HER-2/neu antigen was effective in treating early-stage HER-2/neu-expressing micrometastases. Analysis of the results suggested that further gains in efficacy may require higher specific activity constructs or target antigens that are more highly expressed on tumor cells.

Bismuth-213-labeled anti-microbial cell antibody has also been used as a possible therapeutic against microbial infections (*292*). Studies examining the mechanisms involved in microbial or fungal cell killing have suggested that efficacy is derived from a combination of radiation and immune/inflammatory effects associated with antibody-mediated delivery of the radiation (*293*).

Clinical studies

The initial phase I trial of ^{213}Bi-HuM195 in patients with acute or chronic myelogenous leukemia demonstrated safety, feasibility and anti-leukemic effect but no complete remissions. The large leukemic cell burden in relapsed/refractory leukemia patients (up to 10^{12} cells, yielding approximately 10^{16} target sites), the short range of alpha-particle emissions, and the specific activity of 1 ^{213}Bi atom per 2700 molecules precluded the 99% reduction in cell number required to achieve a tumor burden that would qualify as a complete remission in leukemia patients (*12,294*). Accordingly, this trial has been followed by an on-going Phase I/II trial in which patients are first treated with cytarabine, to reduce tumor burden, and then by escalating activity levels of ^{213}Bi-HuM195. No remissions were seen at the first two activity levels of 18.5 and 27.8 MBq/kg (0.5 and 0.75 mCi/kg). At the higher activity levels – 37 and 46.25 MBq/kg, complete remissions lasting up to 12 months in very high risk patients have been observed (*22,295*).

In addition to the on-going studies at Memorial Sloan-Kettering Cancer Center in New York, there are also two on-going trials in Europe. At the German Cancer Research Center in Heidelberg and at the University Hospital Duesseldorf, Germany, a Phase I trial investigating the safety and efficacy of ^{213}Bi-labeled anti-CD 20 (Rituximab) antibody in patients with relapsed or refractory Non Hodgkin's Lymphoma (NHL) is on-going. The most recent report on this study indicated that 9 patients had been treated in three dose groups with activities of 555 to 1591 MBq of antibody-conjugated ^{213}Bi (*296,297*).

At the University Hospitals in Basel, Switzerland, radiolabeled substance P, an 11-mer peptide that targets the neurokinin type-1 receptor, which is overexpressed in the majority of gliomas was used to deliver, into the tumor or tumor resection cavity ^{213}Bi (2 of 20 patients), ^{177}Lu (3 of 20) or ^{90}Y; with ^{213}Bi or ^{177}Lu being used to reduce the cross-fire in critically located tumors. The feasibility, biodistribution and early and long-term toxicity were assessed in this pilot study. In one of the two ^{213}Bi treated patients (progressive glioblastoma; 375 MBq administered) response assessment was difficult due to bulky residual tumor. In the second patient (low-grade oligodendroglioma; 825 MBq administered) resection of a mass lesion 33 months after alpha therapy disclosed radiation necrosis and absence of viable tumor cells and the patient is still alive 67 months after initial diagnosis (*298*).

The safety and efficacy of intralesional injection of ^{213}Bi -labeled 9.2.27 antibody in patients with metastatic melanoma has been investigated by Allen et al. (*299*), at the St. George Hospital in Kogarah, Australia. Sixteen patients were treated with escalating activity levels of 11.1 MBq, starting at 5.55 MBq. Escalation to 50 MBq did not result in toxicity; histology showed almost complete cell kill at 16.65 MBq and above with few viable cell clusters.

Actimium-225 (^{225}Ac)

Radionuclide properties

Actinium-225 can be obtained either from the natural decay of ^{233}U and its production of ^{229}Th or from the neutron transmutation of ^{226}Ra by successive n,b capture decay reactions *via* ^{227}Ac, ^{228}Th to ^{229}Th (*300-302*). Geerlings *et al.* (*14*) described an ^{225}Ac generator based on a design that adsorbs ^{229}Th oxide onto a titanium phosphate resin. Elution of this ^{229}Th cow yields a mixture of radionuclides: ^{225}Ac, ^{225}Ra, and ^{224}Ra; a subsequent downstream (Dowex 50 WX8) column was used to purify the ^{225}Ac by removing the other decay products. Boll and Mirzadeh *et al.* (*303*) have described the steps for isolating ^{225}Ac from the ^{229}Th at Oak Ridge National

Laboratory. Apostolidis *et al.* have described the method for separation and purification of ^{225}Ac from a ^{229}Th source that is currently employed at the Institute for Transuranium Elements (*304*). A liquid ^{229}Th/^{225}Ac generator has also been proposed by Khalkin *et al* (*305,306*). An alternate strategy to ^{225}Ac production employs proton irradiation of ^{226}Ra which can lead to ^{225}Ac *via* [p,2n] reactions (*300,302,307*) using a cyclotron. Recently, the feasibility of cyclotron produced ^{225}Ac was demonstrated and maximum yields reached with an incident proton energy of 16.8 MeV (*307*) using the ^{226}Ra(p,2n)^{225}Ac reaction. In this work, 0.0125 mg of ^{226}Ra yielded 77.7 kBq (0.0021 mCi) ^{225}Ac after irradiation of a 36 mm^2 target with a 10 μA proton current for 7 h. No significant differences were found in the radionuclidic purity of the cyclotron product when compared to ^{225}Ac produced *via* the ^{229}Th method (*304*).

There are six key (>0.05% yield) radionuclide daughters of ^{225}Ac that are produced in the cascade to stable ^{209}Bi (*5*). A single ^{225}Ac ($t_{1/2}$ = 10.0 d; 6 MeV α particle) decay yields net 4 alpha and 3 beta disintegrations, most of rather high energy and 2 gamma emissions of which the ^{213}Bi 440 keV γ emission has been used in imaging drug distribution (*252*). These daughters are ^{221}Fr ($t_{1/2}$ = 4.8 m; 6 MeV α particle and 218 keV γ emission), ^{217}At ($t_{1/2}$ = 32.3 ms; 7 MeV α particle), ^{213}Bi ($t_{1/2}$ = 45.6 m; 6 MeV α particle, 444 keV β$^-$ particle and 440 keV γ emission), ^{213}Po ($t_{1/2}$ = 4.2 μs; 8 MeV α particle), ^{209}Tl ($t_{1/2}$ = 2.2 m; 659 keV β$^-$ particle), ^{209}Pb ($t_{1/2}$ = 3.25 h; 198 keV β$^-$ particle) and ^{209}Bi (stable). Given the 10.0 d half-life of ^{225}Ac, the large alpha particle emission energies, and the favorable rapid decay chain to stable ^{209}Bi this radionuclide was recognized as a potential candidate for use in cancer therapy (*14*).

In order to take full advantage of the therapeutic potential of ^{225}Ac and the several radionuclidic progeny, an approach was taken which focused on i) stably chelating the ^{225}Ac for delivery *in vivo* to a target cell; ii) internalizing the ^{225}Ac-antibody construct into the target cell; iii) retaining the decay products within the target cell and harnessing their cytotoxic potential; and iv) reducing the loss of the daughters to non-target tissues and mitigating systemic radiotoxic events. This was called the ^{225}Ac nanogenerator system. Targeting agents such as internalizing IgGs transported the ^{225}Ac into the cell where decay daughters were retained if the drug was internalized. This approach proved extremely cytotoxic to the targeted cancer cells and limited the systemic toxicity to the host. The ^{225}Ac delivered to the cancer cell was effectively a therapeutic nanogenerator of multiple alpha particle emissions within the target cell (*4*).

Pre-clinical studies

One of the initial reports on the biodistribution and metabolism of actinium was performed with ^{227}Ac by Taylor, et al. (*308*) Taylor performed intraveneous injections of 18.5 kBq (500 nCi) of ^{227}Ac nitrate solution mixed with serum proteins from isologous rat serum, nitrate ion, 1% sodium citrate or 0.5% sodium diethylenetriaminepentaacetic acid (DTPA). Forty percent of the injected activity of ^{227}Ac-serum protein was excreted in 28 d, and the remainder cleared the rat with a $t_{1/2}$ of 700 d. DTPA, used as a rescue agent for ^{227}Ac contamination, was capable of effecting a 60% reduction in the body burden, but only if administered within 30 minutes of exposure.

The cytotoxicity *in vitro* of an [^{225}Ac]DTPA-antibody construct was reported by Kaspersen *et al.* using a murine IgG1 that targets the EGF receptor expressed on the human epidermoid A431 tumor cell line (*309*). More target cells were killed by the specific than the control radiolabeled antibody, however the DTPA chelate moiety was not able to stably bind the ^{225}Ac in these

experiments as demonstrated by the ^{225}Ac constructs being capable of killing target cells only slightly better than similarly labeled ^{213}Bi-antibodies.

In another study, Beyer *et al.* examined the influence of varying ethylenediamine-tetramethylenephosphonic acid (EDTMP) solution concentrations on the biodistribution of ^{225}Ac and radiolanthanides in tumor-bearing mice (*310*). [^{225}Ac]citrate control and [^{225}Ac]EDTMP solutions (up to 0.1 mM EDTMP) demonstrated high liver uptake (40 %ID/g).

Davis *et al.* examined the biodistribution, dosimetry and radiotoxicity of ^{225}Ac complexed with acetate, ethylenediaminetetraacetic acid (EDTA), 1,4,7,10,13-pentaazacyclopentanadecane-*N,N',N'',N''', N''''*-pentaacetic acid (PEPA), and the A" isomer of *N*-[(*R*)-2-amino-3-(4-nitrophenyl)propyl]-*trans*-(*S,S*-cyclohexane-1,2-diamine-*N,N,N',N'',N''*-pentaacetic acid (CHX-A"-DTPA) in female BALB/c mice (*311*). Data expressed as the %ID/g again demonstrated that the liver is the major site of ^{225}Ac localization for all four small molecule complexes studied. Liver accumulation increases according to the decreasing strength of the ^{225}Ac-complex: CHX-DTPA ~ PEPA > EDTA > acetate. The biodistribution of an antibody carrier molecule was examined in this study. The antibody 201B targets and binds to mouse lung endothelial thrombomodulin and was chemically coupled with CHX-A-DTPA to yield a DTPA-201B construct that was radiolabeled with ^{225}Ac. The [^{225}Ac]DTPA-201B construct efficiently targeted the lung but the ^{225}Ac had a very short tissue $t_{1/2}$ of 4-5 h as compared with the [^{125}I]201B construct with a $t_{1/2}$ of 4-5 d. The DTPA was unable to stably bind the ^{225}Ac at the site *in vivo*. At the 92 kBq dose level, the WBC, spleen and bone marrow were rated as having loss of cellular numbers, integrity, orientation, or structure. At the 185 kBq dose level the WBC, spleen, bone marrow, liver, GI tract, and kidney all were rated as having loss of cellular numbers, integrity, orientation, or structure and evidence of cellular necrosis.

Deal and co-workers prepared a series of ^{225}Ac-labeled chelate complexes and surveyed their biodistribution in normal BALB/c mice (*312*). One of the complexes was reported to exhibit improved *in vivo* stability relative to the others in the series examined. The chelates included EDTA, CHX-A-DTPA, PEPA, DOTA, HEHA, and acetate. 92.5 kBq of each complex (2500 nCi) in MES buffer at pH 6.2 was injected into normal female BALB/c mice *via* the tail vein. All of the complexes rapidly cleared the blood with < 2 %ID/g in 1 h. The order of most ^{225}Ac distributed into tissue to the least was acetate > EDTA > CHX-A"-DTPA ~ PEPA > DOTA > HEHA. The interest in the HEHA chelate led to the synthesis of the isothiocyanate derivative, the conjugation to three different antibodies, and radiolabeling of with ^{225}Ac by Chappell *et al.* (*313*). Serum stability testing of the [^{225}Ac]HEHA-IgG constructs demonstrated <50% stability after 48 h.

In the first reported radiotherapeutic study using ^{225}Ac, *in vivo*, Kennel *et al.* evaluated an [^{225}Ac]HEHA-201B antibody construct for vascular targeted therapy of lung tumors and performed biodistribution, dosimetry and therapeutic efficacy studies (*314*). These and other (*315*) therapeutic studies did not demonstrate a substantial survival advantage in treated mice because of the high systemic toxicity associated with the release of free ^{225}Ac using the HEHA chelate.

McDevitt *et al.* described the design and two-step synthesis of ^{225}Ac-DOTA-radioimmunopharmaceuticals and also the first practical application of ^{225}Ac in targeted drug therapy without accompanying systemic radiotoxicity (*4,21*).

To investigate the therapeutic efficacy *in vivo* of the generator construct, [^{225}Ac]DOTA-J591, McDevitt, *et al.* (*4*) utilized an intramuscular (i.m.) LNCaP tumor model in male nude mice. Male nude mice were treated on day 15 or 12 post-tumor implantation and received 7.2 kBq [^{225}Ac]DOTA-J591 in a single administration. These animals had significantly improved, 63 ($P < 0.006$) and 158 ($P < 0.0001$) day median survival for day 15 or 12 post-tumor implantation, respectively, compared to a 37 -day median survival for mice treated with unlabeled J591 antibody; 14 of the 39 treated animals exhibited prolonged survival. These mice survived at least 10 months and had no measureable PSA or evidence of tumor at the time of sacrifice (293 days). The therapeutic efficacy was dependent on antibody specificity, the administration of the ^{225}Ac-generator, and the treatment time after implantation. Similarly positive results were obtained in a disseminated human Daudi lymphoma cell mouse model. Mice receiving a single injection of [^{225}Ac]DOTA-B4 showed dose-related increases in median survival times of 165 (6.3 kBq), 137 (4.3 kBq), and 99 days (2.1 kBq), respectively. This dose response of [^{225}Ac]B4 was significant with $P = 0.05$. About 40% of mice treated at the highest dose were tumor-free at 300 days and the experiment concluded on day 310. Control mice receiving the irrelevant labeled antibody had median survival times from xenograft of 43 days (5.6 kBq) and 36 days (1.9 kBq). Mice receiving 0.003 mg unlabeled B4 per mouse had a median survival time of 57 days. The time of treatment from tumor innoculation was found to be less relevant in this model, compared to the prostate cancer model.

Borchardt *et al.* explored i.p. radioimmunotherapy in a mouse model of human ovarian cancer using ^{225}Ac-DOTA-trastuzumab, an anti-HER-2/neu antibody (*316*). Therapy, initiated 9 days after tumor seeding, yielded median survival of 52-126 days with [^{225}Ac]DOTA-trastuzumab at various doses and schedules and 48-64 days for [^{225}Ac]DOTA-labeled control IgG. Groups of untreated control mice and those administered native trastuzumab had median survivals of 33 and 44 days, respectively. . Deaths from radiotoxicity occurred with only the highest activity levels administered, the other dose levels were safe. It was concluded that i.p. administration with an internalizing [^{225}Ac]DOTA-labeled anti-HER2/neu antibody could significantly extend survival in a nude mouse model of human ovarian cancer at levels that produce no apparent gross toxicity.

Miederer *et al.* evaluated the pharmacokinetics, dosimetry and toxicity of [^{225}Ac]DOTA-HuM195 (anti-CD33) in disease-free (no CD33 sites) Cynomolgus monkeys (*317*). The blood half-life of [^{225}Ac]DOTA-HuM195 was 12 days and 45% of generated ^{213}Bi daughters were cleared from the blood. Monkey anti-human antibody (MAHA) production was not detected. About 28 kBq/kg of ^{225}Ac caused no toxicity at 6 months, whereas a cumulative dose of about 377 kBq/kg caused severe toxicity. Histopathological evaluation revealed mainly renal tubular damage associated with interstitial fibrosis. Multiple doses of intrathecally administered ^{225}Ac conjugated to an antibody that specifically binds to ganglioside GD2 for neuroblastoma targeting in tumor-free Cynomolgus monkeys did not show any signs of toxicity based on blood chemistry, CBC or clinical examination. Therapeutic efficacy of this labeled antibody was examined in a nude rat xenograft model of meningeal carcinomatosis. In an extremely aggressive nude rat xenograft model of meningeal carcinomatosis, [^{225}Ac]DOTA-3F8 treatment i.t. improved survival time two-fold ($p = 0.01$). Increasing the construct specific activity to > 1 MBq/mg improved the therapeutic efficay relative to lower specific activity preparations (*318*).

The targeted deletion of T-cell clones was examined by Yuan *et al.* using ^{225}Ac-MHC tetramers (*319*). Major histocompatibility complex (MHC) tetramers are multimeric complexes capable of

binding to specific CD8 T-cell clones. These molecules were conjugated to ^{225}Ac using a streptavidin platform to create an agent for CD8 T-cell clonal deletion. The ^{225}Ac-MHC tetramers specifically bound to, killed, and reduced the function of their cognate CD8 T cells while leaving the nonspecific control CD8 T-cell populations unharmed. Biotinylated DOTA was prepared and labeled with ^{225}Ac in high yield (≥ 96%). The ^{225}Ac-LMP1 tetramers (which confer T-cell specificity) effectively killed the targeted LMP1 CD8+ T-cell clones at small doses *in vitro* (ED_{50} = 0.185-0.296 kBq/mL (5 - 8 nCi/mL) or 0.001-0.0016 mg/mL); irrelevant tetramers exhibited much less toxicity. In a murine system, specific cell killing by ^{225}Ac-LLO91-99 tetramers was also demonstrated. LLO91-99 peptide–specific CD8+ T cells were effectively killed after incubation with ^{225}Ac-LLO91-99 tetramers. These results demonstrate that ^{225}Ac-labeled tetramers can selectively delete both numbers and function of specific cytotoxic T lymphocytes (CTLs) with high specificity and induce little cytotoxicity within the other CD8+ T-cell populations.

Ballangrud *et al.* investigated the efficacy of [^{225}Ac]DOTA-trastuzumab against breast cancer spheroids with different HER2/*neu* expression levels (*320*). The breast carcinoma cell lines MCF7, MDA-MB-361, and BT-474 with relative HER2/*neu* expression (by flow cytometry) of 1:4:18 were used. Spheroids of these cell lines were incubated with different concentrations of [^{225}Ac]DOTA-trastuzumab, and spheroid growth was measured by light microscopy over a 50-day period. The activity concentration required to yield a 50% reduction in spheroid volume at day 35 was 18.1, 1.9, and 0.6 kBq/mL (490, 52, 14 nCi/mL) for MCF7, MDA, and BT-474 spheroids, respectively. The radiosensitivity of these three cell lines evaluated as spheroids was described as the activity concentration required to reduce the treated-to-untreated spheroid volume ratio to 0.37, denoted DVR_{37}. The external beam radiosensitivity for spheroids of all three cell lines was found to be 2 Gy. After α-particle irradiation a DVR_{37} of 1.5, 3.0, and 2.0 kBq/mL was determined for MCF7, MDA-MB-361, and BT-474, respectively.

Novel liposomal carriers, multivesicular liposomes (MUVELs), were designed and constructed to enhance the retention of the α-particle emitting daughters of ^{225}Ac by Sofou *et al.* in targeting applications (*321-324*). PEGylated MUVELs yielded 98% ^{225}Ac retention, and 18% retention of the last daughter ^{213}Bi for 30 days. MUVELs were then conjugated to an anti-HER2/neu antibody, trastuzumab, and exhibited strong binding to and significant internalization (83%) by ovarian carcinoma SKOV3 cells. With the i.p. administration of ^{225}Ac-containing MUVELs to animals with disseminated i.p. tumors, significant tumor uptake of ^{225}Ac and its daughters was detected.

The efficacy of ^{225}Ac in peptide receptor radionuclide therapy was examined by Miederer, et al. using the somatastatin analogue, 1,4,7,10-tetra-azacylododecane N,N',N'',N'''-J-tetraacetic acid-Tyr(3)-octreotide (DOTATOC) (*325*). Activities up to 20 kBq had no significant toxic effects in mice; at 30 kBq renal tubular necrosis was observed. Actinium-225-DOTATOC over 12-20kBq reduced the growth of neuroendocrine tumors and showed improved efficacy compared with ^{177}Lu-DOTATOC.

Even with stable chelation of ^{225}Ac to internalizing antibodies, a significant release of alpha-emitting daughters may be expected if targeting and internalization are not rapid. Further efforts to understand and control the progeny of ^{225}Ac have been described by Jaggi *et al.* (*326*). The results indicate that metal chelation, diuresis with furosemide or CTZ, and competitive metal blockade may be considered as adjuvant therapies to modify the potential nephrotoxicity of ^{225}Ac daughters.

The mechanism of radiation nephropathy resulting from targeted radionuclide therapies is poorly understood and was examined by chronologically following the kidneys of Balb/c mice administered 12.95 kBq of [^{225}Ac]DOTA-HuM195 (*327*). These findings suggest that internally delivered alpha particle radiation-induced loss of tubular epithelial cells triggers a chain of adaptive changes that result in progressive morphological damage accompanied by a loss of renal function. In an effort to ameliorate alpha-particle radiation-induced renal toxicity Jaggi *et al* investigated captopril (ACE inhibitor), L-158,809 (Angiotensin II receptor-1 blocker, spironolactone (aldosterone receptor antagonist) or a placebo control. Low-dose spironolactone, and angiotensin receptor-1 blockade to a lesser extent, were found to offer renal protection in a mouse model of internal alpha particle irradiation (*328*).

In order to study the pharmacokinetics of an individual daughter nuclide, ^{221}Fr, the cyclotron production of ^{132}Cs from a natural xenon gas target was undertaken by Finn *et al.* (*329*). In order to determine whether ^{132}Cs is biochemically analogous to ^{221}Fr, a source of ^{221}Fr was developed and comparative biodistribution studies of saline solutions were performed for comparison. The studies showed that ^{132}Cs is not biochemically analogous to ^{221}Fr in mice.

In anticipation of the on-going effort to model the dosimetry of ^{225}Ac and its daughters, Hamacher *et al.* developed a schema for estimating absorbed dose to organs following the administration of radionuclides with multiple unstable daughters (*330*). Such calculations are complicated by the potential differential biological distribution of each of the progeny. The number of decays or cumulated activity of a daughter radionuclide present in a particular tissue is estimated using a probability matrix which describes the likelihood of daughter decay in a particular tissue as a function of the decay site of the parent. An example of three initial compartments is provided to illustrate the use of this formalism.

Clinical studies

Recently, the first patient was treated with [^{225}Ac]DOTA-HuM195 in a Phase I clinical trial at Memorial Sloan-Kettering Cancer Center. The patient presented with relapsed secondary acute myelogenous leukemia (AML). A dose of 1.18 MBq (0.032 mCi) of ^{225}Ac (18.5 kBq/kg) on 0.9 mg HuM195 (0.015 mg/kg) was prepared and administered (*22*). No significant toxicity has been observed

Radium-223 (^{223}Ra)

Radionuclide properties

Radium-223 is a short-lived (half-life = 11.4 d) alpha emitter which decays through a cascade of short-lived alpha- and beta-emitting progeny with the emission of about 28 MeV of energy per starting atom through complete decay of the progeny to stable lead. On average, four alpha particles and two beta particles are emitted. The primary alpha particles emitted by ^{223}Ra are 5.61 and 5.72 MeV; for ^{219}Rn are 6.82 MeV; for ^{215}Po are 7.39 Mev, and for ^{211}Bi are 6.62 MeV. The principal gamma lines for ^{223}Ra in equilibrium with its daughters are at 154 keV, 270 keV, 351 keV, and 405 keV, and ^{223}Ra may be imaged *in vivo* with a gamma camera and low-energy collimator.

The parent (^{227}Ac) of ^{223}Ra can be produced efficiently in thermal or fast reactors by neutron irradiation of common radium (^{226}Ra) according to the reaction:

$^{226}Ra(n,\gamma)^{227}Ra(T_{1/2} = 42\ m) \rightarrow \beta^- + {}^{227}Ac(T_{1/2} = 21.7\ y)$, and (a)

$^{227}Ac \rightarrow \beta^- + {}^{227}Th(T_{1/2} = 18.7\ d) \rightarrow \alpha + {}^{223}Ra(T_{1/2} = 11.4\ d)$ (b)

After irradiation, the ^{227}Ac may be radiochemically separated from the target irradiation product mixture. Actinium-227 can then be purified to remove silica solids, actinide contaminants, and elemental iron. The ^{227}Ac in equilibrium with decay products may then be transferred to an anion exchange column for elution with 0.35 M nitric acid. The ^{227}Th remains alone on the column. Actinium-227 and ^{223}Ra may be recycled. Ten days later, the anion exchange column may be eluted again with 0.35 M nitric acid to obtain pure ^{223}Ra. The resulting solution may then be boiled down with hydrochloric acid to form the final product ($^{223}RaCl_2$).

Pre-clinical studies

Radium is an alkaline earth element and ^{226}Ra is among the most-studied elements in terms of its biological behavior and radiation effects in the body. Biological data on the pharmacokinetics of radium (chloride form) in animals and human are available from literature reviews (*331*) of radium dial-painters (between 1908 and 1925), human ^{226}Ra injection and ingestion studies, human use of ^{224}Ra for treating ankylosing spondylitis and other diseases, and from numerous laboratory experiments on dogs, rats, mice, and other species.

Radium in circulation deposits on bone surfaces, recycles back into blood, and is redeposited again on bone surfaces. The International Commission on Radiological Protection (ICRP) Task Group on Alkaline Earth Metabolism in Adult Man proposed an early compartmental model for radium (*332*). Biokinetic models of radium recycling were first proposed by Johnson and Myers (*333*) and later by additional investigators (*334-337*). Committee 2 of the ICRP updated the ICRP-20 radium model to include systemic recycling and age-dependent factors (*332*). In the ICRP-67 model, bone was divided into cortical and trabecular components, each of which was further divided into bone surface and bone volume. These models dealt primarily with the long-term uptake, retention, exchange, and excretion of ^{226}Ra (half life = 1600 years) in humans, and were applied for setting radiation protection standards for radiation protection. Although radium deposits initially on bone surfaces, over time it becomes part of bone volume. Radium-223 is mainly a surface seeker in bone because it decays long before exchange processes among the bone volume compartments can take place. Although some information is available on the uptake, retention, and clearance of ^{223}Ra in humans, the radium recycling models do not adequately address the short term biokinetics in the soft tissues.

Radium-223 generally mimics the biokinetic behavior of calcium, strontium, and barium. Accordingly, ^{223}Ra circulates in blood and is present in all soft tissues in small amounts, as with calcium, strontium, and barium. The ICRP Task Group on Alkaline Earth Metabolism in Adult Man (*332*) assumed that all short-lived decay products of radium remain with the parent. Follow-up studies by several investigators confirm that in general, the daughter products decay at the same location of ^{223}Ra decay (*125*).

Radium-223 shows no preferential uptake in any organ or soft tissue other than the large intestines, which is transitory and part of the excretion pathway. Clearance half-times from muscle, the lungs, gastrointestinal tract and other soft tissues are relatively short (7 to 12 hours). Radium-223 clears from the liver, kidneys, and spleen with half times of about 58 hours, 75 hours, and 92 hours, respectively. Only a small fraction (2 to 3 percent) of systemic ^{223}Ra clears through the kidneys into the urinary tract. The remainder clears by secretion through the large

intestines directly into the bowel, and less than 1 percent clears the liver through the biliary excretion pathway.

Durbin et al. (*338*) showed that the primary effects of injected ^{223}Ra in rats were due to cell depletion (inhibition of skeletal growth, avascular red marrow, reduction in cartilage cells and osteocytes, and reduced blood counts). At high doses (greater than 185 kBq/kg body weight, or about 5 microcuries/ kg body weight), animal death was attributed to hemorrhage. Acute effects were loss of body weight and reduction in organ weights, with hemorrhagic areas in the lymph nodes, gastrointestinal tract, stomach, and lungs. The effects on kidneys included mild, transient tubular degeneration and atrophic glomeruli not correlated with increasing dose, which quickly returned to normal at times beyond 200 days. Testicular responses to ^{223}Ra showed that it was 5.4 times more lethal to spermatogonial cells than acute external x-rays (*125*).

Henriksen et al. (*339,340*) studied the effects of ^{223}Ra in 19 Han rnu:rnu nude rats to determine therapeutic efficacy in a bone metastis model. They administered about 60 kBq/kg to 5 rats and 110 kBq/kg to 14 rats. They found that ^{223}Ra exhibited a substantial anti-tumor effect at administered activities that were well-tolerated by red marrow, and without significan bone loss (*339*). In a follow-up study, Henriksen et al. studied the comparative biodistributions of ^{89}Sr and ^{223}Ra in five female BALB/C mice (*340*). Although both ^{89}Sr and ^{223}Ra selectively concentrated on bone surfaces with relatively little uptake in the soft-tissue organs, the skeletal uptake of ^{223}Ra was greater than that for ^{89}Sr. Soft-tissue ^{223}Ra activity cleared quickly. Daughter products of ^{223}Ra remained with the parent on bone surfaces, with less than 2% translocating to other parts of the body. Calculations of dose to bone marrow showed a sparing of marrow by the short-range alpha particles compared to high-energy ^{89}Sr beta particles, which more uniformly irradiated the marrow cavities.

The uptake, retention, and clearance of ^{223}Ra were studied in two beagle dogs at the Radium Hospital in Oslo, Norway (*178*). Investigators found that ^{223}Ra cleared circulating blood by direct excretion into the intestines, with activity accumulating in bowel contents (rather than by clearing from liver through bile into the small intestines.)

Fisher and Sgouros (*341*) described methods for calculating radiation doses to tissues and organ from systemically administered ^{223}Ra. For a sphere with large radius and assuming electronic equilibrium, progeny equilibrium, and unit tissue density, the absorbed dose constant for ^{223}Ra and daughters is 163 mGy mBq^{-1} (600 rad mCi^{-1}). Alpha-emission contributes about 93 percent of the total radiation absorbed dose.

Clinical studies

More than 200 patients have been treated with ^{223}Ra-chloride (Alpharadin, Algeta ASA, Oslo, Norway), in several European countries. Radium-223 has been approved for investigational use in the U.S. As noted above, the principal characteristics of this radionuclide are high skeletal uptake with long-term retention, minimal uptake in normal organs and other soft tissues, and clearance via the gastro-intestinal tract.

Clinical investigations in humans using ^{223}Ra for treating prostate and breast cancer metastases (*342,343*) confirmed that intravenously administered $RaCl_2$ clears quickly from circulating blood via the intestinal route and not by urinary excretion with a half-time of 3 to 6 minutes (about 94 percent), with a longer-term fraction due to recycling remaining in blood with a half-time of about 9 hours (6 percent). After ^{223}Ra for therapy of painful skeletal metastases in prostate and

breast cancer patients, a strong and consistent, activity-dependent, reduction in alkaline phosphatase levels occurred, showing that the regions mostly benefiting from treatment included the regions with elevated bone metabolism from developing metastases (*342*). Quality of life was determined compared to baseline at weeks 1, 4, and 8 after infusion, and pain relief was determined for all time points. Myelosuppression was minimal and thrombocytopenia was not dose-limiting. Levels below 200 kBq/kg (5.4 μCi/kg) in adult cancer patients appear to be well-tolerated (*342,343*). Patients receiving ^{223}Ra showed reduced prostate-specific antigen relative to baseline.

In a follow-on phase I study involving six patients with advanced prostate cancer, the feasibility of repeated lower-dose ^{223}Ra administrations was evaluated (*178*). Patients received up to 250 kBq/kg either as two fractions of 125 kBq/kg each, separated by six weeks, or as five fractions of 50 kBq/kg each. Repeated infusions of ^{223}Ra were well-tolerated, and no added toxicity related to repeated injections was observed. Overall hematological toxicity was lower for the patients receiving fractionated therapy. The spacing of fractionated therapy allows blood cell counts to normalize between injections (*178*).

In a phase II randomized clinical trial, late-stage prostate cancer patients received either external beam radiation plus saline injections, or external beam radiation plus four fractions of ^{223}Ra of 50 kBq/kg, at 4-week intervals, for a total of 200 kBq/kg (*344*). Adjuvant treatment with ^{223}Ra resulted in decreased biomarker for metastatic disease (bone alkaline phosphatase relative to baseline) compared to patients receiving the placebo saline injections. Skeletal regions with elevated bone metabolism were most likely to benefit from ^{223}Ra administration. Fifteen of 31 patients also exhibited a decrease (more than 50% from baseline) in prostate-specific antigen compared to only five of 28 patients in the group that received adjuvant placebo after external beam radiation therapy (*344*). This study showed the applicability of ^{223}Ra treatment for skeletal metastases from a wide variety of cancer types.

Terbium-149 (^{149}Tb)

Radionuclide properties

Terbium-149 was first produced by bombarding ^{141}Pr with ^{14}N ions or by spallation reaction on Ta (*345*). However, its potential role as an alpha emitter for targeted cancer therapy was first recongnized in 1996 (*346*). ^{149}Tb, being a lanthanide, was amenable to standard chelation chemistry as for ^{153}Sm. Further, it emits positrons with a 7% branching ratio and its analogue ^{152}Tb could be used for imaging and pharmacokinetics, as it emits a 2.8 MeV positron with 13% branching ratio, offering the potential for PET (*347*). The characteristics of ^{149}Tb are: half-life =4.15 h, alpha energy =3.966 MeV (16.7 % yield), average LET = 143 keV/μm, range in tissue = 28 μm. Terbium-149 also decays by positron emission (7%) and electron capture (76%)

As an analogue for ^{149}Tb, ^{152}Tb (*347*) has been produced at the National Tandem Accelerator, ANU, Australia using the ^{nat}Nd(^{12}C,xn) reaction at 85 MeV for 15.3 h to produce 100 MBq of ^{152}Dy, which decays to ^{152}Tb. Radiochemical purification was achieved by cation exchange column chromotographuy with alpha-hydroxyisobutyric acid as eluent. Yields of Tb-151,152 and 153 were 36, 47 and 13% respectively. Similar activities of ^{149}Tb have also been produced using the 10 MV tandem accelerator (*348*).

The on-line isotope separator ISOLDE at CERN (*349*) was used to produce clinical activities of ^{152}Tb (*347*). A tantalum foil target with thickness of 120 g cm^{-2} was irradiated with 1 GeV

protons from the CERN PS-Booster accelerator. The radio-lanthanide ions generated in the spallation process were released from the 2200°C target and separated electromagnetically according to the charge-mass ratio. Mass number 152 was collected on a high purity aluminium foil over a period of 12 h. The ^{152}Tb was purified by cation exchange chromatography using Aminex A5 resin and α-hydroxyisobutric acid as eluent., then evaporated to dryness and redissolved in 50 μL of 100 mM HCl. Pr and Ce oxide impurities were only 0.2%. The final ^{152}Tb fraction concentration was 770 MBq with 80% yield after chemical separation. The first ^{152}Tb PET image was obtained using a Jaszczak phantom with only 22 MBq.

In a later study, the A-149 isobar radioactive beam was selected, containing ^{149}Dy and ^{149}Tb, as well as the ^{149}Tb daughter nuclides ^{149}Gd and ^{149}Eu. In addition, $^{133}CeO^{+}$ and $^{133}LaO^{+}$ molecular ions were also found in the beam.

The ^{149}Tb was purified as above and the 149 fraction evaporated to dryness and redissolved in 50 μL of 100mM HCl. The final ^{149}Tb concentration was 2 GBq/mL with an isotopic purity of ~100% (*350*).

Pre-clinical studies

The anti-melanoma MAb 9.2.27 was labeled with ^{152}Tb and ^{153}Sm, to study comparative labeling efficiency, conjugate stability and cytotoxicity (*351*).

In colorectal caner (CRC), the c30.6, (chimeric version of the mouse antibody) and 35A7 antibodies against CRC cell surface antigens have been investigated with this radionuclide (*348*). Results showed that both cDTPA and CHX-A" chelators gave similar stability and in vitro specificity. ^{149}Tb was produced and conjugated with the C30.6 and 35A7 monoclonal antibodies and the first cytotoxicity results for ^{149}Tb AIC were reported for colorectal cancer and compared with ^{213}Bi (*352*). The D_0 value for cells in suspension in exponential growth phase was calculated to be 0.24MBq (6.4 μCi) for the ^{213}Bi-35A7, and 11.25 MBq (304 μCi) for free isotope. The D_0 values for ^{149}Tb labeled antibodies were 37 kBq and 140.6 kBq for c30.6 and 35A7 respectively, and 3.66 MBq for the free ^{149}Tb. For ^{152}Tb, a positron emitter, the D_0 values were 27.4 and 88.8 MBq for c30.6 antibody and free ^{152}Tb respectively. These results showed that, in suspension, ^{149}Tb was more cytotoxic to targeted cells than ^{213}Bi. On the other hand, both alpha emitters were very much more toxic than the targeted beta emitter.

Terbium-149 has rather different alpha properties to ^{213}Bi, in that the half-life is much longer (4 h vs 46 min), the alpha energy is about half (3.97 vs 8.4 MeV), the range is less than half (28 vs 72 μm) and the LET is 27% greater (143 vs 113 keV/μm). Further, the branching ratio for alpha emission is much less (17 vs 100%). Of these parameters, the longer half-life provides more time for distribution to hospitals, conjugation and labeling, and for penetrating targeted cell clusters and tumours. The shorter range of ^{149}Tb means that microscopic cross-fire would be less than for ^{213}Bi. The higher LET could be important but overkill may reduce this effect. The lower branching ratio seems like a major disadvantage, but in reality, the dominant EC decay channel is benign, and does not contribute to the non-specific background radiation.

Clearly, specific applications might favour the application of one alpha emitter over the other. Comparative studies have been made using ^{149}Tb produced at the ISOLDE facility at CERN (*263*). The alpha emitters were coupled using the bifunctional chelate CHX-A"-DTPA to the monoclonal antibody d9 that targets the d9 E-cadherin antigen transfected in MDA MB 435S cells. Internalisation of the conjugate was very low (8 % in 240 min). 213Bi and 149Tb were

attached to the MAb with similar efficiency (~100%). The ^{213}Bi conjugate was 1.6 times more cytotoxic at 100 kBq/mL. However, this reflects the relative alpha yield; Bi-213 emits 5.88 times as many alphas per decay as ^{149}Tb. On a per emitted alpha basis, ^{149}Tb was calculated to be ~3.7 times more cytotoxic. Other effects were subject to experimental conditions and the relatively low antigenic expression ($5x10^4$ antigens per cell) that required near saturation to achieve an effect at the specific activity of 111 MBq/mg.

These results were rather indecisive in favouring one emitter over the other. However, it is unlikely that any advantage of ^{149}Tb, for which a local spallation source would be essential, could outweigh in the clinic the practical advantage of the Ac:Bi generator.

Thorium-227 (^{227}Th)

Radionuclide properties

Thorium-227 (T1/2 = 18.7 days) is a member of the ^{235}U series. It can be obtained from the decay of ^{227}Ac which has a 21.8 year half-life. Actinium-227 itself can be produced by thermal neutron irradiation of ^{226}Ra followed by beta decay of ^{227}Ra (T1/2 = 42 min) to ^{227}Ac. Consequently, long-lived generators for ^{227}Th can be prepared (*353,354*).

Thorium-227 decays to ^{223}Ra (see above) by alpha-particle emission with alpha energies ranging from 5.03 (0.00031%) to 6.04 (24.5%) MeV; the average alpha energy is 5.9 MeV. The most abundant alpha emissions have energies of 5.75 (20.3%), 5.98 (23.4%) and 6.04 (24.5%) MeV. High yield photons occur at 12.3 (17%), 15.2 (21%), and 236 (11%) keV (*180*).

Pre-clinical studies

Up until the mid to late 1990s, interest in this radionuclide was driven by its use as a "short lived" bone seeker that could be used, along with ^{224}Ra, to study stochastic biological effects, in particular bone cancer induction. In the 1990's ^{227}Th became important as a generator for ^{223}Ra which was being investigated as a targeted alpha therapeutic (see section above). Most recently, with the demonstration that ^{223}Ra, the immediate daughter of ^{227}Th, yields acceptable myelotoxicity in patients at a dosage level of 250 kBq/kg (6.75 μCi/kg) (*16*), ^{227}Th itself has been evaluated as a canddiate for targeted alpha-emitter therapy (*355*).

Although not directly relevant to the use of this isotope for cancer therapy, the literature describing the stochastic effects of ^{227}Th is briefly reviewed. In a series of publications, starting in the mid-70's, Müller and co-workers examined the biodistribution and long-term sequelae of ^{227}Th inhalation and intraperitoneal injection in mice and rats (*356-359*). Inhalation of ^{227}Th in nitrate form by 250-300 g male Sprague-Dawley rats gave a biological half-time of ^{227}Th in the lungs of approximately 20 days. An initial deposition of 3.7 kBq (100 nCi) in the lungs resulted in mean total doses (including ^{223}Ra and daughters) of 150 cGy to lungs and 36 cGy to bone; the kidneys and liver received 2 and 0.1 cGy, respectively (*356*). In a separate study, Muller and co-workers (*358*) reported that long-term follow-up of 3-4 week old mice IP injected with 0.1 (3.7 kBq/kg) to 50 (185 kBq/kg) μCi/kg of ^{227}Th produced an osteosarcoma incidence of 3% at 3.7 kBq/kg and a maximum incidence of 60% at 18.5 kBq/kg. The latency time for first appearance of osteosarcoma ranged form 8 to 26 months. The tumor incidence vs. time curve dependend strongly on the activity. From 3.7 to 18.5 kBq/kg, the mean tumor latency time decreased with increasing activity. At administered activities >18.5 kBq/kg, the latency time remained constant at approximately 6-24 months. At the higher dose range, an almost linear increase in incidence with activity was observed; the increases occurred in the skeleton of the head (primarily the jaw

region). Skeletal absorbed doses were estimated assuming uniform deposition of ^{227}Th alpha-particles in the individual bones considered; the biodistribution and dosimetry of the daughter, ^{223}Ra, was considered separately and added to the ^{227}Th dose; ^{223}Ra daughters were assumed to decay at site of ^{223}Ra decay (*360*). According to these calculations, the range of administered activity listed above resulted in mean skeletal absorbed doses ranging from 0.2 to 100 Gy. At 100 Gy, corresponding to 185 kBq/kg, bone necrosis preceded the appearance of bone tumors. Drawing upon comparative studies with fractionated administrations of the shorter lived alpha-emitter ^{224}Ra (T1/2 = 3.64 days), the authors concluded that the initial dose-rate and protracted exposure were key factors in the risk of osteosarcoma induction (*357,359*).

To evaluate ^{227}Th- ethylene-diamine-tetramethylene phosphonate (EDTMP) as a therapeutic agent for bone metastases Washiyama *et al*. (*361*) measured the biodistribution of ^{227}Th - EDTMP and ^{227}Th-citrate, following tail vein injection, over a 14-day period in mice; the biodistribution of the daughter nuclide ^{223}Ra in bone was also evaluated. Uptake of ^{227}Th-EDTMP by bone was higher (9.6 and 6.2 %ID/gm in femur and parietal bone, respectively, at 30 min PI) than that in soft tissue (a maximum of 2.7 %ID/gm in the kidneys at 15 min PI). Femur and parietal bone uptake rapidly reached maximum at 30 min and remained at a that level throughout the 14-day measurement period. Except for the kidneys, soft tissue uptake was less than 1 %ID/gm at all measured time-points. Uptake in the femur (maximum of 28 %ID/g at 1 day PI) and parietal bone (17.2 %ID/g at 1 day PI) was higher following ^{227}Th-citrate compared to that seen with ^{227}Th-EDTMP. The concentration in soft tissue remained above 1% (2.3 %ID/gm in kidneys at day 7 PI) even though blood clearance was rapid (0.006 %ID/gm at day 7). Radium-223 was retained in bone throughout the measurement period with approximately 90% of ^{223}Ra produced by the decay of ^{227}Th in bone at day 7 and 14 post-injection.

The initial evaluation of ^{227}Th for low dose rate alpha-particle radioimmunotherapy was completed by Dahle and co-workers (*353*). A two-step approach (*21*) was used to conjugate ^{227}Th to the anti-CD20 antibody, Rituximab, via the metal chelate DOTA. To evaluate stability of the ^{227}Th-labeled antibody, *in vivo*, uptake in balb/c mice of free ^{227}Th, the chelated form, ^{227}Th-*p*-nitrobenzyl-DOTA, and the radioimmunoconjugate, ^{227}Th-DOTA -*p*-nitrobenzyl-Rituximab was compared for several organs and over a range of time periods. The immunoreactive fraction of the antibody radioimmunoconjugate was 56-65%. By measuring ^{227}Th redistribution to bone the authors demonstrated high stability of the radioimmunoconjugate, *in vivo*. Activity in the femur and skull 28 days after injection was 4 to 6 times higher for free ^{227}Th compared to the ^{227}Th-labeled Rituximab. The activity of ^{223}Ra increased with time in the femur and skull up to 21 days after injection and then decreased. The amount of ^{223}Ra in soft tissue was relatively low except for the spleen. The biodistribution for ^{223}Ra generated *in vivo* was in good agreement with results obtained following IV injection of ^{223}Ra (*340*). The measured kinetics were used to estimate tissue absorbed doses for ^{227}Th and ^{223}Ra (including its daughters) separately assuming a 100 kBq/kg administration of ^{227}Th labeled Rituximab and uniform deposition of alpha-particle energy. The femur and skull received the highest total absorbed doses of 1.75 and 1.05 Gy, respectively. The total dose to the spleen was also relatively high at 0.53 Gy. The blood received 97% (0.21 Gy) of the absorbed dose from the decay of ^{227}Th. Incubation of lymphoma cells with the labeled antibody resulted in significant antigen-dependent inhibition of cell growth at Bq/ml concentration levels.

Based upon the promising results obtained in the initial evalution, Dahle and co-workers examined the therapeutic efficacy of ^{227}Th-Rituximab (*355*). In Raji lymphoma xenografted

mice the radioactivity concentration of ^{227}Th in the tumor peaked 4 days after injection of ^{227}Th-Rituximab at a level (1400 Bq/g) approximately 3.5-fold greater than that concentration in any of the normal organs; the concentration of ^{223}Ra in the tumor was 12 times lower than the^{227}Th tumor concentration at this time and also below the concentration observed in the femur and skull (approximately 220 and 170 Bq/g, respectively). Tumor ^{227}Th and ^{223}Ra concentrations were highest for the specific antibody. The radiation doses to normal tissues and tumor for ^{227}Th-Rituximab were determined by calculating the area under the biodistribution curves and multiplying the resulting cumulated activity with the mean alpha-particle energy from ^{227}Th or ^{223}Ra and daughters; only the contribution of alpha-particles was considered and the daughters of ^{223}Ra were assumed to decay in the same tissue as ^{223}Ra. Tumor doses were 0.5, 2 and 4 Gy, respectively, for 50, 200 and 400 kBq/kg injected. At the 200 kBq/kg injected activity, the femur and skull absorbed dose was about 80% and 50% of the tumor dose, respectively; the absorbed doses to liver and spleen (the two highest normal organs) was approximately 0.5 Gy. Sixty percent of mice treated with 200 kBq/kg ^{227}Th-Rituximab survived > 200 days; corresponding % survival following 50, 400 and 1000 kBq/kg was 20, 55 and 40%, respectively. Treatment with 50 kBq/kg had no significant effect on tumor growth or median survival. At 1000 kBq/kg a significant increase in growth delay was observed but long-term survival was reduced. At 200 kBq/kg bone marrow suppression, as measured by drop in white blood cells (WBC) was modest and after 4 weeks WBC counts were in the range of untreated mice. At 400 kBq/kg WBC count recovery required 7 weeks. At 1000 kBq/kg hematologic toxicity was more pronounced and 1 of 37 mice was terminated due to fatigue and weight loss. However, even at this high administered activity only two mice had WBC below 1.3 x 10^9 counts/l. After 14 weeks WBC counts were in the range of controls for this group of mice also. The platelet count was within control range for the majortiy of samples; 3 mice in the 1000 kBq/kg group had slighly lower counts three weeks after treatment.

G. Recommendations for Dosimetry of Deterministic Effects

Introduction

Beyond providing a rational basis for a starting administered activity value for a phase I study, dosimetry has an important role in guiding clinical trial design to help maximize the likelihood of a successful, minimally toxic implementation. This is particularly important since alpha-emitter targeted therapy has the potential to be both highly effective and also very toxic. Which of these two aspects emerges in a therapeutic trial will depend upon having an understanding of the physical and biological factors that impact response and toxicity. It is essential that clinical trials investigating targeted alpha-particle therapy be rationally designed; otherwise there is the risk that alpha-emitters may be abandoned before they have been properly tested in the clinic.

This increased importance of dosimetric analysis is coupled with a greater difficulty in obtaining the human data necessary to perform dosimetry. In contrast to the majority of targeted therapy trials to date, collection of biodistribution data for dosimetry from pre-treatment imaging studies will not be possible for the majority of alpha-particle emitting radionuclides with therapeutic potential. This places a greater emphasis on pre-clinical studies and extrapolation of results obtained from such studies to the human. Several of the alpha-emitting radiotherapeutics decay to alpha-emitting daughters whose distribution may not be that of the carrier. Aside from understanding the biodistribution/dosimetry of the alpha-emitter labeled carrier, therefore, the

biodistribution/dosimetry of the daughter must also be considered (*317,330,341,353,355,360,362,363*).

In this section the focus of the discussion and the recommendations that are made are specific to deterministic effects.

Recommendations

After stability and radiochemical purity of the radiopharmaceutical has been established and an appropriate target identified, the following progression of studies is proposed. Elements of these recommendations have also been described elsewhere (*364-366*).

1. Determine cellular targeting kinetics and properties

   number of sites per cell and fraction of cells expressing target
   distribution of binding sites per cell among the targeted cells
   binding and dissociation constants for cell targeting (*e.g.*, Ab affinity)
   internalization rate and fraction internalized
   fate of internalized radionuclide
   LD_{50} in targeted versus non-targeted cells
   cell-level dosimetry for targeted and non-targeted cells

2. Animal (xenograft or transgenic) model studies

   evaluate maximum tolerated administered activity (MTD)
   identify likely dose-limiting organs (DLOs)
   collect macroscopic (whole-organ) pharmacokinetics
   collect microscopic (*e.g.*, by autoradiography or optical imaging) biodistribution in DLOs
   evaluate stability of the radiopharmaceutical *in vivo*
   evaluate efficacy at MTD
   perform cell- and organ-level dosimetry for the animal model

3. Extrapolate data obtained in 1 and 2 to the human to arrive at initial activity for phase I study.

   develop and fit a pharmacokinetic model to data obtained in 1 and 2
   replace model parameter values with estimated human values, simulate biodistribution in human
   use model-derived biodistribution to estimate absorbed dose to DLOs identified in 2b.

4. Assess radiopharmaceutical distribution during the phase I study.

   Image (if possible)
   Collect and count blood samples
   Collect, count and autoradiograph biopsy samples (if practical)

If there are concerns related to possible renal, urinary bladder wall or GI toxicity related to the localization of activity in luminal contents versus the organ wall that have not been addressed by animal studies:.

   Collect and count urine samples
   Collect and count fecal samples

Items 1-3, above are general guidelines. The primary objective is to collect adequate pre-clinical data so as to have an understanding of the alpha-emitters' likely biodistribution and kinetics in

humans. This is particularly important since pre-therapy patient imaging will not be possible. It is essential that this approach not be seen as mandatory for moving alpha-emitter labeled radiopharmaceuticals to the clinic, in particular, step 3 may be replaced by a projected conservative (worst-case) scenario analysis or by a direct translation of small-animal pharmacokinetics to the human using standard methods to adjust for differences in body size and organ mass (*367*). The autoradiography proposed in items 2d and 4c will clearly be subject to the practical constraint of alpha-emitter half-life. For short-lived alpha-emitters, microscopic imaging of fluorescently tagged agents may be a viable alternative to autoradiography in animals models.

Conventional versus cell-level dosimetry

In most cases a microdosimetric analysis will not be necessary for targeted therapy applications because the activity level administered and mean absorbed doses to targeted cells are larger than in the cases described above and the resulting stochastic deviation is expected to be substantially less than 20%. In such cases standard dosimetry methods may be applied (*166,252*). The standard approach to dosimetry calculations has been described by the Medical Internal Radionuclide Dose (MIRD) Committee (*166*). In this formalism the absorbed dose to a target volume from a source region is given as the total number of disintegrations in the source region multiplied by a factor (the S value) that provides the absorbed dose to a target volume per disintegration in the source region. The sum of these products across all source regions gives the total absorbed dose to the target. MIRD cellular S values have been published for cell level dosimetry calculations for situations in which the number of disintegrations in different cellular compartments can be measured or modeled (*151*). Using these S values, the absorbed dose to the nucleus may be calculated from alpha-particle emissions uniformly distributed on the cell surface, in the cytoplasm or in the nucleus.

Conventional dosimetry for organs and tumors

Estimation of the average absorbed dose to a particular normal organ or tumor volume is based upon the assumption that the radioactivity is uniformly distributed in the organ and that the energy deposited by the emitted alpha particles is also distributed uniformly within the organ. With some exceptions (*368-372*), the cross-organ dose from alpha-particle and electron emissions can be assumed negligible for human organ and tumor dosimetry. Care is required in applying S-values for alpha-emitters since alpha emitters may have multiple decay pathways as well as multiple radioactive daughters that should be taken into account. For example, S values for ^{213}Bi will not include the emissions from the ^{213}Po daughter which has a 4 μs half-life and which contributes 98% of the alphas emitted by ^{213}Bi decay (the remaining 2% come from decay of ^{213}Bi itself).. This consideration and also the importance of separately accounting for absorbed dose due to electron and photon emissions from that due to alphas requires that the dosimetry calculations be performed based upon absorbed fraction calculations rather than upon S-values. The methodology is described by the following equations (presented using the recently published updated MIRD schema) (*373*)

$$D_{\alpha}(r_T, T_D) = \tilde{A}(r_S, T_D) \cdot \frac{\sum_i \Delta_i^{\alpha} \phi(r_T \leftarrow r_S; E_i^{\alpha})}{M(r_T)} \qquad \text{G.1}$$

$$D_e(r_T,T_D) = \tilde{A}(r_S,T_D)\cdot\frac{\sum_i \Delta_i^e \phi(r_T \leftarrow r_S;E_i^e)}{M(r_T)} \quad \text{G.2}$$

$$D_{ph}(r_T,T_D) = \frac{\sum_{r_S}\left(\tilde{A}(r_S,T_D)\cdot\sum_i \Delta_i^{ph}\phi(r_T \leftarrow r_S;E_i^{ph})\right)}{M(r_T)} \quad \text{G.3}$$

$$D_{RBE}(r_T,T_D) = RBE_\alpha \cdot D_\alpha(r_T,T_D) + RBE_e \cdot D_e(r_T,T_D) + RBE_{ph}\cdot D_{ph}(r_T,T_D) \quad \text{G.4}$$

with:

$D_x(r_T,T_D)$	absorbed dose to target region, r_T from emission type x.
$D_{RBE}(r_T,T_D)$	RBE-weighted dose to target region, r_T.
r_T, r_S	target, source region (or tissue), respectively.
$\tilde{A}(r_T,T_D)$	time-integrated activity or total number of nuclear transitions in target region, r_T.
$M(r_T)$	mass of target region.
Δ_i^x	mean energy emitted per nuclear transition for i^{th} emission of particle type x (= alpha, electron or photon).
$\phi(r_T \leftarrow r_S;E_i^x)$	fraction of energy emitted per nuclear transition in source region, r_S, that is absorbed in target region, r_T by the i^{th} emission of particle type x that is emitted with initial energy, E.
RBE_α, RBE_e	
RBE_{ph}	relative biological effectiveness for alpha-particles (α), electrons (e) and photons (ph). $RBE_e = RBE_{ph} = 1$

The total number of nuclear transitions in a particular tissue or region is typically obtained by longitudinal imaging, or counting tissue samples for radioactivity. Values for the Δ_i's are obtained from decay-scheme tabulations published for each radionuclide (*233*). The absorbed fraction for each decay type, ϕ, must be calculated from tabulations of absorbed fractions for the particular tissue geometry. In almost all cases non-cell-level dose calculations, the absorbed fractions for alpha-particles can be assumed equal to 1; the absorbed fractions for electrons are likewise usually assumed equal to 1. A description of the methods used to calculate these values is beyond the scope of this review but are provided in references (*372,374,375*). Reference (*372*), in particular, describes absorbed fractions that are tabulated by alpha-particle energy for bone marrow trabeculae. For alpha-emitters that decay via a branched decay scheme, as in ^{213}Bi, for example, (Fig. 11) it is important to account for the relative yield of each branch in determining the total energy emitted by each type of emission (*i.e.*, the Δ_i's). In the case of ^{213}Bi, Tables 6 and 7 summarize the electron and alpha-particle emissions. The tables illustrate how to tally the total electron and alpha-particle energy. As shown, 2.2% of ^{213}Bi decays result in ^{209}Tl with the emission of an alpha particle, the initial energy of the emitted alpha is either 5.5 or 5.8 MeV with the probability of each given by the yields shown on table 2. In the remaining 97.8% of decays, ^{213}Bi decays to ^{213}Po with the emission of a beta particle. Polonium-213, itself decays very rapidly via the emission of an 8.4 MeV alpha to ^{209}Pb which in turn decays to ^{209}Bi with the emission of a 198-keV beta particle. The exercise illustrates that a careful accounting of emissions is required in tallying the energy emitted per disintegration of the administered alpha-emitter, even when the decay scheme is relatively simple as for ^{213}Bi. Although outside the scope of this review, the photon S values (Table 8) can be calculated based on tabulations of photon absorbed fractions to different source-target organ combinations and photon energies (*376*).

Units

The issue of identifying the most appropriate dosimetry quantities and units is particularly important for alpha emitters because, as noted earlier, there can be confusion regarding the calculation of dosimetry quantities that relate to stochastic versus deterministic effects. It is incorrect to assign the unit sievert (Sv) to the quantity defined by equation G.4. The sievert is not a unit in the conventional sense, but rather, is intended to indicate that the absorbed dose value has been scaled to reflect a biological risk that is associated with stochastic effects. Although the product of deterministic RBEs and absorbed dose in Gy has been referred to as a Sv, this is not strictly correct since Sv should only be used to designate the risk of incurring stochastic biological effects such as cancer. No special named unit has been widely adopted to reflect a dose value that has been multiplied by an RBE and that specifically reflects the magnitude of deterministic effects. The MIRD Committee has proposed that the barendsen (Bd) be defined as the special named unit for the product of deterministic RBE and absorbed dose has published a commentary to this effect (*377*). To avoid confusion during the transition period, the MIRD Committee recommends that the three absorbed dose values, for alpha, electron and photon emissions be provided separately, and reported in the absorbed dose unit, Gy. This removes any ambiquity as to interpretation of reported absorbed doses for alpha-emitter therapy applications.

Daughters

The example provided above is for an alpha-emitter with a relatively simple decay scheme. Each disintegration of the parent ^{213}Bi leads to a single alpha-particle emission; there are no long-lived alpha-emitting daughters. This is not the case for the longer-lived alpha-emitters ^{223}Ra, ^{225}Ac and ^{227}Th which decay via alpha-emitting daughters. Because emission of an alpha by the parent atom leads to a 50- to 100-nm recoil of the resulting daughter, daughter atoms may not remain conjugated to the molecular carrier. In the most complex scenario, the biological distribution of the daughter will depend upon the site of parent decay (*330*). In practice, the biological distribution of long-lived daughters tends to be dominated by the chemical fate of the daughter atom. For example, ^{213}Bi, the longest lived daughter of ^{225}Ac concentrates in the kidneys. Likewise, ^{223}Ra, the daughter of ^{227}Th localizes to bone. Dosimetry calculations for such radionuclides must, therefore account for the biodistribution of both the parent and all daughters.

Efficacy Modeling

A key parameter for evaluating tumor cell kill is the cumulated activity (*i.e.*, number of nuclear transitions) per target cell, $\tilde{A}$(cell). An estimate of this would provide information regarding the likelihood of effective cell killing for a single, isolated cell, defined as a cell that is irradiated only from emissions on its surface as is especially relevant in radiolabeled antibody targeting of micrometastases or low tumor burden leukemia or ascetic disease. Using a formulation adapted from (*378*), this can be estimated as follows:

$$\tilde{A}(cell) = \int_{t_1}^{t_2} A(cell,t) \qquad \text{G.5}$$

$$A(cell,t) = Ag_0 \cdot SA(t) \qquad \text{G.6}$$

$$SA(t) = SA_0 \cdot e^{-\lambda t} \qquad \text{G.7}$$

where:

$\tilde{A}(cell)$	Number of disintegrations per cell.
$A(cell,t)$	Disintegration rate per cell at time t.
Ag_0	Number of target sites (receptors or antigens) per cell
SA_0	Initial specific activity of the targeting agent.
t_1,t_2	Estimated start and end time that define time-interval during which activity is target cell associated.
λ	effective decay rate constant of the radionuclide (= ln(2)/radionuclide half-life). This folds in the physical decay as well as biological elimination from the cell as a consequence of cell division or migration of the radionuclide.

Once the number of cell-associated decays are known, then the MIRD cellular S values (*151,363*) may be used to estimate the absorbed dose to the cell nucleus (n) or to the whole cell from a cell-surface (cs) and/or cytosolic (cy) distribution of the total number of decays:

$$D(n) = \tilde{A}(cs) \cdot S(n \leftarrow cs) + \tilde{A}(cy) \cdot S(n \leftarrow cy) \qquad \text{G.8.}$$

where $\tilde{A}(cs)$ and $\tilde{A}(cy)$ are the cumulated activity on the cell surface and in the cytoplasm, respectively. The quantities $S(n \leftarrow cs)$ and $S(n \leftarrow cy)$ are the absorbed dose to the nucleus per nuclear transformation (Bq s) on the cell surface and in cytoplasm, respectively. Calcuation of cellular absorbed dose in this manner applies only to isolated cells. This is a worst-case approximation for a tumor cell eradication since, depending upon the range of the emitted alpha-particle and the cellular geometry of the target tumor tissue, some cross-fire from adjacent cells may otherwise be expected.

The estimated absorbed dose to the nucleus can then be used with an estimate of the radiosensitivity (D_0) of the cell line to calculate surviving fraction (SF) and, from this, the tumor control probability (TCP) for a given number of target cells (N):

$$SF = e^{-D/D_0} \qquad \text{G.9.}$$

$$TCP = e^{-N \cdot SF} \qquad \text{G.10.}$$

It is important to note that equation G.9 is strictly valid only if D_0 is measured for the source/target configuration for which one is doing the *TCP* calculation. If this condition is not approximated, the microdosimetric parameter, z_0, should be used and the microdosimetric spectra should be calculated and used to calculate *SF* (*379*). Equation G.10 is derived assuming that the probability distribution for cell survival is given by Poisson statistics and reflects the probability of 0 cells surviving when the average number surviving is $N \cdot SF$ (*380*). If, for a given number of initial target cells, *N*, the surviving fraction is such that, on average, only a single cell is expected to survive then the probability of no cell surviving is 0.37. If the therapeutic efficacy of the approach is such that ten times n cells could be reduced to 1 (*i.e.*, efficacy is improved by a factor of 10 giving, $N \cdot SF = 0.1$), then the *TCP* would be 0.9.

Recently, the non-uniformity in antigen expression was identified as having an important impact on the *TCP* (*49*). The effect of accounting for a variable antigen distribution among targeted cells compared to a single value for Ag_0 can be examined by assuming Ag_0 follows a normal distribution centered about a mean value. By performing a simulation to randomly sample the normal distribution the number of antigens, *Ag(i)*, on the surface of cell *i,* are obtained for *N* cells. Using the equations listed above, the number of disintegrations for each cell, i, and its survival probability (given by the expression for *SF*) can be calculated. The *TCP* for a single simulation is then given by:

$$TCP = e^{-\sum_{i=1}^{N} SF(i)} \qquad \text{G.11.}$$

The average of the *TCP* obtained from multiple simulations provides an estimate of the final *TCP* for a cell population with an assumed variable antigen expression.

Illustrative example

The following example, illustrates use of equations G.5 through G.11.

The cell-surface expression of HER2/*neu* is set to 0.5 or 1 x 10^6 sites/cell; these values are consistent, with established values on HER2/*neu*-expressing breast cancer cells (*320,381*). The specific activity of ^{213}Bi-trastuzumab is approximately 440 MBq/ mg Ab (*12,256*); a breast cancer cell is modeled as two concentric spheres with nuclear radius of 4 μm and a cellular radius of 5 μm. The radiosensitivity is set to 0.7 Gy (*61*); the half-life of ^{213}Bi is 45.6 min. For purposes of illustration, rapid targeting of intravascularly disseminated metastases is assumed such that all administered activity decays occur on the target cells ($t_1 = 0; t_2 = \infty$). The relevant parameter values are:

Ag_0 0.5, 1 x 10^6 sites/cell

SA_0 440 MBq/mg Ab

R_N 4 μm

R_C 5 μm

D_0 0.7 Gy

$T_{1/2}$ 45.6 min

The values chosen do not necessarily simulate any one specific experiment, but rather are taken as reasonable values to illustrate use of equations G.5-G.11. Using the values for t_1 and t_2 provided above, Equation G.5 reduces to:

$$\tilde{A}(cell) = \frac{SA_0}{\lambda} \cdot Ag_0 \qquad \text{G.12}$$

The effect of variable antigen expression is illustrated by assuming Ag_0 is normally distributed with a mean of 0.5 or 1 x 10^6 and standard deviations of 10 or 25%.

Results are depicted in table 5.

The analysis reveals the exquisite sensitivity of tumor control to the number of cell-associated decays and to the uniformity of expression. Note that the same results would be obtained by increasing the specific activity by a factor of 2. Estimation of the number of cell-associated decays is one of the most important parameter values in targeted alpha-emitter therapy.

It is important to note that the calculations described above are provided for illustration, and the results reflect the worst case of an isolated cell that is subject only to self-irradiation and the best case that all of the target sites on the cell surface will be occupied by the delivery molecule. Whether these conditions are met will depend upon the geometry of the cancer; for example, in the targeting of leukemia after substantial cytoreduction, the assumptions are a reasonable representation of what might happen. In the targeting of metastastic tumor cell clusters, the results will be a balance between the fraction of sites occupied and the cross-fire from one cell to another. If the cells are clustered together then the assumed 100% target antigen occupancy is optimistic, on the other hand, clustering will increase cross-fire and the assumption of only self-irradiation is convervative. It is also important to note that a microdosimetric calculation was not performed. In most cases, given a sufficient number of cell-associated decays, microdosimetry

will not be necessary and the use of cellular S-values is valid. A microdosimetric treatment of TCP for alpha-particle emitting radionuclides has been developed by Roeske and Stinchcomb (*379*).

Hematologic toxicity

Depending upon the data available, the delivery vehicle and the alpha-emitting radionuclide a number of different approaches may be used to evaluate hematologic toxicity prior to an initial therapeutic administration. If the stability of the radiolabeled delivery molecule has been confirmed in pre-clinical studies and data are available for the kinetics of the delivery molecule in humans using a radionuclide that has similar chemical properties and a similar catabolic and intracellular fate, then human data may be used to obtain the residence time or cumulated activity in the marrow of the alpha-emitter. If these conditions are not met, then the initial estimate can be based on pre-clinical biodistribution data.

Once the total number of radionuclide decays in the red marrow (RM) has been determined ($\tilde{A}(r_{RM})$), a first-order estimate of the absorbed dose to the red marrow ($D_{\alpha}(r_{RM})$) may be obtained by reformulating equation G.1:

$$D_{\alpha}(r_{RM},T_D)=\frac{\tilde{A}(r_{RM},T_D)}{M(r_{RM})}\cdot\sum_i \Delta_i^{\alpha}\phi(r_{RM};E_i^{\alpha}) \qquad \text{G.13}$$

with

M_{RM} red marrow mass.

Note that in equation G.13, the photon and electron dose contributions are assumed negligible relative to the alpha-particle contribution. The estimate outlined above, along with pre-clinical toxicity studies can be used to provide the rationale for a starting administered activity level in a human Phase I trial. During the phase I trial a more detailed estimation of red-marrow absorbed dose should be obtained. This would require either direct (*e.g.*, biopsy) or indirect sampling (*e.g.*, by imaging or the use of blood kinetics as a surrogate) of the red marrow.

Illustrative example

The example provided previously is expanded to illustrate initial estimation of red marrow absorbed dose in targeting breast cancer metastases using ^{231}Bi-labeled Trastuzumab. Since the circulation half-time of intact antibody is much greater than the 45.6-minute half-life of ^{213}Bi, all IV-administered ^{213}Bi may be assumed to decay in circulation, with the radioimmunoconjugate assumed to be stable over the relevant 5 to 6-hr time-period. Under these conditions, the cumulated activity in the marrow may be calculated as the administered activity divided by the physical decay rate constant, λ, for ^{213}Bi. This actually gives the total number of disintegrations or cumulated activity in the blood. Dividing this by the blood volume yields the blood cumulated activity concentration. Multiplying the cumulated activity concentration in blood by the red marrow to blood (activity concentration) ratio (RMBLR) gives the cumulated activity concentration in the red marrow. Assuming a blood volume of 3.9L (with density ≈ 1 g/cc) (*382*) corresponding to the adult female and RMBLR = 0.36 (*383*), the cumulated activity concentration is 3.6 x 10^6 Bq-s/gm per MBq ^{213}Bi injected. Recognizing that this value replaces

the quotient in equation G.13 and using $\sum_i \Delta_i^\alpha \phi(r_{RM}; E_i^\alpha) = 1.33 \times 10^{-12}$ Gy-kg/Bq-s (17.7 g-rad/μCi-hr) (*252*) by assuming $\phi(r_{RM}; E_i^\alpha) = 1$ for all alpha emissions, *i*, the red marrow absorbed dose is 4.85 mGy/MBq (17.9 rad/mCi).

The estimate of red marrow absorbed dose shown was obtained assuming all alpha-particle energy is absorbed in the red marrow ($\phi(r_{RM}) = 1$). If the microarchitecture of the marrow (pelvis) is considered and a cellularity of 50%, which is typical of 30- to 50-year old adults is used (*384,385*), $\phi(r_{RM}) = 0.57$ for ^{213}Bi alpha-particle emissions (*372,386*), and the mean red marrow absorbed dose is 2.76 mGy/MBq. To relate this value to red marrow toxicity experience with beta-particle emitters or with external beam, the dose estimate should be multiplied by an RBE value. Human data on red marrow RBE are limited but suggest RBE ≈ 1 (see Table 4). However, until additional data are collected, a more conservative RBE factor of 2 to 3 is recommended if the red-marrow absorbed dose will be used to establish a starting administered activity in a dose-escalation trial.

H. Summary

The potential of alpha-particle emitters to treat cancer has been recognized since the early 1900s. Early experience with alpha-particle emitters, however, occurred when the hazards were not appreciated, resulting in their indiscriminant use and negative consequences. Continuing interest in alpha-particle emitting radionuclides for cancer therapy is driven by the physical and radiobiological properties of alpha-particles as compared to photons and electrons. The energy deposition along the path of an alpha-particle can be two to three orders of magnitude greater than that of emissions arising from the decay of ^{131}I, ^{90}Y, and other beta-particle emitters. The number of alpha-particle nuclear traversals required to kill a cell (excluding bystander effects) has been found to range from as low as 1 to as high as 20. The variability in this value arises because of the high sensitivity of this determination to the geometry of the cell and nucleus during irradiation and also the LET of the incident alphas and the LET distribution within the nucleus. The alpha-particle RBE for initial yield of DSB relative to acute ^{60}Co gamma-rays ranges from 0.7 to 4.4. While the repair rate of repairable damage is independent of LET, the fraction not repaired and the fraction repaired very slowly both increase with LET. Since high LET damage is not easily repaired, a minimal OER effect is observed with alpha-particle radiation; at an LET greater than 140 keV/μm, OER = 1. The initial LET of 4- to 8-MeV alpha-particles which are typical of the alpha-emitters of interest in targeted alpha-emitter therapy ranges from 110 to 61 keV/μm. The OER values in this LET range are 1.3 to 2.1. Since the LET of the emitted alpha-particles increases well beyond 140 keV/μm as the Bragg peak is approached, the ability of alpha-particles to overcome radioresistance due to hypoxia will depend upon the spatial distribution of the alpha-emitters relative to the hypoxic region. Alpha-particle induced kill is also minimally susceptible to differences in dose rate. Over a dose-rate range of 0.005 to 1 Gy/min no dose-rate effect is observed. Reported values for the RBE of alpha-particles, for cell killing *in vivo*, range from approximately 1 to 5, depending upon the reference radiation, alpha particle energy, and the biological end-point.

Because of the high LET of alpha-particles, a single energy-deposition event in the nucleus of a cell can deposit an absorbed dose that corresponds to a large fraction of the total energy deposited. When the relative deviation of the local dose exceeds 20%, the stochastic variation of

energy deposited within a target must be taken into account and microdosimetric methods must be used. In most cases of alpha-emitter therapy it is expected that the number of alpha-particle energy deposition events will be large enough so that each individual event will contribute substantially less than 20% of the total dose. In most cases, therefore, a mean absorbed dose calculation will be valid.

Beyond providing a starting administered activity for Phase I studies, dosimetry has an important role in guiding clinical trial design to help maximize the likelihood of a successful, minimally toxic implementation. An outline of recommended studies has been provided as well as specific examples illustrating how dosimetry/modeling analyses can provide valuable information for trial design.

Finally, it should be recognized that although DNA damage and its repair are at the core of alpha-emitter radiobiological effects, almost all of the foundation work in support of this conclusion was performed well before modern molecular biology came into existence. Gains in knowledge and the emergence of new experimental techniques have made it possible to examine the role of cell signaling and DNA repair pathways on cell and tissue response to alpha-particle radiation. Such studies will contribute to our understanding of the biological effects of targeted alpha-particle therapy and very likely impact the recommendations made in this review.

I. Acknowledgements

The authors thank D.E.Charlton for vigorous discussions and his careful reading of this paper.

References

(1) Bloomer WD, McLaughlin WH, Lambrecht RM, Atcher RW, Mirzadeh S, Madara JL et al. 211At radiocolloid therapy: further observations and comparison with radiocolloids of 32P, 165Dy, and 90Y. *Int J Radiat Oncol Biol Phys.* 1984; 10(3):341-348.

(2) Macklis RM, Kinsey BM, Kassis AI, Ferrara JLM, Atcher RW, Hines JJ et al. Radioimmunotherapy with Alpha-Particle Emitting Immunoconjugates. *Science.* 1988; 240(4855):1024-1026.

(3) Zalutsky MR, Vaidyanathan G. Astatine-211-Labeled Radiotherapeutics: An Emerging Approach to Targeted Alpha-Particle Radiotherapy. *Curr Pharm Des.* 2000; 6(14):1433-1455.

(4) McDevitt MR, Ma D, Lai LT, Simon J, Borchardt P, Frank RK et al. Tumor therapy with targeted atomic nanogenerators. *Science.* 2001; 294(5546):1537-40.

(5) McDevitt MR, Sgouros G, Finn RD, Humm JL, Jurcic JG, Larson SM et al. Radioimmunotherapy with alpha-emitting nuclides. *Eur J Nucl Med.* 1998; 25(9):1341-51.

(6) Zalutsky MR, Vaidyanathan G. Astatine-211-labeled radiotherapeutics: An emerging approach to targeted alpha-particle radiotherapy. *Curr Pharm Des.* 2000; 6(14):1433-1455.

(7) Mulford DA, Scheinberg DA, Jurcic JG. The promise of targeted {alpha}-particle therapy. *J Nucl Med.* 2005; 46 Suppl 1:199S-204S.

(8) Jurcic JG. Antibody therapy for residual disease in acute myelogenous leukemia. *Crit Rev Oncol Hematol.* 2001; 38(1):37-45.

(9) Wilbur DS. Potential use of alpha-emitting radionuclides in the treatment of cancer. *Antibody Immunoconj Radiopharm.* 1990; 4:85-97.

(10) Wicha MS. Cancer stem cells and metastasis: Lethal seeds - Commentary. *Clin Cancer Res.* 2006; 12(19):5606-5607.

(11) Sgouros G, Song H. Cancer stem cell targeting using the alpha-particle emitter, 213Bi: mathematical modeling and feasibility analysis. *Cancer Biother Radiopharm.* 2008; 23(1):74-81.

(12) Jurcic JG, Larson SM, Sgouros G, McDevitt MR, Finn RD, Divgi CR et al. Targeted alpha particle immunotherapy for myeloid leukemia. *Blood.* 2002; 100(4):1233-9.

(13) Jurcic JG, McDevitt MR, Sgouros G, Ballangrud A, Finn RD, Geerlings MW et al. Targeted alpha-particle therapy for myeloid leukemias: A phase I trial of bismuth-213-HuM195 (anti-CD33). *Blood.* 1997; 90(10):2245.

(14) Geerlings MW, Kaspersen FM, Apostolidis C, van der Hout R. The feasibility of 225Ac as a source of alpha-particles in radioimmunotherapy. *Nucl Med Commun.* 1993; 14(2):121-5.

(15) Zalutsky MR, Reardon DA, Akabani G, Coleman RE, Friedman AH, Friedman HS et al. Clinical experience with alpha-Particle emitting 211At: treatment of recurrent brain tumor patients with 211At-labeled chimeric antitenascin monoclonal antibody 81C6. *J Nucl Med.* 2008; 49(1):30-38.

(16) Nilsson S, Larsen RH, Fossa SD, Balteskard L, Borch KW, Westlin JE et al. First clinical experience with alpha-emitting radium-223 in the treatment of skeletal metastases. *Clinical Cancer Research.* 2005; 11(12):4451-4459.

(17) Hultborn R, Andersson H, Back T, Divgi C, Elgqvist J, Himmelman J et al. Pharmacokinetics and dosimetry of (211)AT-MX35 F(AB ')(2) in therapy of ovarian cancer - Preliminary results from an ongoing phase I study. *Cancer Biother Radiopharm.* 2006; 21(4):395.

(18) Kennel SJ, Mirzadeh S, Eckelman WC, Waldmann TA, Garmestani K, Yordanov AT et al. Vascular-targeted radioimmunotherapy with the alpha-particle emitter 211At. *Radiat Res.* 2002; 157(6):633-641.

(19) Kennel SJ, Mirzadeh S. Vascular targeted radioimmunotherapy with 213Bi--an alpha-particle emitter. *Nucl Med Biol.* 1998; 25(3):241-6.

(20) Akabani G, McLendon RE, Bigner DD, Zalutsky MR. Vascular targeted endoradiotherapy of tumors using alpha-particle-emitting compounds: Theoretical analysis. *Int J Radiat Oncol Biol Phys.* 2002; 54(4):1259-1275.

(21) McDevitt MR, Ma D, Simon J, Frank RK, Scheinberg DA. Design and synthesis of 225Ac radioimmunopharmaceuticals. *Appl Radiat Isot.* 2002; 57(6):841-847.

(22) Jurcic JG, McDevitt MR, Pandit-Taskar N, Divgi CR, Finn RD, Sgouros G et al. Alpha-particle immunotherapy for acute myeloid leukemia (AML) with bismuth-213 and actinium-225. *Cancer Biother Radiopharm.* 2006; 21(4):396.

(23) Bell AG. The uses of radium. *Am Med.* 1903; 6:261.

(24) Schales F. Brief History of Ra-224 Usage in Radiotherapy and Radiobiology. *Health Phys.* 1978; 35(1):25-32.

(25) Macklis RM. The Great Radium Scandal. *Sci Am.* 1993; 269(2):94-99.

(26) Bertrand A, Legras B, Martin J. Use of Radium-224 in Treatment of Ankylosing-Spondylitis and Rheumatoid Synovitis. *Health Phys.* 1978; 35(1):57-60.

(27) Lassmann M, Nosske D, Reiners C. Therapy of ankylosing spondylitis with Ra-224-radium chloride: dosimetry and risk considerations. *Radiat Environ Biophys.* 2002; 41(3):173-178.

(28) Martland HS. Occupational poisoning in manufacture of luminous watch dials - General review of hazard caused by ingestion of luminous paint, with especial reference to the New Jersey cases. *J Am Med Assoc.* 1929; 92:466-473.

(29) Baserga R, Yokoo H, Henegar GC. Thorotrast-Induced Cancer in Man. *Cancer.* 1960; 13(5):1021-1031.

(30) Seidlin SM, Marinelli LD, Oshry E. Radioactive Iodine Therapy - Effect on Functioning Metastases of Adenocarcinoma of the Thyroid. *J Am Med Assoc.* 1946; 132(14):838-847.

(31) Larson SM, Carrasquillo JA, Krohn KA, Brown JP, McGuffin RW, Ferens JM et al. Localization of 131I-labeled p97-specific Fab fragments in human melanoma as a basis for radiotherapy. *J Clin Invest.* 1983; 72(6):2101-14.

(32) Zirkle RE. Some effects of alpha radiation upon plant cells. *J Cell Comp Physiol.* 1932; 2(3):251-274.

(33) Andrew BA, Suit H. The centenary of the discovery of the Bragg peak. *Radiother Oncol.* 2004; 73(3):265-268.

(34) Barendsen GW, Koot CJ, van Kerson GR, Bewley DK, Field SB, Parnell CJ. The effect of oxygen on the impairment of the proliferative capacity of human cells in culture by ionizing radiations of different LET. *Int J Radiat Biol.* 1966; 10:317-327.

(35) Barendsen GW, Walter HMD. Effects of Different Ionizing Radiations on Human Cells in Tissue Culture .4. Modification of Radiation Damage. *Radiat Res.* 1964; 21(2):314-329.

(36) Barendsen GW. Modification of Radiation Damage by Fractionation of Dose Anoxia + Chemical Protectors in Relation to Let. *Ann N Y Acad Sci.* 1964; 114(A1):96-114.

(37) Barendsen GW. Impairment of the Proliferative Capacity of Human Cells in Culture by Alpha-Particles with Differing Linear-Energy Transfer. *Int J Radiat Biol Relat Stud Phys Chem Med.* 1964; 8(5):453-466.

(38) Barendsen GW, Walter HMD, Bewley DK, Fowler JF. Effects of Different Ionizing Radiations on Human Cells in Tissue Culture .3. Experiments with Cyclotron-Accelerated Alpha-Particles and Deuterons. *Radiat Res.* 1963; 18(1):106-&.

(39) Barendsen GW. Dose-Survival Curves of Human Cells in Tissue Culture Irradiated with Alpha-, Beta-, 20-Kv X- and 200-Kv X-Radiation. *Nature.* 1962; 193(4821):1153-&.

(40) Barendsen GW, Beusker TLJ. Effects of Different Ionizing Radiations on Human Cells in Tissue Culture .1. Irradiation Techniques and Dosimetry. *Radiat Res.* 1960; 13(6):832-840.

(41) Barendsen GW, Beusker TLJ, Vergroesen AJ, Budke L. Effect of Different Ionizing Radiations on Human Cells in Tissue Culture .2. Biological Experiments. *Radiat Res.* 1960; 13(6):841-849.

(42) Barendsen GW, Vergroesen AJ. Irradiation of Human Cells in Tissue Culture with Alpha-Rays, Beta-Rays and X-Rays. *Int J Radiat Biol Relat Stud Phys Chem Med.* 1960; 2(4):441.

(43) Goodhead DT, Munson RJ, Thacker J, Cox R. Mutation and Inactivation of Cultured Mammalian-Cells Exposed to Beams of Accelerated Heavy-Ions .4. Biophysical Interpretation. *Int J Radiat Biol.* 1980; 37(2):135-167.

(44) Munson RJ, Bance DA, Stretch A, Goodhead DT. Mutation and Inactivation of Cultured Mammalian-Cells Exposed to Beams of Accelerated Heavy-Ions .1. Irradiation Facilities and Methods. *Int J Radiat Biol.* 1979; 36(2):127-136.

(45) Thacker J, Stretch A, Stephens MA. Mutation and Inactivation of Cultured Mammalian-Cells Exposed to Beams of Accelerated Heavy-Ions .2. Chinese-Hamster V79-Cells. *Int J Radiat Biol.* 1979; 36(2):137-148.

(46) Cox R, Masson WK. Mutation and Inactivation of Cultured Mammalian-Cells Exposed to Beams of Accelerated Heavy-Ions .3. Human-Diploid Fibroblasts. *Int J Radiat Biol.* 1979; 36(2):149-160.

(47) Fisher DR, Frazier ME, Andrews T.K. Jr. Energy distribution and the relative biological effects of internal alpha emitters. *Radiat Prot Dosim.* 1985; 13:223-227.

(48) Humm JL, Chin LM. A model of cell inactivation by alpha-particle internal emitters. *Radiat Res.* 1993; 134(2):143-50.

(49) Kvinnsland Y, Stokke T, Aurlien E. Radioimmunotherapy with alpha-particle emitters: Microdosimetry of cells with a heterogeneous antigen expression and with various diameters of cells and nuclei. *Radiat Res.* 2001; 155(2):288-296.

(50) Neti PVSV, Howell RW. Log normal distribution of cellular uptake of radioactivity: Implications for biologic responses to radiopharmaceuticals. *J Nucl Med.* 2006; 47(6):1049-1058.

(51) Munro TR. Relative Radiosensitivity of Nucleus and Cytoplasm of Chinese Hamster Fibroblasts. *Radiat Res.* 1970; 42(3):451-70.

(52) Lloyd EL, Gemmell MA, Henning CB, Gemmell DS, Zabransky BJ. Cell Survival Following Multiple-Track Alpha-Particle Irradiation. *Int J Radiat Biol.* 1979; 35(1):23-31.

(53) Raju MR, Eisen Y, Carpenter S, Inkret WC. Radiobiology of Alpha-Particles .3. Cell Inactivation by Alpha-Particle Traversals of the Cell-Nucleus. *Radiat Res.* 1991; 128(2):204-209.

(54) Bird RP, Rohrig N, Colvett RD, Geard CR, Marino SA. Inactivation of Synchronized Chinese-Hamster V79-Cells with Charged-Particle Track Segments. *Radiat Res.* 1980; 82(2):277-289.

(55) Todd P, Wood JCS, Walker JT, Weiss SJ. Lethal, Potentially Lethal, and Nonlethal Damage Induction by Heavy-Ions in Cultured Human-Cells. *Radiat Res.* 1985; 104(2):S5-S12.

(56) Roberts CJ, Goodhead DT. The Effect of Pu-238 Alpha-Particles on the Mouse Fibroblast Cell-Line C3H 10T1/2 - Characterization of Source and Rbe for Cell-Survival. *Int J Radiat Biol.* 1987; 52(6):871-882.

(57) Barendsen GW. Let Dependence of Linear and Quadratic Terms in Dose-Response Relationships for Cellular-Damage - Correlations with the Dimensions and Structures of Biological Targets. *Radiat Prot Dosim.* 1990; 31(1-4):235-239.

(58) Howell RW, Rao DV, Hou DY, Narra VR, Sastry KSR. The Question of Relative Biological Effectiveness and Quality Factor for Auger Emitters Incorporated Into Proliferating Mammalian-Cells. *Radiation Research.* 1991; 128(3):282-292.

(59) Macklis RM, Lin JY, Beresford B, Atcher RW, Hines JJ, Humm JL. Cellular kinetics, dosimetry, and radiobiology of alpha-particle radioimmunotherapy: induction of apoptosis. *Radiat Res.* 1992; 130(2):220-6.

(60) Charlton DE, Nikjoo H, Humm JL. Calculation of Initial Yields of Single-Strand and Double-Strand Breaks in Cell-Nuclei from Electrons, Protons and Alpha-Particles. *Int J Radiat Biol.* 1989; 56(1):1-19.

(61) Charlton DE, Turner MS. Use of chord lengths through the nucleus to simulate the survival of mammalian cells exposed to high LET alpha-radiation. *Int J Radiat Biol.* 1996; 69(2):213-217.

(62) Crawford-Brown DJ, Hofmann W. A generalized state-vector model for radiation-induced cellular transformation. *Int J Radiat Biol.* 1990; 57(2):407-423.

(63) Crawford-Brown DJ, Hofmann W. Correlated hit probability and cell transformation in an effect-specific track length model applied to in vitro alpha irradiation. *Radiat Environ Biophys.* 2001; 40(4):317-323.

(64) Jenner TJ, Delara CM, Oneill P, Stevens DL. Induction and Rejoining of Dna Double-Strand Breaks in V79-4 Mammalian-Cells Following Gamma-Irradiation and Alpha-Irradiation. *Int J Radiat Biol.* 1993; 64(3):265-273.

(65) Delara CM, Jenner TJ, Townsend KMS, Marsden SJ, Oneill P. The Effect of Dimethyl-Sulfoxide on the Induction of Dna Double-Strand Breaks in V79-4 Mammalian-Cells by Alpha-Particles. *Radiat Res.* 1995; 144(1):43-49.

(66) Rydberg B, Heilbronn L, Holley WR, Lobrich M, Zeitlin C, Chatterjee A et al. Spatial distribution and yield of DNA double-strand breaks induced by 3-7 MeV helium ions in human fibroblasts. *Radiat Res.* 2002; 158(1):32-42.

(67) Hoglund E, Blomquist E, Carlsson J, Stenerlow B. DNA damage induced by radiation of different linear energy transfer: initial fragmentation. *Int J Radiat Biol.* 2000; 76(4):539-547.

(68) Stenerlow B, Hoglund E, Carlsson J, Blomquist E. Rejoining of DNA fragments produced by radiations of different linear energy transfer. *Int J Radiat Biol.* 2000; 76(4):549-557.

(69) Rydberg B, Cooper B, Cooper PK, Holley WR, Chatterjee A. Dose-dependent misrejoining of radiation-induced DNA double-strand breaks in human fibroblasts: Experimental and theoretical study for high- and low-LET radiation. *Radiat Res.* 2005; 163(5):526-534.

(70) Goodhead DT, Nikjoo H. Track Structure-Analysis of Ultrasoft X-Rays Compared to High-Let and Low-Let Radiations. *Int J Radiat Biol.* 1989; 55(4):513-529.

(71) Brenner DJ, Ward JF. Constraints on Energy Deposition and Target Size of Multiply Damaged Sites Associated with Dna Double-Strand Breaks. *Int J Radiat Biol.* 1992; 61(6):737-748.

(72) Michalik V. Model of Dna Damage Induced by Radiations of Various Qualities. *Int J Radiat Biol.* 1992; 62(1):9-20.

(73) Goodhead DT. Initial Events in the Cellular Effects of Ionizing-Radiations - Clustered Damage in Dna. *Int J Radiat Biol.* 1994; 65(1):7-17.

(74) Barendsen GW. The Relationships Between Rbe and Let for Different Types of Lethal Damage in Mammalian-Cells - Biophysical and Molecular Mechanisms. *Radiat Res.* 1994; 139(3):257-270.

(75) Holthusen H. Articles on the biology of radiation effects - Analysis on nematode eggs. *Pflugers Archiv fur Die Gesamte Physiologie des Menschen und der Tiere.* 1921; 187:1-24.

(76) Thomlinson RH, Gray LH. The Histological Structure of Some Human Lung Cancers and the Possible Implications for Radiotherapy. *Br J Cancer.* 1955; 9(4):539-&.

(77) Unruh A, Ressel A, Mohamed HG, Johnson RS, Nadrowitz R, Richter E et al. The hypoxia-inducible factor-1 alpha is a negative factor for tumor therapy. *Oncogene.* 2003; 22(21):3213-3220.

(78) Ewing D, Powers EL. Oxygen-dependent sensitization of irradiated cells. In: Meyn RE, Withers HR, eds. *Radiation biology in cancer research*. New York: Raven Press; 1979:143-168.

(79) Hall EJ. *Radiobiology for the Radiologist*. Philadelphia: J.B. Lippincott Co.; 1994:118.

(80) Goodhead DT, O'Neill P, Menzel HG, editors. The separation of spatial and temporal effects of high LET radiation. 96 Sep 29; Cambridge, UK: The Royal Society of Chemistry; 1997.

(81) Hill MA, Stevens DL, Marsden SJ, Allott R, Turcu ICE, Goodhead DT. Is the increased relative biological effectiveness of high LET particles due to spatial or temporal effects? Characterization and OER in V79-4 cells. *Phys Med Biol.* 2002; 47(19):3543-3555.

(82) Machinami R, Ishikawa Y, Boecker BB. The international workshop on health effects of Thorotrast, radium, radon and other alpha-emitters 1999 - Preface. *Radiat Res.* 1999; 152(6):S1-S2.

(83) ICRP. ICRP Publication 92: Relative Biological Effectiveness (RBE), Quality Factor (Q), and Radiation Weighting Factor (wR), 92. 2004.

(84) Harrison JD, Muirhead CR. Quantitative comparisons of cancer induction in humans by internally deposited radionuclides and external radiation. *Int J Radiat Biol.* 2003; 79(1):1-13.

(85) Brown I, Mitchell JS. The development of a [At-211]-astatinated endoradiotherapeutic drug: Part IV - Late radiation effects. *Int J Radiat Oncol Biol Phys.* 1998; 40(5):1177-1183.

(86) Durbin PW, Asling CW, Johnston ME, Parrott MW, Jeung N, Williams MH et al. The Induction of Tumors in the Rat by Astatine-211. *Radiat Res.* 1958; 9(3):378-397.

(87) Yokoro K, Kunii A, Furth J, Durbin PW. Tumor Induction with Astatine-211 in Rats - Characterization of Pituitary Tumors. *Cancer Res.* 1964; 24(4P1):683-&.

(88) Mothersill C, Seymour C. Radiation-induced bystander effects: Past history and future directions. *Radiat Res.* 2001; 155(6):759-767.

(89) Moiseenko VV, Battista JJ, Hill RP, Travis EL, Van Dyk J. In-field and out-of-field effects in partial volume lung irradiation in rodents: Possible correlation between early dna damage and functional endpoints. *Int J Radiat Oncol Biol Phys.* 2000; 48(5):1539-1548.

(90) Van Luijk P, Novakova-Jiresova A, Faber H, Steneker MNJ, Kampinga HH, Meertens H et al. Relation between radiation-induced whole lung functional loss and regional structural changes in partial irradiated rat lung. *Int J Radiat Oncol Biol Phys.* 2006; 64(5):1495-1502.

(91) Murphy JB, Liu JH, Sturm E. Studies on x-ray effects. IX. The action of serum from x-rayed animals on lymphoid cells in vitro. *Journal of Experimental Medicine.* 1922; 35(3):373-U14.

(92) Parsons WB, Watkins CH, Pease GL, Childs DS. Changes in Sternal Marrow Following Roentgen-Ray Therapy to the Spleen in Chronic Granulocytic Leukemia. *Cancer.* 1954; 7(1):179-189.

(93) Nagasawa H, Little JB. Induction of Sister Chromatid Exchanges by Extremely Low-Doses of Alpha-Particles. *Cancer Res.* 1992; 52(22):6394-6396.

(94) Azzam EI, de Toledo SM, Gooding T, Little JB. Intercellular communication is involved in the bystander regulation of gene expression in human cells exposed to very low fluences of alpha particles. *Radiat Res.* 1998; 150(5):497-504.

(95) Azzam EI, de Toledo SM, Little JB. Direct evidence for the participation of gap junction-mediated intercellular communication in the transmission of damage signals from alpha-particle irradiated to nonirradiated cells. *Proc Natl Acad Sci U S A.* 2001; 98(2):473-478.

(96) Azzam EI, de Toledo SM, Little JB. Expression of CONNEXIN43 is highly sensitive to ionizing radiation and other environmental stresses. *Cancer Res.* 2003; 63(21):7128-7135.

(97) Hall EJ. The bystander effect. *Health Phys.* 2003; 85(1):31-35.

(98) Zhou HN, Randers-Pehrson G, Waldren CA, Vannais D, Hall EJ, Hei TK. Induction of a bystander mutagenic effect of alpha particles in mammalian cells. *Proc Natl Acad Sci U S A.* 2000; 97(5):2099-2104.

(99) Sawant SG, Zheng W, Hopkins KM, Randers-Pehrson G, Lieberman HB, Hall EJ. The radiation-induced bystander effect for clonogenic survival. *Radiat Res.* 2002; 157(4):361-364.

(100) Boyd M, Ross SC, Dorrens J, Fullerton NE, Tan KW, Zalutsky MR et al. Radiation-induced biologic bystander effect elicited in vitro by targeted radiopharmaceuticals labeled with alpha-, beta-, and Auger electron-emitting radionuclides. *J Nucl Med.* 2006; 47(6):1007-1015.

(101) Boyd M, Mairs RJ, Keith WN, Ross SC, Welsh P, Akabani G et al. An efficient targeted radiotherapy/gene therapy strategy utilising human tetomerase promoters and radioastatine and harnessing radiation-mediated bystander effects. *Journal of Gene Medicine.* 2004; 6(8):937-947.

(102) Persaud R, Zhou HN, Baker SE, Hei TK, Hall EJ. Assessment of low linear energy transfer radiation-induced bystander mutagenesis in a three-dimensional culture model. *Cancer Res.* 2005; 65(21):9876-9882.

(103) Bishayee A, Hill HZ, Stein D, Rao DV, Howell RW. Free radical-initiated and gap junction-mediated bystander effect due to nonuniform distribution of incorporated radioactivity in a three-dimensional tissue culture model. *Radiat Res.* 2001; 155(2):335-344.

(104) Bishayee A, Rao DV, Howell RW. Evidence for pronounced bystander effects caused by nonuniform distributions of radioactivity using a novel three-dimensional tissue culture model. *Radiat Res.* 1999; 152(1):88-97.

(105) Morgan WF, Sowa MB. Non-targeted bystander effects induced by ionizing radiation. Mutat Res. In press.

(106) Brooks AL. Evidence for 'bystander effects' in vivo. *Hum Exp Toxicol.* 2004; 23(2):67-70.

(107) Brooks AL, Retherford JC, McClellan RO. Effect of 239 PuO2 particle number and size on the frequency and distribution of chromosome aberrations in the liver of the Chinese hamster. *Radiat Res.* 1974; 59(3):693-709.

(108) Tamplin AR, Cochran TB. Radiation standards for hot particles: A report on the inadequacy of existing radiation protection standards related to internal exposures of man to insoluble particles of plutonium and other alphs-emitting hot particles. 1974. Washington, DC. Natural Resources Defense Council Report.

(109) Hall EJ, Brenner DJ. The Radiobiology of Radiosurgery - Rationale for Different Treatment Regimes for Avms and Malignancies. *Int J Radiat Oncol Biol Phys.* 1993; 25(2):381-385.

(110) Dale RG, Jones B. The assessment of RBE effects using the concept of biologically effective dose. *Int J Radiat Oncol Biol Phys.* 1999; 43(3):639-645.

(111) Takata M, Sasaki MS, Sonoda E, Morrison C, Hashimoto M, Utsumi H et al. Homologous recombination and non-homologous end-joining pathways of DNA double-strand break repair have overlapping roles in the maintenance of chromosomal integrity in vertebrate cells. *EMBO J.* 1998; 17(18):5497-5508.

(112) Oliveira NG, Castro M, Rodrigues AS, Concalves IC, Gil OM, Fernandes AP et al. Wortmannin enhances the induction of micronuclei by low and high LET radiation (vol 18, pg 37, 2003). *Mutagenesis.* 2003; 18(2):217.

(113) Oliveira NG, Castro M, Rodrigues AS, Goncalves IC, Gil OM, Fernandes AP et al. Wortmannin enhances the induction of micronuclei by low and high LET radiation. *Mutagenesis.* 2003; 18(1):37-44.

(114) Harapanhalli RS, Narra VR, Yaghmai V, Azure MT, Goddu SM, Howell RW et al. Vitamins As Radioprotectors In-Vivo .2. Protection by Vitamin-A and Soybean Oil Against Radiation-Damage Caused by Internal Radionuclides. *Radiat Res.* 1994; 139(1):115-122.

(115) Narra VR, Harapanhalli RS, Goddu SM, Howell RW, Rao DV. Radioprotection Against Biological Effects of Internal Radionuclides In-Vivo by S-(2-Aminoethyl)Isothiouronium Bromide Hydrobromide (Aet). *J Nucl Med.* 1995; 36(2):259-266.

(116) Rao DV, Howell RW, Narra VR, Govelitz GF, Sastry KSR. Invivo Radiotoxicity of Dna-Incorporated I125 Compared with That of Densely Ionizing Alpha-Particles. *Lancet.* 1989; 2(8664):650-653.

(117) Rao DV, Narra VR, Howell RW, Lanka VK, Sastry KSR. Induction of Sperm Head Abnormalities by Incorporated Radionuclides - Dependence on Subcellular-Distribution, Type of Radiation, Dose-Rate, and Presence of Radioprotectors. *Radiat Res.* 1991; 125(1):89-97.

(118) Goddu SM, Narra VR, Harapanhalli RS, Howell RW, Rao DV. Radioprotection by DMSO against the biological effects of incorporated radionuclides in vivo - Comparison with other radioprotectors and evidence for indirect action of Auger electrons. *Acta Oncol.* 1996; 35(7):901-907.

(119) Narra VR, Harapanhalli R, Howell RW, Sastry KSR, Rao DV. Vitamins As Radioprotectors In-Vivo .1. Protection by Vitamin-C Against Internal Radionuclides in Mouse Testes - Implications to the Mechanism of Damage Caused by the Auger Effect. *Radiat Res.* 1994; 137(3):394-399.

(120) Wright HA, Magee JL, Hamm RN, Chatterjee A, Turner JE, Klots CE. Calculations of Physical and Chemical-Reactions Produced in Irradiated Water Containing Dna. *Radiat Prot Dosimetry.* 1985; 13(1-4):133-136.

(121) ICRP. ICRP Publication 58: RBE for Deterministic Effects. 1990. ICRP.

(122) Schwartz JL, Rotmensch J, Atcher RW, Jostes RF, Cross FT, Hui TE et al. Interlaboratory Comparison of Different Alpha-Particle and Radon Sources - Cell-Survival and Relative Biological Effectiveness. *Health Phys.* 1992; 62(5):458-461.

(123) Jostes RF, Hui TE, James AC, Cross FT, Schwartz JL, Rotmensch J et al. Invitro Exposure of Mammalian-Cells to Radon - Dosimetric Considerations. *Radiat Res.* 1991; 127(2):211-219.

(124) Charlton DE, Utteridge TD, Allen BJ. Theoretical treatment of human haemopoietic stem cell survival following irradiation by alpha particles. *Int J Radiat Biol.* 1998; 74(1):111-8.

(125) Howell RW, Goddu SM, Narra VR, Fisher DR, Schenter RE, Rao DV. Radiotoxicity of gadolinium-148 and radium-223 in mouse testes: relative biological effectiveness of alpha-particle emitters in vivo. *Radiat Res.* 1997; 147(3):342-8.

(126) Howell RW, Rao DV, Hou DY, Narra VR, Sastry KSR. The Question of Relative Biological Effectiveness and Quality Factor for Auger Emitters Incorporated Into Proliferating Mammalian-Cells. *Radiation Research.* 1991; 128(3):282-292.

(127) Howell RW, Goddu SM, Rao DV. Design and performance characteristics of an experimental cesium-137 irradiator to simulate internal radionuclide dose rate patterns. *J Nucl Med.* 1997; 38(5):727-731.

(128) Goddu SM, Bishayee A, Bouchet LG, Bolch WE, Rao DV, Howell RW. Marrow toxicity of 33P-versus 32P-orthophosphate: implications for therapy of bone pain and bone metastases. *J Nucl Med.* 2000; 41(5):941-51.

(129) Feinendegen LE, McClure JJ. Meeting report - Alpha-emitters for medical therapy - Workshop of the United States Department of Energy - Denver, Colorado, May 30-31, 1996. *Radiat Res.* 1997; 148(2):195-201.

(130) Harrison A, Royle L. Determination of Absorbed Dose to Blood, Kidneys, Testes and Thyroid in Mice Injected with At-211 and Comparison of Testes Mass and Sperm Number in X-Irradiated and At-211 Treated Mice. *Health Phys.* 1984; 46(2):377-383.

(131) Howell RW, Azure MT, Narra VR, Rao DV. Relative biological effectiveness of alpha-particle emitters in vivo at low doses [see comments]. *Radiat Res.* 1994; 137(3):352-60.

(132) Behr TM, Behe M, Stabin MG, Wehrmann E, Apostolidis C, Molinet R et al. High-linear energy transfer (LET) alpha versus low-LET beta emitters in radioimmunotherapy of solid tumors: therapeutic efficacy and dose- limiting toxicity of 213Bi- versus 90Y-

labeled CO17-1A Fab' fragments in a human colonic cancer model. *Cancer Res.* 1999; 59(11):2635-43.

(133) Yoriyaz H, Stabin M. Electron and photon transport in a model of a 30 g mouse. *J Nucl Med.* 1997; 38(5):967.

(134) Elgqvist J, Bernhardt P, Hultborn R, Jensen H, Karlsson B, Lindegren S et al. Myelotoxicity and RBE of At-211-conjugated monoclonal antibodies compared with Tc-99m-conjugated monoclonal antibodies and Co-60 irradiation in nude mice. *J Nucl Med.* 2005; 46(3):464-471.

(135) Muthuswamy MS, Roberson PL, Buchsbaum DJ. A mouse bone marrow dosimetry model. *J Nucl Med.* 1998; 39(7):1243-7.

(136) Berger MJ. Improved Point Kernels for Electron and Beta Ray Dosimetry. 1973. Washington DC, National Bureau of Standards.

(137) ICRU. ICRU 49, Stopping Powers and Ranges for Protons and Alpha Particles. 49. 1993. Bethesda, MD, ICRU.

(138) Back T, Andersson H, Divgi CR, Hultborn R, Jensen H, Lindegren S et al. At-211 radioimmunotherapy of subcutaneous human ovarian cancer xenografts: Evaluation of relative biologic effectiveness of an alpha-emitter in vivo. *J Nucl Med.* 2005; 46(12):2061-2067.

(139) Sgouros G, Ballangrud AM, Jurcic JG, Panageas KS, McDevitt MR, Finn RD et al. Beta vs alpha-emitter dose-response analysis in patients. *J Nucl Med.* 2000; 41(5):82P.

(140) ICRP Publication 60: 1990 Recommendations of the International Commission on Rabiological Protection. *Ann ICRP.* 1991; 21(1).

(141) ICRP Publication 105: Radiological Protection in Medicine. *Annals of the ICRP.* 2008; 37(6).

(142) ICRP 92: Relative biological effectiveness (RBE), quality factor (Q), and radiation weighting factor (WR), 92. 2003.

(143) Neti PVSV, Howell RW. Biological response to nonuniform distributions of Po-210 in. *Radiat Res.* 2007; 168(3):332-340.

(144) Goddu SM, Rao DV, Howell RW. Multicellular dosimetry for micrometastases: dependence of self-dose versus cross-dose to cell nuclei on type and energy of radiation and subcellular distribution of radionuclides. *J Nucl Med.* 1994; 35(3):521-530.

(145) Charlton DE. Radiation effects in spheroids of cells exposed to alpha emitters. *Int J Radiat Biol.* 2000; 76(11):1555-1564.

(146) Akabani G, Zalutsky MR. Microdosimetry of astatine-211 using histological images: application to bone marrow. *Radiat Res.* 1997; 148(6):599-607.

(147) Humm JL, Macklis RM, Bump K, Cobb LM, Chin LM. Internal dosimetry using data derived from autoradiographs. *J Nucl Med.* 1993; 34(10):1811-7.

(148) Baxter LT, Jain RK. Transport of fluid and macromolecules in tumors. IV. A microscopic model of the perivascular distribution. *Microvasc Res.* 1991; 41(2):252-272.

(149) Jain RK, Baxter LT. Mechanisms of heterogeneous distribution of monoclonal antibodies and other macromolecules in tumors: significance of elevated interstitial pressure. *Cancer Res.* 1988; 48(24 Pt 1):7022-32.

(150) Sgouros G. Plasmapheresis in radioimmunotherapy of micrometastases: a mathematical modeling and dosimetrical analysis [see comments]. *J Nucl Med.* 1992; 33(12):2167-79.

(151) Goddu SM, Howell RL, Bouchet LG, Bolch WE, Rao DV. *MIRD Cellular S Values*. Reston VA: Society of Nuclear Medicine; 1997

(152) Goddu SM, Howell RW, Rao DV. Cellular dosimetry: absorbed fractions for monoenergetic electron and alpha particle sources and S-values for radionuclides uniformly distributed in different cell compartments. *J Nucl Med.* 1994; 35(2):303-316.

(153) Polig E. Localized alpha-dosimetry. In: Eberg MHA, ed. *Current Topics in Radiation Research*. Amsterdam: North-Holland; 1978:189-327.

(154) Rossi HH. Microdosimetric energy distribution in irradiated matter. In: Attx FH, Roesch WC, eds. *Radiation Dosimetry Vol. 1 Fundamentals*. New York: Academic Press; 1968.

(155) Roesch WC. Microdosimetry of Internal Sources. *Radiat Res.* 1977; 70(3):494-510.

(156) Fisher DR. The microdosimetry of monoclonal antibodies labeled with alpha emitters. In: Schlafke-Stelson AT, Watson EE, eds. *Fourth International Radiopharmaceutical Dosimetry Symposium*. Oak Ridge, TN: Oak Ridge Associated Universities; 1986:26-36.

(157) Stinchcomb TG, Roeske JC. Analysis of Survival of C-18 Cells After Irradiation in Suspension with Chelated and Ionic Bismuth-212 Using Microdosimetry. *Radiat Res.* 1994; 140(1):48-54.

(158) Stinchcomb TG, Roeske JC. Analytic microdosimetry for radioimmunotherapeutic alpha emitters. *Med Phys.* 1992; 19(6):1385-93.

(159) Ebert HG, editor. Analysis of patterns of energy deposition; a survey of theoretical relations in microdosimetry. Brussels: Commission of European Communities; 1970.

(160) Olko P, Booz J. Energy Deposition by Protons and Alpha-Particles in Spherical Sites of Nanometer to Micrometer Diameter. *Radiat Environ Biophys.* 1990; 29(1):1-17.

(161) Ziegler JF, Biersack JP, Littmark U. The stopping and range of ions in matter. 1985. New York, Pergamon Press.

(162) Ziegler JF. The stopping and range of ions in solids. 3-61. 1998. San Diego, Academic Press. Ion Implantation: Science and Technology.

(163) Bichsel H. Stopping powers of fast charged particles in heavy elements. 1992. Springield VA, U.S. National Technical Information Service. NIST Report IR-4550.

(164) Kellerer AM, Chmelevsky D. Criteria for Applicability of Let. *Radiat Res.* 1975; 63(2):226-234.

(165) Roeske JC, Stinchcomb TG. Dosimetric framework for therapeutic alpha-particle emitters. *J Nucl Med.* 1997; 38(12):1923-9.

(166) Loevinger R, Budinger TF, Watson EE. *MIRD Primer for Absorbed Dose Calculations, Revised Edition*. New York, NY: The Society of Nuclear Medicine, Inc.; 1991

(167) Stinchcomb TG, Roeske JC. Values of "S," <z1>, and <(z1)2> for dosimetry using alpha-particle emitters. *Med Phys.* 1999; 26(9):1960-71.

(168) Fisher DR. Specific energy distributions for alpha emitters in the dog lung. *Ann Occup Hyg.* 1988; 32 (Suppl 1):1095-1104.

(169) Humm JL. A microdosimetric model of astatine-211 labeled antibodies for radioimmunotherapy. *Int J Radiat Oncol Biol Phys.* 1987; 13(11):1767-73.

(170) Stinchcomb TG, Roeske JC. Survival of Alpha Particle Irradiated Cells as a Function of the Shape and Size of the Sensitive Volume (Nucleus). *Radiat Prot Dosimetry.* 1995; 62(3):157-164.

(171) Aubineau-Laniece I, Pihet P, Winkler R, Hofmann W, Charlton DE. Monte Carlo Code for Microdosimetry of Inhaled a Emitters. *Radiat Prot Dosimetry.* 2002; 99(1-4):463-467.

(172) Fakir H, Hofmann W, Aubineau-Laniece I. Modelling the effect of non-uniform radon progeny activities on transformation frequencies in human bronchial airways. *Radiat Prot Dosimetry.* 2006; 121(3):221-235.

(173) Fakir H, Hofmann W, Aubineau-Laniece I. Microdosimetry of radon progeny alpha particles in bronchial airway bifurcations. *Radiat Prot Dosimetry.* 2005; 117(4):382-394.

(174) Fakir H, Hofmann W, Caswell RS, Aubineau-Laniece I. Microdosimetry of inhomogeneous radon progeny distributions in bronchial airways. *Radiat Prot Dosimetry.* 2005; 113(2):129-139.

(175) Palm S, Humm JL, Rundqvist R, Jacobsson L. Microdosimetry of astatine-211 single-cell irradiation: Role of daughter polonium-211 diffusion. *Med Phys.* 2004; 31(2):218-225.

(176) Iyer R, Lehnert BE. Alpha-particle-induced increases in the radioresistance of normal human bystander cells. *Radiat Res.* 2002; 157(1):3-7.

(177) Utteridge TD, Charlton DE, Allen BJ. Monte Carlo modeling of the effects of injected short-, medium- and longer-range alpha-particle emitters on human marrow at various ages. *Radiat Res.* 2001; 156(4):413-418.

(178) ICRP. Age-dependent Doses to Members of the Public from Intake of Radionuclides: Part 2; Ingestion Dose Coefficients, ICRP Publication 67. 67. 1993. ICRP. Annalsof the ICRP.

(179) Eckerman KF, Endo A. MIRD Radionuclide Data and Decay Scheme. 2007.

(180) Browne E, Firestone RB. *Table of Radioactive Isotopes*. New York: John Wiley & Sons; 1986

(181) Lambrecht RM, Mirzadeh S, Wolf AP, Milius RA, McLaughlin WH, Bloomer WD et al. Astatine-211 - Production and Radiochemistry for the Development of Therapeutic Radiopharmaceuticals. *Abstr Pap Am Chem Soc.* 1985; 189(APR-):109-NUCL.

(182) Larsen RH, Wieland BW, Zalutsky MR. Evaluation of an internal cyclotron target for the production of At-211 via the Bi-209 (alpha,2n)At-211 reaction. *Appl Radiat Isot.* 1996; 47(2):135-143.

(183) Hadley SW, Wilbur DS, Gray MA, Atcher RW. Astatine-211 Labeling of An Antimelanoma Antibody and Its Fab Fragment Using N-Succinimidyl Para-Astatobenzoate - Comparisons Invivo with the Para-[125I]Iodobenzoyl Conjugate. *Bioconjug Chem.* 1991; 2(3):171-179.

(184) Wilbur DS, Vessella RL, Stray JE, Goffe DK, Blouke KA, Atcher RW. Preparation and Evaluation of Para-[At-211]Astatobenzoyl Labeled Antirenal Cell-Carcinoma Antibody A6H F(Ab')2 - In-Vivo Distribution Comparison with Para-[I-125]Iodobenzoyl Labeled A6H F(Ab')2. *Nucl Med Biol.* 1993; 20(8):917-927.

(185) Schwarz UP, Plascjak P, Beitzel MP, Gansow OA, Eckelman WC, Waldmann TA. Preparation of 211At-labeled humanized anti-Tac using 211At produced in disposable internal and external bismuth targets. *Nucl Med Biol.* 1998; 25(2):89-93.

(186) Lindegren S, Back T, Jensen HJ. Dry-distillation of astatine-211 from irradiated bismuth targets: a time-saving procedure with high recovery yields. *Appl Radiat Isot.* 2001; 55(2):157-160.

(187) Corson DR, MacKenzie KR, Segré E. Artificially radioactive element 85. *Phys Rev.* 1940; 58(8):672-678.

(188) Hamilton JG, Soley MH. Studies in iodine metabolism of the thyroid gland in situ by the use of radio-iodine in normal subjects and in patients with various types of goiter. *Am J Physiol.* 1940; 131(1):0135-0143.

(189) Hamilton JG, Durbin PW, Parrott M. The Accumulation and Destructive Action of Astatine211 (Eka-Iodine) in the Thyroid Gland of Rats and Monkeys. *J Clin Endocrinol Metab.* 1954; 14(10):1161-1178.

(190) McLendon RE, Archer GE, Garg PK, Bigner DD, Zalutsky MR. Radiotoxicity of systemically administered [At-211]astatide in B6C3F1 and BALB/c (nu/nu) mice: A long-term survival study with histologic analysis. *Int J Radiat Oncol Biol Phys.* 1996; 35(1):69-80.

(191) Bloomer WD, McLaughlin WH, Neirinckx RD, Adelstein SJ, Gordon PR, Ruth TJ et al. Astatine-211--tellurium radiocolloid cures experimental malignant ascites. *Science.* 1981; 212(4492):340-341.

(192) Larsen RH, Hassfjell SP, Hoff P, Alstad J, Olsen E, Vergote IB et al. At-211-Labeling of Polymer Particles for Radiotherapy - Synthesis, Purification and Stability. *J Labelled Comp Radiopharm.* 1993; 33(10):977-986.

(193) Larsen RH, Hoff P, Vergote IB, Bruland OS, Aas M, Devos L et al. Alpha-Particle Radiotherapy with At-211-Labeled Monodisperse Polymer Particles, At-Labeled Igg Proteins, and Free At-211 in A Murine Intraperitoneal Tumor-Model. *Gynecol Oncol.* 1995; 57(1):9-15.

(194) Brown I, Carpenter RN, Mitchell JS. 6-I-125-Iodo-2-Methyl-1,4-Naphthoquinol Bis (Diammonium Phosphate) As A Potential Radio-Halogenated Anticancer Agent - Invitro Investigations and Possible Clinical Implications. *Eur J Nucl Med.* 1982; 7(3):115-120.

(195) Brown I, Mitchell JS. The Development Op A [At-211]-Astatinated Endoradiotherapeutic Drug .2. Therapeutic Results for Transplanted Adenocarcinoma of the Rectum in Mice and Associated Studies. *International Journal of Radiation Oncology Biology Physics.* 1994; 29(1):115-124.

(196) Brown I, Carpenter RN, Mitchell JS. The Development of A [At-211]-Astatinated Endoradiotherapeutic Drug .1. Localization by Alpha-Particle Autoradiography in A Murine Tumor-Model. *Int J Radiat Oncol Biol Phys.* 1992; 23(3):563-572.

(197) Brown I, Carpenter RN, Link E, Mitchell JS. Potential Diagnostic and Therapeutic Agents for Malignant-Melanoma - Synthesis of Heavy Radiohalogenated Derivatives of Methylene-Blue by Electrophilic and Nucleophilic Methods. *J Radioanalytic Nucl Chem-Let.* 1986; 107(6):337-351.

(198) Link EM, Brown I, Carpenter RN, Mitchell JS. Uptake and Therapeutic Effectiveness of I-125 Methylene and At-211 Methylene Blue for Pigmented Melanoma in An Animal-Model System. *Cancer Res.* 1989; 49(15):4332-4337.

(199) Link EM, Carpenter RN. At-211-Methylene Blue for Targeted Radiotherapy of Human-Melanoma Xenografts - Treatment of Micrometastases. *Cancer Res.* 1990; 50(10):2963-2967.

(200) Link EM, Carpenter RN. Astatine-211-Methylene Blue for Targeted Radiotherapy of Human-Melanoma Xenografts - Treatment of Cutaneous Tumors and Lymph-Node Metastases. *Cancer Res.* 1992; 52(16):4385-4390.

(201) Vaidyanathan G, Larsen RH, Zalutsky MR. 5-[At-211]astato-2'-deoxyuridine, an alpha-particle-emitting endoradiotherapeutic agent undergoing DNA incorporation. *Cancer Res.* 1996; 56(6):1204-1209.

(202) Walicka MA, Vaidyanathan G, Zalutsky MR, Adelstein SJ, Kassis AI. Survival and DNA damage in Chinese hamster V79 cells exposed to alpha particles emitted by DNA-incorporated astatine-211. *Radiat Res.* 1998; 150(3):263-268.

(203) Vaidyanathan G, Zalutsky MR. Preparation of 5-[I-131]Iodo- and 5-[At-211]astato-1-(2-deoxy-2-fluoro-beta-D-arabinofuranosyl)uracil by a halodestannylation reaction. *Nucl Med Biol.* 1998; 25(5):487-496.

(204) Vaidyanathan G, Zalutsky MR. 1-(M-[At-211]Astatobenzyl)Guanidine - Synthesis Via Astato Demetalation and Preliminary Invitro and Invivo Evaluation. *Bioconjug Chem.* 1992; 3(6):499-503.

(205) Vaidyanathan G, Strickland DK, Zalutsky MR. Meta-[(211)At]Astatobenzylguanidine - Further Evaluation of A Potential Therapeutic Agent. *Int J Cancer.* 1994; 57(6):908-913.

(206) Strickland DK, Vaidyanathan G, Zalutsky MR. Cytotoxicity of Alpha-Particle-Emitting M-[At-211] Astatobenzylguanidine on Human Neuroblastoma-Cells. *Cancer Res.* 1994; 54(20):5414-5419.

(207) Vaidyanathan G, Friedman HS, Keir ST, Zalutsky MR. Evaluation of meta-[At-211]astatobenzylguanidine in an athymic mouse human neuroblastoma xenograft model. *Nucl Med Biol.* 1996; 23(6):851-856.

(208) Vaidyanathan G, Zhao XG, Larsen RH, Zalutsky MR. 3-[At-211]astato-4-fluorobenzylguanidine: a potential therapeutic agent with prolonged retention by neuroblastoma cells. *Br J Cancer.* 1997; 76(2):226-233.

(209) Vaidyanathan G, Affleck DJ, Zalutsky MR. No-carrier-added (4-fluoro-3-[I-131]iodobenzyl)guanidine and (3-[At-211]astato-4-fluorobenzyl) guanidine. *Bioconjug Chem.* 1996; 7(1):102-107.

(210) Murud KM, Larsen RH, Hoff P, Zalutsky MR. Synthesis, purification, and in vitro stability of At-211- and I-125-labeled amidobisphosphonates. *Nucl Med Biol.* 1999; 26(4):397-403.

(211) Murud KM, Larsen RH, Bruland OS, Hoff P. Influence of pretreatment with 3-amino-1-hydroxypropylidene-1,1-bisphosphonate (APB) on organ uptake of At-211 and I-125-labeled amidobisphosphonates in mice. *Nucl Med Biol.* 1999; 26(7):791-794.

(212) Aaij C, Tschroots WR, Lindner L, Feltkamp TE. Preparation of Astatine Labeled Proteins. *Int J Appl Radiat Isot.* 1975; 26(1):25-&.

(213) Visser GWM, Diemer EL, Kaspersen FM. Preparation and Stability of Astato-Tyrosine and Astato-Iodotyrosine. *Int J Appl Radiat Isot.* 1979; 30(12):749-752.

(214) Friedman AM, Zalutsky MR, Wung W, Buckingham F, Harper PV, Scherr GH et al. Preparation of A Biologically Stable and Immunogenically Competent Astatinated Protein. *Int J Nucl Med Biol.* 1977; 4(3-4):219-&.

(215) Zalutsky MR, Narula AS. Astatination of Proteins Using An N-Succinimidyl Tri-Normal-Butylstannyl Benzoate Intermediate. *Appl Radiat Isot.* 1988; 39(3):227-232.

(216) Zalutsky MR, Garg PK, Friedman HS, Bigner DD. Labeling monoclonal antibodies and F(ab')2 fragments with the alpha- particle-emitting nuclide astatine-211: preservation of immunoreactivity and in vivo localizing capacity. *Proc Natl Acad Sci U S A.* 1989; 86(18):7149-53.

(217) Larsen RH, Bruland OS, Hoff P, Alstad J, Lindmo T, Rofstad EK. Inactivation of human osteosarcoma cells in vitro by 211At-TP-3 monoclonal antibody: comparison with astatine-211-labeled bovine serum albumin, free astatine-211 and external-beam X rays. *Radiat Res.* 1994; 139(2):178-84.

(218) Hauck ML, Larsen RH, Welsh PC, Zalutsky MR. Cytotoxicity of alpha-particle-emitting astatine-211-labelled antibody in tumour spheroids: no effect of hyperthermia. *Br J Cancer.* 1998; 77(5):753-9.

(219) Garg PK, Bigner DD, Zalutsky MR. Tumour dose enhancement via improved antibody radiohalogenation. In: Epenetos AA, ed. *Monoclonal Antibodies-Applications in Clinical Oncology*. London: Chapman and Hall; 1991:103-114.

(220) Reist CJ, Foulon CF, Alston K, Bigner DD, Zalutsky MR. Astatine-211 labeling of internalizing anti-EGFRvIII monoclonal antibody using N-succinimidyl 5-[At-211]astato-3-pyridinecarboxylate. *Nucl Med Biol.* 1999; 26(4):405-411.

(221) Wikstrand CJ, Hale LP, Batra SK, Hill ML, Humphrey PA, Kurpad SN et al. Monoclonal-Antibodies Against Egfrviii Are Tumor-Specific and React with Breast and Lung Carcinomas and Malignant Gliomas. *Cancer Res.* 1995; 55(14):3140-3148.

(222) Zalutsky MR, Stabin MG, Larsen RH, Bigner DD. Tissue distribution and radiation dosimetry of astatine-211-labeled chimeric 81C6, an alpha-particle-emitting immunoconjugate. *Nucl Med Biol.* 1997; 24(3):255-261.

(223) McLendon RE, Archer GE, Larsen RH, Akabani G, Bigner DD, Zalutsky MR. Radiotoxicity of systemically administered At-211-labeled human/mouse chimeric monoclonal antibody: A long-term survival study with histologic analysis. *Int J Radiat Oncol Biol Phys.* 1999; 45(2):491-499.

(224) Zalutsky MR, McLendon RE, Garg PK, Archer GE, Schuster JM, Bigner DD. Radioimmunotherapy of neoplastic meningitis in rats using an alpha- particle-emitting immunoconjugate. *Cancer Res.* 1994; 54(17):4719-25.

(225) Zalutsky MR, Schuster JM, Garg PK, Archer GE, Jr., Dewhirst MW, Bigner DD. Two approaches for enhancing radioimmunotherapy: alpha emitters and hyperthermia. *Recent Results Cancer Res.* 1996; 141:101-22.

(226) Elgqvist J, Andersson H, Back T, Claesson I, Hultborn R, Jensen H et al. alpha-Radioimmunotherapy of intraperitoneally growing OVCAR-3 tumors of variable dimensions: Outcome related to measured tumor size and mean absorbed dose. *J Nucl Med.* 2006; 47(8):1342-1350.

(227) Elgqvist J, Andersson H, Back T, Hultborn R, Jensen H, Karlsson B et al. Therapeutic efficacy and tumor dose estimations in radioimmunotherapy of intraperitoneally growing OVCAR-3 cells in nude mice with At-211-labeled monoclonal antibody MX35. *J Nucl Med.* 2005; 46(11):1907-1915.

(228) Elgqvist J, Andersson H, Back T, Claesson I, Hultborn R, Jensen H et al. Fractionated radio immunotherapy of intraperitoneally growing ovarian cancer in nude mice with At-211-MX35 F(ab ')(2): therapeutic efficacy and myelotoxicity. *Nucl Med Biol.* 2006; 33(8):1065-1072.

(229) Hamilton JG, Durbin PW, Parrott MW. Accumulation of Astatine211 by Thyroid Gland in Man. *Proc Soc Exp Biol Med.* 1954; 86(2):366-369.

(230) Doberenz I, Doberenz W, Wunderlich G, Franke WG, Heidelbach JG, Fischer S et al. Endoarterial theraphy of lingual carcinoma using 211At-labelled-Human Serum Albumin-Microspheres - Preliminary clinical experience. *NUC Compact.* 1990; 21(4):124-127.

(231) Zalutsky MR, Reardon DA, Akabani G, Friedman AH, Herndon JE. Astatine-211 labeled human/mouse chimeric anti-tenascin monoclonal antibody via surgically created resection cavities for patients with recurrent glioma: Phase I study. [abstract]. *Neuro-oncol.* 2002; 4:S10.

(232) Zalutsky MR, Pozzi OR. Radioimmunotherapy with alpha-particle emitting radionuclides. *Q J Nucl Med Mol Imaging.* 2004; 48(4):289-296.

(233) Weber DA, Eckerman KF, Dillman LT, Ryman JC. *MIRD: Radionuclide Data and Decay Schemes*. New York: The Society of Nuclear Medicine; 1989

(234) Atcher RW, Friedman AM, Hines JJ. An Improved Generator for the Production of Pb-212 and Bi-212 from Ra-224. *Appl Radiat Isot.* 1988; 39(4):283-286.

(235) Nicoline M, Mazzi U, editors. Therapeutic potential of alpha-emitters: Chemistry to biology to clinical applications. Padova, Italy: SGE Editorali; 1999.

(236) Kozak RW, Atcher RW, Gansow OA, Friedman AM, Hines JJ, Waldmann TA. Bismuth-212-Labeled Anti-Tac Monoclonal-Antibody - Alpha-Particle-Emitting Radionuclides As Modalities for Radioimmunotherapy. *Proceedings of the National Academy of Sciences of the United States of America.* 1986; 83(2):474-478.

(237) Brechbiel MW, Gansow OA, Atcher RW, Schlom J, Esteban J, Simpson DE et al. Synthesis of 1-(Para-Isothiocyanatobenzyl) Derivatives of Dtpa and Edta - Antibody Labeling and Tumor-Imaging Studies. *Inorg Chem.* 1986; 25(16):2772-2781.

(238) Brechbiel MW, Pippin CG, McMury TJ, Milenic D, Roselli M, Colcher D et al. An effective chelating agent for labeling of monoclonal antibody with 212Bi for alpha-particle mediated radioimmunotherapy. *J Chem Soc Chem Commun.* 1991; 17:1169-1170.

(239) Brechbiel MW, Gansow OA. Synthesis of C-functionalzied trans-cyclohexyldiethylenetriaminepenta-acetic acids for labeling of monoclonal antibodies with bismuth-212 alpha-particle emitter. *J Chem Soc Perkin Trans I.* 1992; 1:1173-1178.

(240) Junghans RP, Dobbs D, Brechbiel MW, Mirzadeh S, Raubitschek AA, Gansow OA et al. Pharmacokinetics and bioactivity of 1,4,7,10-tetra-azacylododecane off',N",N"'-tetraacetic acid (DOTA)-bismuth-conjugated anti-Tac antibody for alpha-emitter (212Bi) therapy. *Cancer Res.* 1993; 53(23):5683-9.

(241) Milenic DE, Roselli M, Mirzadeh S, Pippin CG, Gansow OA, Colcher D et al. In vivo evaluation of bismuth-labeled monoclonal antibody comparing DTPA-derived bifunctional chelates. *Cancer Biother Radiopharm.* 2001; 16(2):133-146.

(242) Jones SB, Tiffany LJ, Garmestani K, Gansow OA, Kozak RW. Evaluation of dithiol chelating agents as potential adjuvants for anti-IL-2 receptor lead or bismuth alpha radioimmunotherapy. *Nucl Med Biol.* 1996; 23(2):105-113.

(243) Huneke RB, Pippin CG, Squire RA, Brechbiel MW, Gansow OA, Strand M. Effective alpha-particle-mediated radioimmunotherapy of murine leukemia. *Cancer Res.* 1992; 52(20):5818-20.

(244) Hartmann F, Horak EM, Garmestani K, Wu C, Brechbiel MW, Kozak RW et al. Radioimmunotherapy of nude mice bearing a human interleukin 2 receptor alpha-expressing lymphoma utilizing the alpha-emitting radionuclide- conjugated monoclonal antibody 212Bi-anti-Tac. *Cancer Res.* 1994; 54(16):4362-70.

(245) Rotmensch J, Whitlock JL, Schwartz JL, Hines JJ, Reba RC, Harper PV. In vitro and in vivo studies on the development of the alpha-emitting radionuclide bismuth 212 for intraperitoneal use against microscopic ovarian carcinoma. *Am J Obstet Gynecol.* 1997; 176(4):833-840.

(246) Macklis RM, Beresford BA, Lin JY, Atcher RW, Humm JL. Murine Hematopoietic Ablation by Alpha-Particle-Emitting Radiopharmaceuticals - A Potential Preparative Regimen for Bone-Marrow Transplantation. *Int J Oncol.* 1993; 2(4):711-715.

(247) Hassfjell S, Brechbiel MW. The development of the alpha-particle emitting radionuclides Bi-212 and Bi-213, and their decay chain related radionuclides, for therapeutic applications. *Chem Rev.* 2001; 101(7):2019-2036.

(248) Hassfjell SP, Bruland OS, Hoff P. Bi-212-DOTMP: An alpha particle emitting bone-seeking agent for targeted radiotherapy. *Nucl Med Biol.* 1997; 24(3):231-237.

(249) Miao Y, Hylarides M, Fisher DR, Shelton T, Moore H, Wester DW et al. Melanoma therapy via peptide-targeted {alpha}-radiation. *Clin Cancer Res.* 2005; 11(15):5616-5621.

(250) Hui TE, Fisher DR, Kuhn JA, Williams LE, Nourigat C, Badger CC et al. A mouse model for calculating cross-organ beta doses from yttrium-90- labeled immunoconjugates. *Cancer.* 1994; 73(3 Suppl):951-7.

(251) Jurcic JG, Larson SM, Sgouros G, McDevitt MR, Finn RD, Divgi CR et al. Targeted at particle immunotherapy for myeloid leukemia. *Blood.* 2002; 100(4):1233-1239.

(252) Sgouros G, Ballangrud AM, Jurcic JG, McDevitt MR, Humm JL, Erdi YE et al. Pharmacokinetics and dosimetry of an alpha-particle emitter labeled antibody: 213Bi-HuM195 (anti-CD33) in patients with leukemia. *J Nucl Med.* 1999; 40(11):1935-46.

(253) McDevitt MR, Finn RD, Sgouros G, Ma D, Scheinberg DA. An 225Ac/213Bi generator system for therapeutic clinical applications: construction and operation. *Appl Radiat Isot.* 1999; 50(5):895-904.

(254) Nikula TK, McDevitt MR, Finn RD, Wu C, Kozak RW, Garmestani K et al. Alpha-emitting bismuth cyclohexylbenzyl DTPA constructs of recombinant humanized anti-CD33 antibodies: pharmacokinetics, bioactivity, toxicity and chemistry. *J Nucl Med.* 1999; 40(1):166-76.

(255) Nikula TK, Curcio MJ, Brechbiel MW, Gansow OA, Finn RD, Scheinberg DA. A Rapid, Single-Vessel Method for Preparation of Clinical Grade Ligand Conjugated Monoclonal-Antibodies. *Nucl Med Biol.* 1995; 22(3):387-390.

(256) McDevitt MR, Finn RD, Ma D, Larson SM, Scheinberg DA. Preparation of alpha-emitting 213Bi-labeled antibody constructs for clinical use. *J Nucl Med.* 1999; 40(10):1722-7.

(257) Davis IA, Kennel SJ. Radioimmunotherapy using vascular targeted 213Bi: the role of tumor necrosis factor alpha in the development of pulmonary fibrosis. *Clin Cancer Res.* 1999; 5(10 Suppl):3160s-3164s.

(258) Kennel SJ, Boll R, Stabin M, Schuller HM, Mirzadeh S. Radioimmunotherapy of micrometastases in lung with vascular targeted 213Bi. *Br J Cancer.* 1999; 80(1-2):175-84.

(259) Kennel SJ, Lankford T, Davern S, Foote L, Taniguchi K, Ohizumi I et al. Therapy of rat tracheal carcinoma IC-12 in SCID mice: vascular targeting with [Bi-213]-MAb TES-23. *Eur J Cancer.* 2002; 38(9):1278-1287.

(260) Kennel SJ, Stabin M, Yoriyaz H, Brechbiel MW, Mirzadeh S. Treatment of lung tumor colonies with 90Y targeted to blood vessels: comparison with the alpha-particle emitter 213Bi. *Nucl Med Biol.* 1999; 26(1):149-57.

(261) McDevitt MR, Barendswaard E, Ma D, Lai L, Curcio MJ, Sgouros G et al. An alpha-particle emitting antibody ([213Bi]J591) for radioimmunotherapy of prostate cancer. *Cancer Res.* 2000; 60(21):6095-100.

(262) Li Y, Rizvi SM, Ranson M, Allen BJ. 213Bi-PAI2 conjugate selectively induces apoptosis in PC3 metastatic prostate cancer cell line and shows anti-cancer activity in a xenograft animal model. *Br J Cancer.* 2002; 86(7):1197-1203.

(263) Miederer M, Seidl C, Beyer GJ, Charlton DE, Vranjes-Duric S, Comor JJ et al. Comparison of the radiotoxicity of two alpha-particle-emitting immunoconjugates, terbium-149 and bismuth-213, directed against a tumor-specific, exon 9 deleted (d9) E-cadherin adhesion protein. *Radiat Res.* 2003; 159(5):612-620.

(264) Ballangrud AM, Yang WH, Charlton DE, McDevitt MR, Hamacher KA, Panageas KS et al. Response of LNCaP spheroids after treatment with an alpha-particle emitter (213Bi)-labeled anti-prostate-specific membrane antigen antibody (J591). *Cancer Res.* 2001; 61(5):2008-14.

(265) Kennel SJ, Stabin M, Roeske JC, Foote LJ, Lankford PK, Terzaghi-Howe M et al. Radiotoxicity of bismuth-213 bound to membranes of monolayer and spheroid cultures of tumor cells. *Radiat Res.* 1999; 151(3):244-56.

(266) Adams GP, Shaller CC, Chappell LL, Wu C, Horak EM, Simmons HH et al. Delivery of the alpha-emitting radioisotope bismuth-213 to solid tumors via single-chain Fv and diabody molecules. *Nucl Med Biol.* 2000; 27(4):339-346.

(267) Yao Z, Zhang M, Garmestani K, Axworthy DB, Mallett RW, Fritzberg AR et al. Pretargeted alpha emitting radioimmunotherapy using (213)Bi 1,4,7,10-tetraazacyclododecane-N,N',N",N"'-tetraacetic acid-biotin. *Clin Cancer Res.* 2004; 10(9):3137-3146.

(268) Senekowitsch-Schmidtke R, Schuhmacher C, Becker KF, Nikula TK, Seidl C, Becker I et al. Highly specific tumor binding of a Bi-213-labeled monoclonal antibody against mutant E-cadherin suggests its usefulness for locoregional alpha-radioimmunotherapy of diffuse-type gastric cancer. *Cancer Res.* 2001; 61(7):2804-2808.

(269) Bloechl S, Beck R, Seidl C, Morgenstern A, Schwaiger M, Senekowitsch-Schmidtke R. Fractionated locoregional low-dose radioimmunotherapy improves survival in a mouse model of diffuse-type gastric cancer using a Bi-213-conjugated monoclonal antibody. *Clin Cancer Res.* 2005; 11(19):7070S-7074S.

(270) Seidl C, Schrock H, Seidenschwang S, Beck R, Schmid E, Abend M et al. Cell death triggered by alpha-emitting Bi-213-immunoconjugates in HSC45-M2 gastric cancer cells is different from apoptotic cell death. *Eur J Nucl Med Mol Imaging.* 2005; 32(3):274-285.

(271) Milenic DE, Garmestani K, Brady ED, Albert PS, Ma DS, Abdulla A et al. Targeting of HER2 antigen for the treatment of disseminated peritoneal disease. *Clin Cancer Res.* 2004; 10(23):7834-7841.

(272) Milenic D, Garmestani K, Dadachova E, Chappell L, Albert P, Hill D et al. Radioimmunotherapy of human colon carcinoma xenografts using a Bi-213-labeled domain-deleted humanized monoclonal antibody. *Cancer Biother Radiopharm.* 2004; 19(2):135-147.

(273) Michel RB, Rosario AV, Brechbiel MW, Jackson TJ, Goldenberg DM, Mattes MJ. Experimental therapy of disseminated B-Cell lymphoma xenografts with Bi-213-labeled anti-CD74. *Nucl Med Biol.* 2003; 30(7):715-723.

(274) Li Y, Wang J, Rizvi SMA, Jager MJ, Conway RM, Billson FA et al. In vitro targeting of NG2 antigen by Bi-213-9.2.27 alpha-immunoconjugate induces cytotoxicity in human uveal melanoma cells. *Invest Ophthalmol Vis Sci.* 2005; 46(12):4365-4371.

(275) Rizvi SMA, Qu CF, Song YJ, Raja C, Allen BJ. In vivo studies of pharmacokinetics and efficacy of bismuth-213 labeled antimelanoma monoclonal antibody 9.2.27. *Cancer Biol Ther.* 2005; 4(7):763-768.

(276) Allen BJ, Rizvi SM, Tian Z. Preclinical targeted alpha therapy for subcutaneous melanoma. *Melanoma Res.* 2001; 11(2):175-182.

(277) Song YJ, Qu CF, Rizvi SMA, Li Y, Robertson G, Raja C et al. Cytotoxicity of PAI2, C595 and Herceptin vectors labeled with the alpha-emitting radioisotope Bismuth-213 for ovarian cancer cell monolayers and clusters. *Cancer Lett.* 2006; 234(2):176-183.

(278) Qu CF, Song EY, Li Y, Rizvi SMA, Raja C, Smith R et al. Pre-clinical study of Bi-213 labeled PAI2 for the control of micrometastatic pancreatic cancer. *Clin Exp Metastasis.* 2005; 22(7):575-586.

(279) Qu CF, Li Y, Song YJ, Rizvi SMA, Raja C, Zhang D et al. MUC1 expression in primary and metastatic pancreatic cancer cells for in vitro treatment by Bi-213-C595 radioimmunoconjugate. *Br J Cancer.* 2004; 91(12):2086-2093.

(280) Allen BJ, Tian Z, Rizvi SMA, Li Y, Ranson M. Preclinical studies of targeted alpha therapy for breast cancer using Bi-213-labelled-plasminogen activator inhibitor type 2. *Br J Cancer.* 2003; 88(6):944-950.

(281) Allen BJ, Raja C, Rizvi S, Li Y, Tsui W, Zhang D et al. Targeted alpha therapy for cancer. *Phys Med Biol.* 2004; 49(16):3703-3712.

(282) Li Y, Rizvi SMA, Blair JM, Cozzi PJ, Qu CF, Ow KT et al. Antigenic expression of human metastatic prostate cancer cell lines for in vitro multiple-targeted alpha-therapy with (213)bi-conjugates. *Int J Radiat Oncol Biol Phys.* 2004; 60(3):896-908.

(283) Rizvi SMA, Li Y, Song EYJ, Qu CF, Raja C, Morgenstern A et al. Preclinical studies of Bismuth-213 labeled plasminogen activator inhibitor type 2 (PAI2) in a prostate cancer nude mouse xenograft model. *Cancer Biol Ther.* 2006; 5(4):386-393.

(284) Qu CF, Song YJ, Rizvi SMA, Li Y, Smith R, Perkins AC et al. In vivo and in vitro inhibition of pancreatic cancer growth by targeted alpha therapy using Bi-213-CHX.A"-C595. *Cancer Biol Ther.* 2005; 4(8):848-853.

(285) McDevitt MR, Barendswaard E, Ma D, Lai L, Curcio MJ, Sgouros G et al. An alpha-particle emitting bismuth-213 labeled antibody (J591) to the external domain of prostate specific membrane antigen. *Cancer Res.* 2000; 60:6095-6100.

(286) Norenberg JP, Krenning BJ, Konings IRHM, Kusewitt DF, Nayak TK, Anderson TL et al. Bi-213-[DOTA(0),Tyr(3)]octreotide peptide receptor radionuclide therapy of pancreatic tumors in a preclinical animal model. *Clin Cancer Res.* 2006; 12(3):897-903.

(287) Zhang ML, Yao ZS, Garmestani K, Axworthy DB, Zhang Z, Mallett RW et al. Pretargeting radioinimunotherapy of a murine model of adult T-cell leukemia with the alpha-emitting radionuclide, bismuth 213. *Blood.* 2002; 100(1):208-216.

(288) Sandmaier BM, Bethge WA, Wilbur DS, Hamlin DK, Santos EB, Brechbiel MW et al. Bismuth 213-labeled anti-CD45 radioimmunoconjugate to condition dogs for nonmyeloablative allogeneic marrow grafts. *Blood.* 2002; 100(1):318-326.

(289) Bethge WA, Wilbur DS, Storb R, Hamlin DK, Santos EB, Brechbiel MW et al. Radioimmunotherapy with bismuth-213 as conditioning for nonmyeloablative allogeneic hematopoietic cell transplantation in dogs: A dose deescalation study. *Transplantation.* 2004; 78(3):352-359.

(290) Song H, Shahverdi K, Huso DL, Esaias C, Fox J, Liedy A et al. Bi-213 (alpha-emitter)-antibody targeting of breast cancer metastases in the neu-N transgenic mouse model. *Cancer Res.* 2008; 68(10):3873-3880.

(291) Song H, Shahverdi K, Fox J, Wang Y, Gimi B, Pomper M et al. A model of metastatic breast carcinoma for targeted alpha-emitter therapy modeling/dosimetry studies. *Cancer Biother Radiopharm.* 2004; 19(4):518.

(292) Dadachova E, Nakouzi A, Bryan RA, Casadevall A. Ionizing radiation delivered by specific antibody is therapeutic against a fungal infection. *Proc Natl Acad Sci U S A.* 2003; 100(19):10942-10947.

(293) Dadachova E, Casadevall A. Treatment of infection with radiolabeled antibodies. *Q J Nucl Med.* 2006; 50(3):193-204.

(294) Sgouros G. Single-cell targeting with Bi-213-labeled antibodies: A microdosimetric analysis. *J Nucl Med.* 1998; 39:111P.

(295) Mulford DA, Pandit-Taskar N, McDevitt MR, Finn RD, Weiss MA, Apostolidis C et al. Sequential therapy with cytarabine and bismuth-213 (Bi-213)-labeled-HuM195 (anti-CD33) for acute myeloid leukemia (AML). *Blood.* 2004; 104(11):496A.

(296) Heeger S, Moldenhauer G, Egerer G, Wesch H, Martin S, Nikula T et al. Alpha-radioimmunotherapy of B-lineage non-Hodgkin's lymphoma using 213Bi-labelled anti-CD19-and anti-CD20-CHX-A "-DTPA conjugates. *Abstr Pap Am Chem Soc.* 2003; 225:U261.

(297) Phase I clinical study on alpha-therapy for Non Hodgkin Lymphoma. 04 Jun 28; Dusseldorf, Germany.: 2004.

(298) Kneifel S, Cordier D, Good S, Ionescu MCS, Ghaffari A, Hofer S et al. Local targeting of malignant gliomas by the diffusible peptidic vector 1,4,7,10-tetraazacyclododecane-1-glutaric acid-4,7,10-triacetic acid-substance P. *Clin Cancer Res.* 2006; 12(12):3843-3850.

(299) Allen BJ, Raja C, Rizvi S, Li Y, Tsui W, Graham P et al. Intralesional targeted alpha therapy for metastatic melanoma. *Cancer Biol Ther.* 2005; 4(12):1318-1324.

(300) Anonymous. Methods for the production of Ac-225 and Bi-213 for alpha immunotherapyy, ITU Annual Report 1995-(EUR 16368). 55-56. 1995. ITU. Basic Actinide Research.

(301) Mirzadeh S. Generator-produced alpha-emitters. *Appl Radiat Isot.* 1998; 49(4):345-349.

(302) Production of Bi-213 and Ac-225. 97 Oct 27; Karlsruhe, Germany: 1997.

(303) Boll RA, Malkemus D, Mirzadeh S. Production of actinium-225 for alpha particle mediated radioimmunotherapy. *Appl Radiat Isot.* 2005; 62(5):667-679.

(304) Apostolidis C, Molinet R, Rasmussen G, Morgenstern A. Production of Ac-225 from Th-229 for targeted alpha therapy. *Anal Chem.* 2005; 77(19):6288-6291.

(305) Khalkin VA, Tsupko-Sitnikov VV, Zaitseva NG. Radionuclides for radiotherapy. Properties, preparation, and application of actinium-225. *Radiochemistry.* 1997; 39(6):483-492.

(306) Lambrecht RM, Tomiyoshi K, Sekine T. Radionuclide generators. *Radiochimica Acta.* 1997; 77(1-2):103-123.

(307) Apostolidis C, Molinet R, McGinley J, Abbas K, Mollenbeck J, Morgenstern A. Cyclotron production of Ac-225 for targeted alpha therapy. *Appl Radiat Isot.* 2005; 62(3):383-387.

(308) Taylor DM. Metabolism of Actinium in Rat. *Health Phys.* 1970; 19(3):411-8.

(309) Kaspersen FM, Bos E, Doornmalen AV, Geerlings MW, Apostolidis C, Molinet R. Cytotoxicity of 213Bi- and 225Ac-immunoconjugates. *Nucl Med Commun.* 1995; 16(6):468-76.

(310) Beyer GJ, Offord R, Kunzi G, Aleksandrova Y, Ravn U, Jahn S et al. The influence of EDTMP-concentration on the biodistribution of radio- lanthanides and 225-Ac in tumor-bearing mice. The ISOLDE Collaboration. *Nucl Med Biol.* 1997; 24(5):367-72.

(311) Davis IA, Glowienka KA, Boll RA, Deal KA, Brechbiel MW, Stabin M et al. Comparison of 225actinium chelates: tissue distribution and radiotoxicity. *Nucl Med Biol.* 1999; 26(5):581-9.

(312) Deal KA, Davis IA, Mirzadeh S, Kennel SJ, Brechbiel MW. Improved in vivo stability of actinium-225 macrocyclic complexes. *J Med Chem.* 1999; 42(15):2988-92.

(313) Chappell LL, Deal KA, Dadachova E, Brechbiel MW. Synthesis, conjugation, and radiolabeling of a novel bifunctional chelating agent for 225Ac radioimmunotherapy applications. *Bioconjug Chem.* 2000; 11(4):510-519.

(314) Kennel SJ, Chappell LL, Dadachova K, Brechbiel MW, Lankford TK, Davis IA et al. Evaluation of 225Ac for vascular targeted radioimmunotherapy of lung tumors [In Process Citation]. *Cancer Biother Radiopharm.* 2000; 15(3):235-44.

(315) Kennel SJ, Brechbiel MW, Milenic DE, Schlom J, Mirzadeh S. Actinium-225 conjugates of MAb CC49 and humanized delta CH2CC49. *Cancer Biother Radiopharm.* 2002; 17(2):219-31.

(316) Borchardt PE, Yuan RR, Miederer M, McDevitt MR, Scheinberg DA. Targeted actinium-225 in vivo generators for therapy of ovarian cancer. *Cancer Res.* 2003; 63(16):5084-5090.

(317) Miederer M, McDevitt MR, Sgouros G, Kramer K, Cheung NK, Scheinberg DA. Pharmacokinetics, dosimetry, and toxicity of the targetable atomic generator, 225Ac-HuM195, in nonhuman primates. *J Nucl Med.* 2004; 45(1):129-137.

(318) Miederer M, McDevitt MR, Borchardt P, Bergman I, Kramer K, Cheung NKV et al. Treatment of neuroblastoma meningeal carcinomatosis with intrathecal application of ?-emitting atomic nanogenerators targeting disialo-ganglioside GD2. *Clin Cancer Res.* 2004; 10(20):6985-6992.

(319) Yuan RR, Wong P, McDevitt MR, Doubrovina E, Leiner I, Bornmann W et al. Targeted deletion of T-cell clones using alpha-emitting suicide MHC tetramers. *Blood.* 2004; 104(8):2397-2402.

(320) Ballangrud AM, Yang WH, Palm S, Enmon R, Borchardt PE, Pellegrini VA et al. Alpha-Particle Emitting Atomic Generator (Actinium-225)-Labeled Trastuzumab (Herceptin) Targeting of Breast Cancer Spheroids: Efficacy versus HER2/neu Expression. *Clin Cancer Res.* 2004; 10(13):4489-4497.

(321) Sofou S, Thomas JL, Lin HY, McDevitt MR, Scheinberg DA, Sgouros G. Engineered Liposomes for Potential {alpha}-Particle Therapy of Metastatic Cancer. *J Nucl Med.* 2004; 45(2):253-260.

(322) Sofou S, Enmon RM, McDevitt MR, Jaggi J, Thomas JL, Scheinberg DA et al. Multivesicular radioimmunoliposomes with encapsulated actinium-225 for targeted alpha-particle therapy of intraperitoneal micrometastatic cancer. *Cancer Biother Radiopharm.* 2004; 19(4):518-519.

(323) Chang MY, Seideman J, Sofou S. Enhanced loading efficiency and retention of Ac-225 in rigid liposomes for potential targeted therapy of micrometastases. *Bioconjug Chem.* 2008; 19(6):1274-1282.

(324) Sofou S, Kappel BJ, Jaggi J, McDevitt MR, Scheinberg DA, Sgouros G. Enhanced Retention of the alpha-particle Emitting Daughters of Actinium-225 by Liposome Carriers. *Bioconjug Chem.* 2007;In Press.

(325) Miederer M, Henriksen G, Alke A, Mossbrugger I, Quintanilla-Martinez L, Senekowitsch-Schmidtke R et al. Preclinical evaluation of the alpha-particle generator nuclide Ac-225 for somatostatin receptor radiotherapy of neuroendocrine tumors. *Clin Cancer Res.* 2008; 14(11):3555-3561.

(326) Jaggi JS, Kappel BJ, McDevitt MR, Sgouros G, Flombaum CD, Cabassa C et al. Efforts to control the errant products of a targeted in vivo generator. *Cancer Res.* 2005; 65(11):4888-4895.

(327) Jaggi JS, Seshan SV, McDevitt MR, LaPerle K, Sgouros G, Scheinberg DA. Renal tubulointerstitial changes after internal irradiation with ?-particle-emitting actinium daughters. *J Am Soc Nephrol.* 2005; 16(9):2677-2689.

(328) Jaggi JS, Seshan SV, McDevitt MR, Sgouros G, Hyjek E, Scheinberg DA. Mitigation of radiation nephropathy after internal ?-particle irradiation of kidneys. *Int J Radiat Biol.* 2006; 64(5):1503-1512.

(329) Finn R, McDevitt M, Sheh Y, Lom C, Qiao J, Cai S et al. Cyclotron production of cesium radionuclides as analogues for francium-221 biodistribution. *Nucl Instrum Methods Phys Res B.* 2005; 241(1-4):649-651.

(330) Hamacher KA, Sgouros G. A schema for estimating absorbed dose to organs following the administration of radionuclides with multiple unstable daughters: a matrix approach. *Med Phys.* 1999; 26(12):2526-8.

(331) Rowland RE. *Radium in Humans: A Review of U.S. Studies*. Chicago, IL: University of Chicago Press; 1994

(332) ICRP. ICRP Publication 20. Alkaline Earth Metabolism in AdultMan. 1973. Oxford, Pergamon Press.

(333) Johnson JR, Myers RC. Alkaline earth metabolism: A model useful in calculating organ burdens, excretion rates and committed effective dose equivalent conversion factors. *Radiat Prot Dosimetry.* 1981; 1(2):87-95.

(334) Harrison GE, Carr TE, Sutton A. Distribution of radioactive calcium, strontium, barium and radium following intravenous injection into a healthy man. *Int J Radiat Biol Relat Stud Phys Chem Med.* 1967; 13(3):235-247.

(335) Leggett RW. A generic age-specific biokinetic model for calcium-like elements. *Radiat Prot Dosimetry.* 1992; 41:183-198.

(336) Leggett RW, Eckerman KF, Williams LR. An elementary method for implementing complex biokinetic models. *Health Phys.* 1993; 64(3):260-271.

(337) Polig E, Lloyd RD, Bruenger FW, Miller SC. Biokinetic model of radium in humans and beagles. *Health Phys.* 2004; 86(1):42-55.

(338) Durbin PW, Asling CW, Jeung N, Williams MH, Post J, Johnston ME et al. The metabolism and toxicity of radium-223 in rats. UCRL-8189. 1958. Berkely, CA, University of California Radiation Laboratory.

(339) Henriksen G, Breistol K, Bruland OS, Fodstad O, Larsen RH. Significant antitumor effect from bone-seeking, alpha-particle-emitting Ra-223 demonstrated in an experimental skeletal metastases model. *Cancer Res.* 2002; 62(11):3120-3125.

(340) Henriksen G, Fisher DR, Roeske JC, Bruland OS, Larsen RH. Targeting of osseous sites with alpha-emitting Ra-223: Comparison with the beta-emitter Sr-89 in mice. *J Nucl Med.* 2003; 44(2):252-259.

(341) Fisher DR, Sgouros G. Dosimetry of radium-223 and progeny. In: Stelson AT, Stabin MG, Sparks RB, eds. Gatlinburg, TN: US Dept of Energy & Oak Ridge Assoc. Universities; 1999:375-391.

(342) Bruland OS, Nilsson S, Fisher DR, Larsen RH. High-linear energy transfer irradiation targeted to skeletal metastases by the alpha-emitter Ra-223: Adjuvant or alternative to conventional modalities? *Clin Cancer Res.* 2006; 12(20):6250S-6257S.

(343) Nilsson S, Larsen RH, Fossa? SD, Balteskard L, Borch KW, Westlin JE et al. First clinical experience with ?-emitting radium-223 in the treatment of skeletal metastases. *Clin Cancer Res.* 2005; 11(12):4451-4459.

(344) Nilsson S, Franzen L, Parker C, Tyrrell C, Blom R, Tennvall J et al. Bone-targeted radium-223 in symptomatic, hormone-refractory prostate cancer: a randomised, multicentre, placebo-controlled phase II study. *Lancet Oncol.* 2007; 8(7):587-594.

(345) Toth KS, Rasmussen JO. Studies of Rare Earth Alpha-Emitters. *Phys Rev.* 1958; 109(1):121-125.

(346) Allen BJ, Blagojevic N. Alpha- and beta-emitting radiolanthanides in targeted cancer therapy: The potential role of terbium-149. *Nucl Med Commun.* 1996; 17(1):40-47.

(347) Allen BJ, Goozee G, Sarkar S, Beyer G, Morel C, Byrne AP. Production of terbium-152 by heavy ion reactions and proton induced spallation. *Appl Radiat Isot.* 2001; 54(1):53-58.

(348) Rizvi SMA, Allen BJ, Tian Z, Goozee G, Sarkar S. In vitro and preclinical studies of targeted alpha therapy (TAT) for colorectal cancer. *Colorectal Dis.* 2001; 3(5):345-353.

(349) Beyer GJ. Radioactive ion beams for biomedical research and nuclear medical application. *Hyperfine Interact.* 2000; 129(1-4):529-553.

(350) Beyer GJ, Comor JJ, Dakovic M, Soloviev D, Tamburella C, Hageb E et al. Production routes of the alpha emitting 149Tb for medical application. *Radiochim Acta.* 2002; 90(5):247-252.

(351) Imam SK, Allen BJ, Goozee G, Sarkar S, Hersey P. In vitro & in vivo studies with Tb-152 and Sm-153 RICs of the melanoma antibody 9.2.27. *Melanoma Res.* 1997; 7:S35.

(352) Allen BJ, Rizvi S, Li Y, Tian Z, Ranson M. In vitro and preclinical targeted alpha therapy for melanoma, breast, prostate and colorectal cancers. *Crit Rev Oncol Hematol.* 2001; 39(1-2):139-146.

(353) Dahle J, Borrebaek J, Melhus KB, Bruland OS, Salberg G, Olsen DR et al. Initial evaluation of (227)Th-p-benzyl-DOTA-rituximab for low-dose rate alpha-particle radioimmunotherapy. *Nucl Med Biol.* 2006; 33(2):271-279.

(354) Henriksen G, Bruland OS, Larsen RH. Thorium and actinium polyphosphonate compounds as bone-seeking alpha particle-emitting agents. *Anticancer Res.* 2004; 24(1):101-105.

(355) Dahle J, Borrebaek J, Jonasdottir TJ, Hjelmerud AK, Melhus KB, Bruland OS et al. Targeted cancer therapy with a novel low dose rate alpha-emitting radioimmunoconjugate. *Blood.* 2007; 110(6):2049-2056.

(356) Muller WA, Nenot JC, Daburon ML, Lafuma J. Metabolic and dosimetric studies after inhalation of 227Th in rats with regard to the risk of lung and bone tumors. *Radiat Environ Biophys.* 1975; 11(4):309-311.

(357) Gossner W, Hug O, Luz A, Muller WA. Experimental induction of bone tumors by short-lived bone-seeking radionuclides. *Recent Results Cancer Res.* 1976;(54):36-49.

(358) Muller WA, Gossner W, Hug O, Luz A. Late effects after incorporation of the short-lived alpha-emitters 224Ra and 227Th in mice. *Health Phys.* 1978; 35(1):33-55.

(359) Luz A, Muller WA, Linzner U, Strauss PG, Schmidt J, Muller K et al. Bone tumor induction after incorporation of short-lived radionuclides. *Radiat Environ Biophys.* 1991; 30(3):225-227.

(360) Muller WA. Studies on Short-Lived Internal Alpha-Emitters in Mice and Rats .2. Th-227. *Int J Radiat Biol Relat Stud Phys Chem Med.* 1971; 20(3):233-43.

(361) Washiyama K, Amano R, Sasaki J, Kinuya S, Tonami N, Shiokawa Y et al. 227Th-EDTMP: a potential therapeutic agent for bone metastasis. *Nucl Med Biol.* 2004; 31(7):901-908.

(362) Sgouros G. Long-lived alpha emitters in radioimmunotherapy: the mischievous progeny. *Cancer Biother Radiopharm.* 2000; 15(3):219-21.

(363) Hamacher KA, Den RB, Den EI, Sgouros G. Cellular dose conversion factors for alpha-particle-emitting radionuclides of interest in radionuclide therapy. *J Nucl Med.* 2001; 42(8):1216-1221.

(364) Siegel JA, Thomas SR, Stubbs JB, Stabin MG, Hays MT, Koral KF et al. MIRD pamphlet no. 16: Techniques for quantitative radiopharmaceutical biodistribution data acquisition and analysis for use in human radiation dose estimates. *J Nucl Med.* 1999; 40(2):37S-61S.

(365) Schlafke-Stelson AT, Watson EE, editors. Treatment planning for internal emitter therapy: Methods, applications and clinical implications. 96 May 7; Oak Ridge, TN: Oak Ridge Associated Universities; 1999.

(366) Sgouros G. Radioimmunotherapy of Micrometastases. In: Riva P, ed. *Cancer Radioimmunotherapy - Present and Future*. Newark, NJ: Harwood Academic Publishers; 1998:191-207.

(367) Kirschner AS, Ice RD, Beierwaltes WH. Radiation-Dosimetry of I-131-19-Iodocholesterol - Pitfalls of Using Tissue Concentration Data - Reply. *J Nucl Med.* 1975; 16(3):248-249.

(368) Patton PW, Rajon DA, Shah AP, Jokisch DW, Inglis BA, Bolch WE. Site-specific variability in trabecular bone dosimetry: considerations of energy loss to cortical bone. *Med Phys.* 2002; 29(1):6-14.

(369) Bolch WE, Patton PW, Rajon DA, Shah AP, Jokisch DW, Inglis BA. Considerations of marrow cellularity in 3-dimensional dosimetric models of the trabecular skeleton. *J Nucl Med.* 2002; 43(1):97-108.

(370) Shah AP, Patton PW, Rajon DA, Bolch WE. Adipocyte spatial distributions in bone marrow: implications for skeletal dosimetry models. *J Nucl Med.* 2003; 44(5):774-783.

(371) Shah AP, Rajon DA, Patton PW, Jokisch DW, Bolch WE. Accounting for beta-particle energy loss to cortical bone via paired-image radiation transport (PIRT). *Med Phys.* 2005; 32(5):1354-1366.

(372) Watchman CJ, Jokisch DW, Patton PW, Rajon DA, Sgouros G, Bolch WE. Absorbed fractions for alpha-particles in tissues of trabecular bone: Considerations of marrow cellularity within the ICRP reference male. *J Nucl Med.* 2005; 46(7):1171-1185.

(373) Bolch WE, Eckerman KF, Sgouros G, Thomas SR. MIRD Pamphlet No. 21: A Generalized Schema for Radiopharmaceutical Dosimetry--Standardization of Nomenclature. *J Nucl Med.* 2009; 50(3):477-484.

(374) Snyder WS, Fisher HL, Ford MR, Warner GG. Estimates of absorbed fractions for monoenergetic photon sources uniformly distributed in various organs of a heterogeneous phantom. *J Nucl Med.* 1969; 10(3S):7-52.

(375) Bouchet LG, Jokisch DW, Bolch WE. A three-dimensional transport model for determining absorbed fractions of energy for electrons within trabecular bone. *J Nucl Med.* 1999; 40(11):1947-1966.

(376) Snyder WS, Ford MR, Warner GG. Estimates of specific absorbed fractions for photon sources uniformly distributed in various organs of a heterogeneous phantom. MIRD Pamphlet No. 5, Revised, 5-67. 1978. The Society of Nuclear Medicine. 1978.

(377) Sgouros G, Howell RW, Bolch WE, Fisher DR. MIRD Commentary: Proposed Name for a Dosimetry Unit Applicable to Deterministic Biological Effects--The Barendsen (Bd). *J Nucl Med.* 2009; 50(3):485-487.

(378) Sgouros G, Song H. Cancer stem cell targeting using the alpha-particle emitter, 213Bi: mathematical modeling and feasibility analysis. *Cancer Biother Radiopharm.* 2008; 23(1):74-81.

(379) Roeske JC, Stinchcomb TG. The average number of alpha-particle hits to the cell nucleus required to eradicate a tumour cell population. *Phys Med Biol.* 2006; 51(9):N179-N186.

(380) Munro TR, Gilbert CW. The Relation Between Tumour Lethal Doses and the Radiosensitivity of Tumour Cells. *Br J Radiol.* 1961; 34(400):246-251.

(381) Shepard HM, Lewis GD, Sarup JC, Fendly BM, Maneval D, Mordenti J et al. Monoclonal antibody therapy of human cancer: taking the HER2 protooncogene to the clinic. *J Clin Immunol.* 1991; 11(3):117-127.

(382) ICRP 89: Basic anatomical and physiological data for use in radiological protection: Reference values. Valentin J, editor. 2005. Pergamon. Annals of the ICRP.

(383) Sgouros G. Bone marrow dosimetry for radioimmunotherapy: theoretical considerations. *J Nucl Med.* 1993; 34(4):689-694.

(384) Snyder WS, Cook MJ, Nasset ES, Karhausen LR, Howells GP, Tipton IH. Report of the task group on reference man, ICRP publication 23. 1975. Elmsford, NY, International Commission on Radiological Protection.

(385) Hartsock RJ, Smith EB, Petty CS. Normal Variations with Aging of Amount of Hematopoietic Tissue in Bone Marrow from Anterior Iliac Crest - A Study Made from 177 Cases of Sudden Death Examined by Necropsy. *Am J Clin Pathol.* 1965; 43(4):326-31.

(386) Sgouros G, Bolch WE, Shah A, Watchman CJ, Jurcic JG, Scheinberg DA. Relative biological effectiveness for efficacy and toxicity in leukemia patients of the alpha-particle emitter, bismuth-213. *Cancer Biother Radiopharm.* 2006; 21(4):397-398.

(387) Heeger S, Moldenhauer G, Egerer G, Wesch H, Martin S, Nikula T et al. Alpha-radioimmunotherapy of B-lineage non-Hodgkin's lymphoma using 213Bi-labelled anti-CD19-and anti-CD20-CHX-A "-DTPA conjugates. *Abstracts of Papers of the American Chemical Society.* 2003; 225:U261.

Tables

Table 1 – Summary of recently reported clinical trials using alpha-particle emitters

Radionuclide	Delivery vehicle	Cancer	Comments	reference
^{211}At	Anti-Tenascin IgG	Glioblastoma Multiforme (GBM)	On-going Phase I using surgical cavity injection of labeled anti-Tenascin IgG, median survival 60 wks, 2 patients with recurrent GBM survived nearly 3 years.	(*15*)
	MX35 $F(ab')_2$	Ovarian	On-going Phase I using MX35 $F(ab')_2$, BM, peritoneal absorbed dose = 0.08, 8 mGy/MBq, respectively	(*17*)
^{213}Bi	Anti-CD33 IgG	Leukemia (AML or CML)	Phase I completed with no toxicity, substantial reduction in circulating and BM blasts. Phase I/II in cytoreduced patients, 4/23 very high risk patients showed lasting CRs (up to 12 months).	(*12,22*)
	Anti-neurokinin receptor peptide	glioblastoma	2 patients treated with ^{213}Bi, one w/ oligodendroglioma treated by distillation in resection cavity alive more than 67 months	(*298*)
	Anti CD20 IgG (Rituximab)	Relapsed/refractory Non-Hodgkin's lymphoma (NHL)	Phase I study, 9 patients treated to date	(*387*)
	9.2.27 IgG	melanoma	16 patients, intralesional administration led to massive tumor cell kill and resolution of lesions; significant decline in serum marker melanoma-inhibitory-activity protein (MIA) at 2 weeks post-treatment was observed.	(*299*)
^{223}Ra	$RaCl_2$	Skeletal breast and prostate cancer metastases	Phase IA dose-escalation studies completed involving single-dose infusion of 46 to 250 kBq/kg in 25 patients with no dose-limiting hematological toxicity. Phase IB study in six patients to evaluate repeated injections (two or five fractions) totaling up to 250 kBq/kg. Phase II randomized trial in 33 metastatic breast or prostate cancer patients with external beam plus saline or four times 50 kBq/kg ^{223}Ra at 4-week intervals; shows significant (-66%) decrease in bone alkaline	(*342,344*)

			phosphatase compared to placebo and 15 of 31 patients with PSA decrease >50% PSA reduction from baseline vs 5 of 28 in the control group.	
^{225}Ac	Anti-CD33 IgG	AML	Phase I trial, on-going, at first dose-level of 0.5 μCi/kg (18.5 kBq/kg), one of 2 patients reported had elimination of peripheral blasts and a reduction in marrow blasts.	(*22*)

Table 2 – Alpha-particle beam findings that are also applicable to internally administered alpha-particle emitters

1. RBE>1 for cell sterilization, chromosomal damage/cancer induction relative to low LET radiation
2. Reduced susceptibility to modulation by radiosensitizers and radioprotectors
3. Reduced capacity to repair sub-lethal damage
4. Higher induction of double-strand DNA breaks at low total absorbed doses
5. Monoexponential surviving fraction curve after uniform irradiation (absence of a shoulder)

Table 3 – RBE values for testicular sperm head survival

Radionuclide	initial alpha-particle energy (MeV)	RBE at D_0	Reference
^{148}Gd*	3.2	7.4 ± 2.4	(*125*)
^{210}Po*	5.3	6.7 ± 1.4	(*116*)
^{212}Bi†	6.0	6.0	(*131*)
^{212}Po†	8.8	4.6	(*131*)

*Citrate

†In equilibrium with the parent, ^{212}Pb, and with its daughters, ^{212}Bi, ^{212}Po and ^{208}Tl.

Table 4 – RBE values for radioimmunotherapy studies, *in vivo*

Radionuclide	biological end-point	reference radiation	RBE	Reference
^{213}Bi (Fab')	MTD (marrow)	^{90}Y (Fab')	≈1	(*132*)
^{213}Bi (Fab')	tumor growth delay	^{90}Y (Fab')	2-14	(*132*)
^{211}At (IgG)	WBC reduction	whole-body ^{60}Co	5.0 ± 0.9	(*134*)
^{211}At (IgG)	WBC reduction	^{99m}Tc (F(ab')$_2$)	3.4 ± 0.6	(*134*)
^{211}At (F(ab')$_2$)	tumor growth delay	whole-body ^{60}Co	4.8 ± 0.7	(*138*)
^{213}Bi (IgG)	nadir duration,	^{90}Y (IgG)	≈1	(*139*)
^{213}Bi (IgG)	leukemia reduction	^{90}Y (IgG)	≈1	(*139*)

Table 5 – Tumor Control Probabilities for simulated targeting analysis

	TCP			
N (cell number)	10^2	10^4	10^5	10^8
0.5 x 10^6 sites/cell	1	0.99	0.87	0
0.5 x 10^6 sites/cell ± 10%*	1	0.97	0.71	0
0.5 x 10^6 sites/cell ± 25%	0.98	0.04	0	0
1 x 10^6 sites/cell	1	1	1	1
1 x 10^6 sites/cell ± 10%	1	1	1	0.99
1 x 10^6 sites/cell ± 25%	1	0.49	0.002	0

*Standard deviation

Table 6. Electron emissions considered in the absorbed dose calculations; mean energy and range values are listed for beta emissions. The dominant contributors to electron absorbed dose are shown in bold.

	ELECTRONS					
ISOTOPE	Energy (keV)	Isotope % per disint.	Effective % per disint.	Mean energy (keV/disint.)	Δ^e (Gy-kg/Bq-s)	Elec. range (mm)
Bi-213	200	0.20	0.20	0.40	6.41E-17	0.5
Bi-213	347	2.55	2.55	8.85	1.42E-15	1.4
Bi-213	423	0.40	0.40	1.69	2.71E-16	1.9
Bi-213 (beta)	**444**	**97.80**	**97.80**	**434.23**	**6.96E-14**	2.1
Tl-209 (beta)	659	100.00	2.20	14.50	2.32E-15	4.2
Pb-209 (beta)	**198**	**100.00**	**100.00**	**198.00**	**3.17E-14**	0.5
SUM				657.67	1.05E-13	

Table 7. Alpha particle emissions considered in the absorbed dose calculations.

	ALPHA PARTICLES					
ISOTOPE	Energy (keV)	Isotope % per disint.	Effective % per disint.	Mean energy (keV/disint.)	Δ^α (Gy-kg/Bq-s)	Alpha range (μm)
Bi-213	5549	0.16	0.16	8.88	1.42E-15	42.0
Bi-213	5869	2.01	2.01	117.97	1.89E-14	45.5
Po-213	7614	0.003	0.003	0.22	3.58E-17	66.0
Po-213	8375	100.00	97.80	8190.75	1.31E-12	75.6
SUM				8317.82	1.33E-12	

Table 8. Individual photon S-factors and summed photon S-factor used for ^{213}Bi photon dosimetry (26).

ISOTOPE	Photon Energy (keV)	S-factor (Gy/MBq-s)
Bi-213	440	5.78E-11
Bi-213	79	9.84E-13
Tl-209	117	1.60E-12
Tl-209	467	6.71E-12
Tl-209	1566	2.37E-11
SUM=$S_{WB\leftarrow WB}$		9.08E-11

Figures

Figure 1

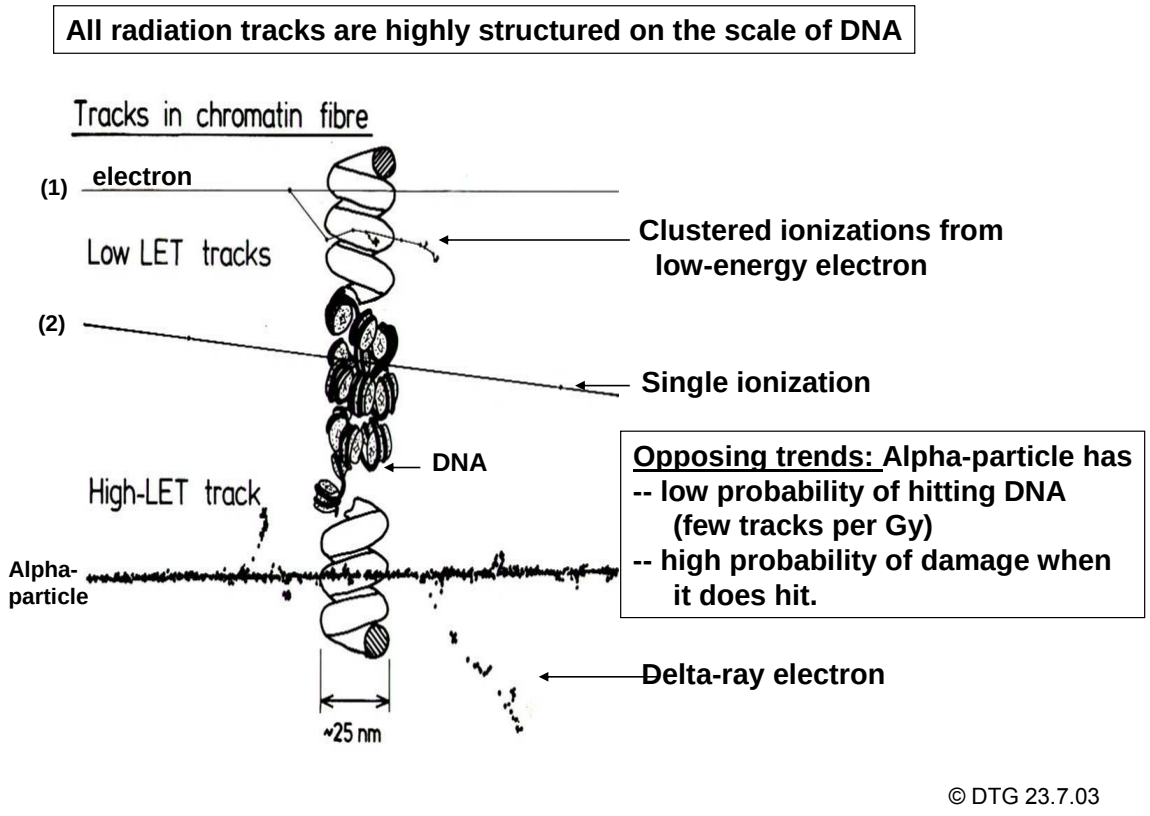

Fig. 1 – Illustration of difference in ionization density between low and high LET tracks. (from D.T.Goodhead, CERRIE Workshop 2003; with permission).

Figure 2

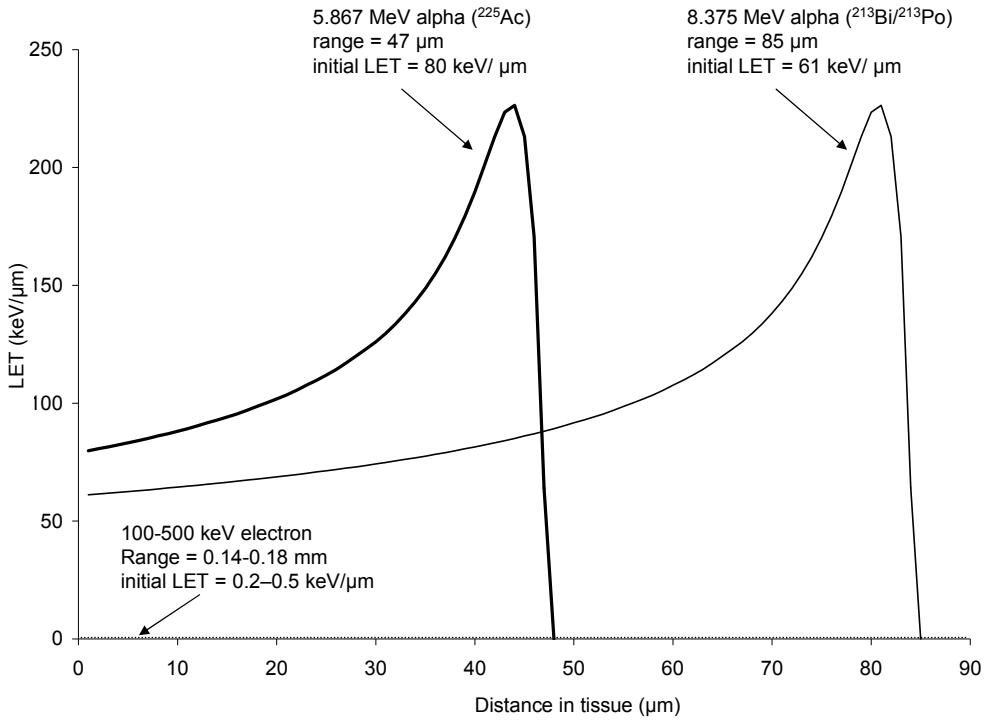

Fig. 2 – LET vs distance traveled in tissue for alpha-particles with two different initial kinetic energies. Note that alpha-particles emitted with a lower initial energy are closer to their Bragg peak and, therefore, start out with a higher LET. The LET of electrons with initial energy of 100 to 500 keV is also shown at the bottom of the plot for comparision. The plot was generated using data from ICRU 49 (*137*).

Figure 3

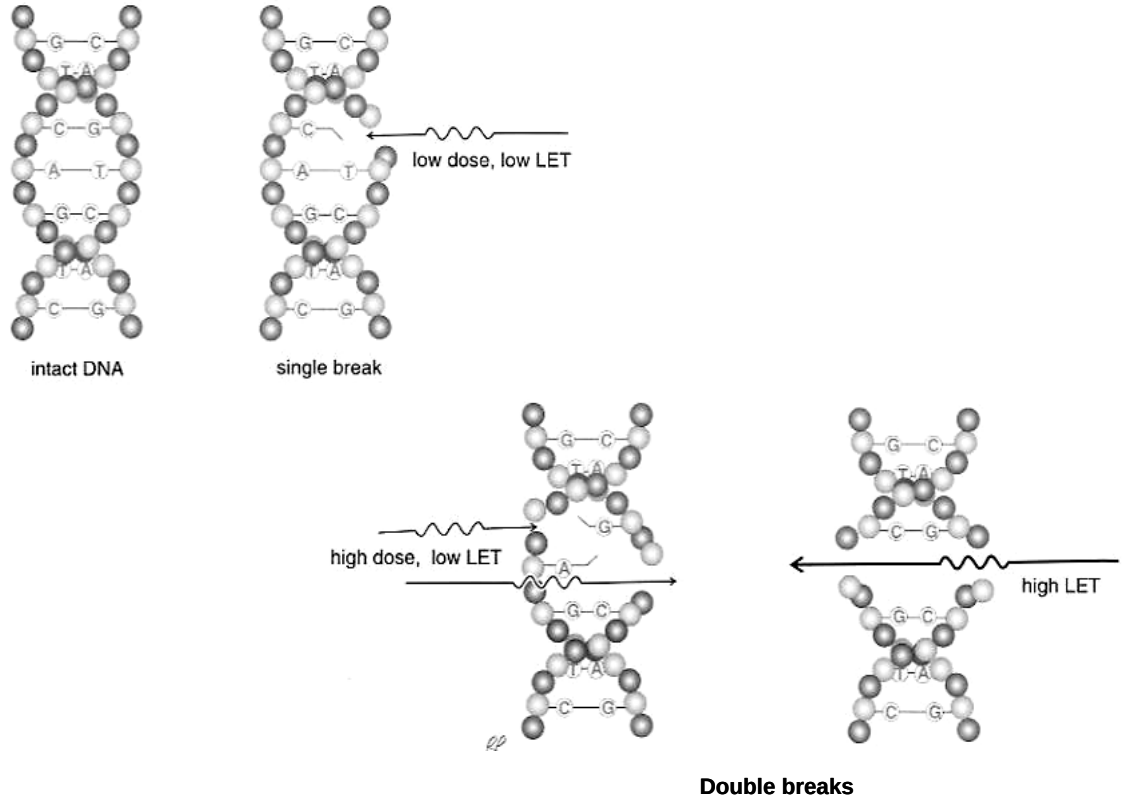

Figure 3 – Single high LET track has a high probability of yielding a double-strand DNA break while probability of DSB induction with low LET tracks becomes comparable only at higher absorbed doses. (Figure from Essentials of Nuclear Medicine Physics, Powsner RA and Powsner ER, Blackwell Science, Inc., Malden MA, 1998)

Figure 4

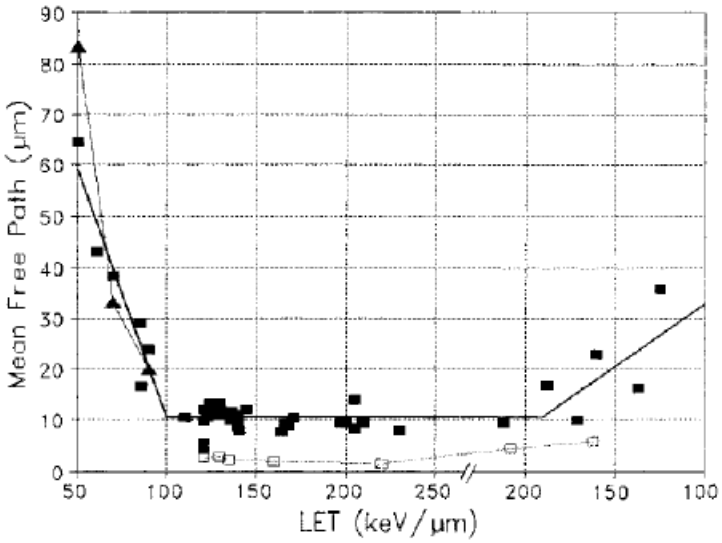

Figure 4 – Dependence of mean free path on LET. Note that LET is plotted (*e.g.*, from 200 to 100 keV/μm after 250 keV/μm) so that the stopping powers on the low energy side of the Bragg peak can be identified ((from Charlton DE, et al. Int J Radiat Biol 69:213-217, 1996.)

Figure 5

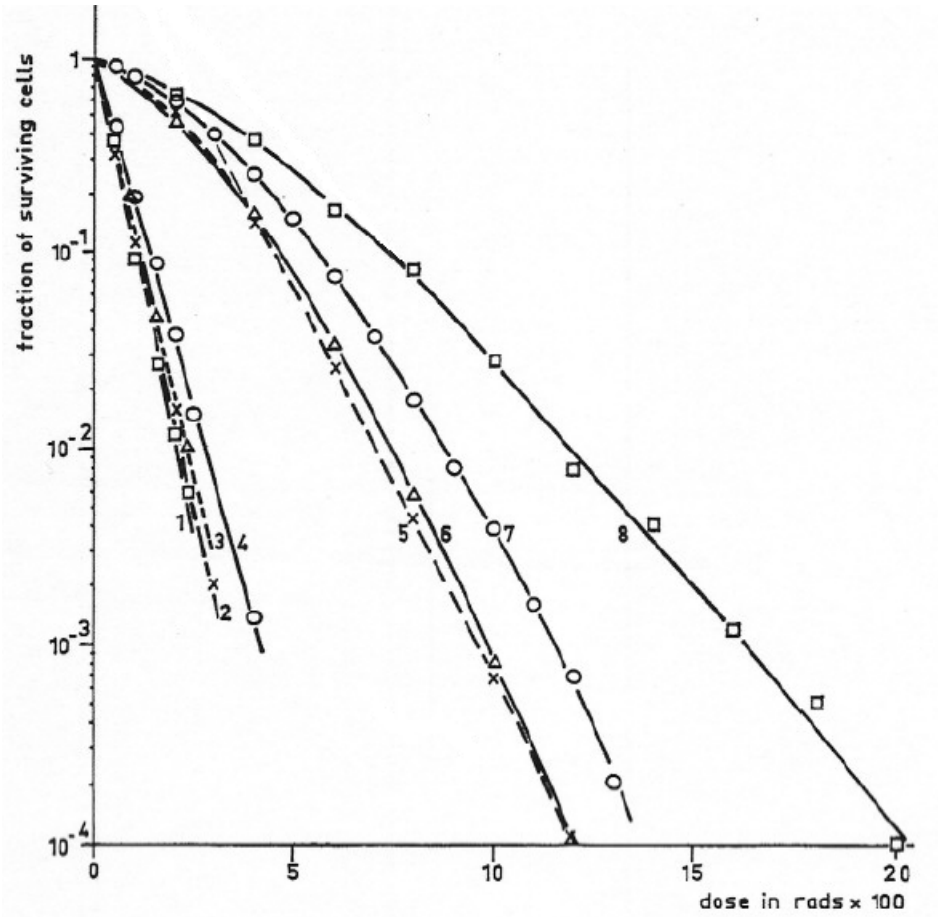

Figure 5 – Survival curves obtained with different cell lines and ^{210}Po alphas (1-4) or 250 kVp X-rays (5-8). 1 and 8: R_1 cells derived from a rhabdomyosarcoma of a rat. 2 and 5: sub-line of the human kidney cell line T_1 with a mean chromosome number of 121. 3 and 6: sub-line of T_1 with 62 chromosomes. 4 and 7: sub-line of T_1 with 63 chromosomes. (adapted from Barendsen GW in Theoretical and Experimental Biophysics, Cole A, editor, Marcel Dekker, Inc. New York, 1967)

Figure 6

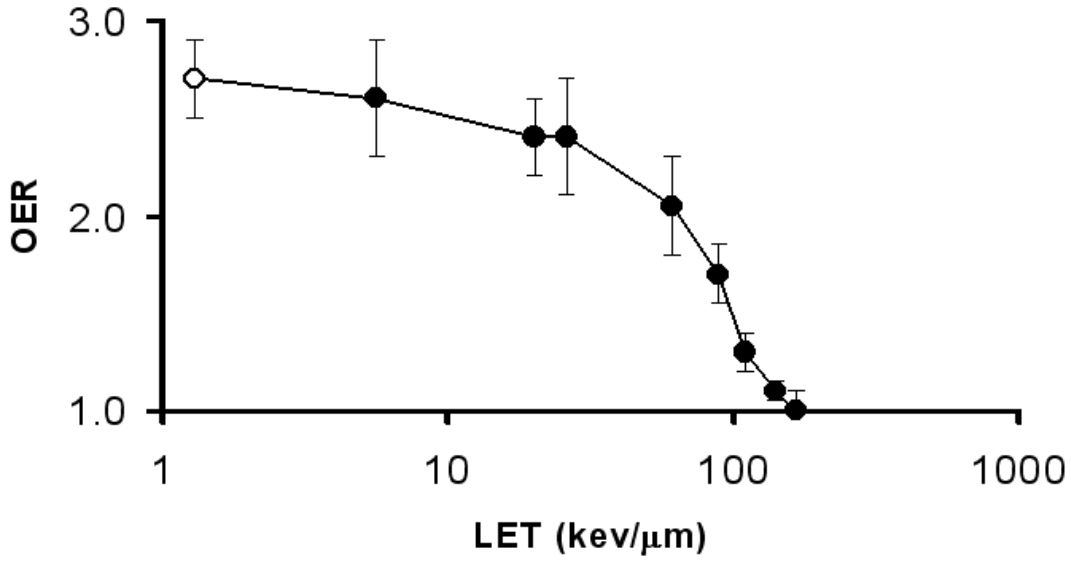

Figure 6 – OER as a function of LET. OER was measured using cultured human kidney derived cells incubated in air or nitrogen. Closed circles correspond to alpha-particles of different energies generated by cyclotron. The open circle corresponds to 250 kVp X-rays (average LET ≈ 1.3 keV/μm). (Data re-plotted from Barendsen, et al., Int J Radiat Biol 10:317-327, 1966.)

Figure 7

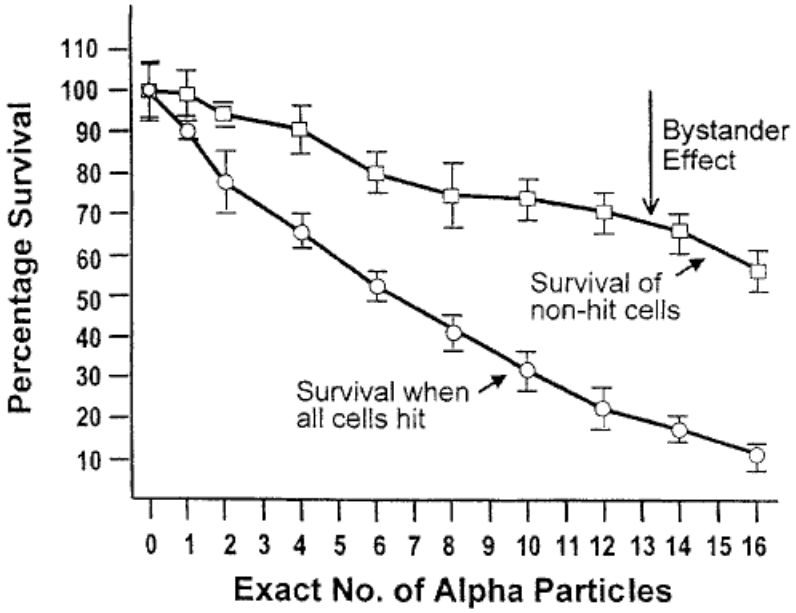

Figure 7 – Illustration of the bystander effect. The square symbols correspond to cell survival of non-hit cells when 10% of the cells in the dish are hit with a defined number of alpha-particles (circles). Since the results are normalized to plating efficiency, survival below 100% for the non-hit cells reflects a bystander effect. In this study, the effect appears to be dose dependent; the alpha-particles were aimed at the centroid of the nucleus of each of the targeted cells. (From Hall EJ. The Bystander Effect. Health Phys 85:2003).

Figure 8

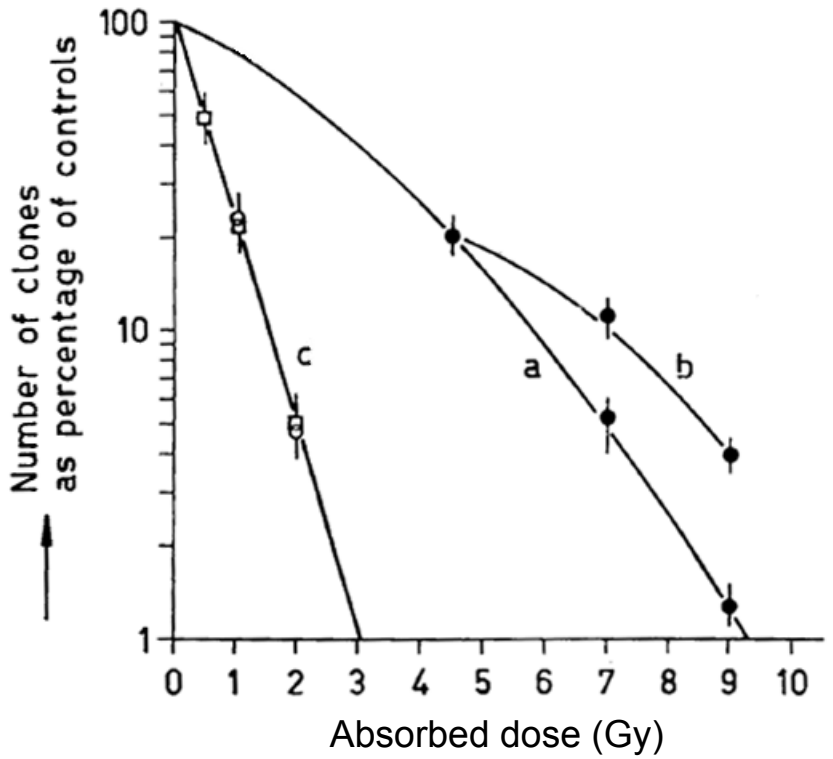

Figure 8 – Effect of fractionation on cell survival. a. cell curvival curve obtained with single doses of 200 kV X-rays. b. curve obtained when 200 kV X-ray doses are separated by 12 hours (4.5 Gy, then 2.5 Gy or 4.5 Gy). c. curve obtained with 3.4 MeV alpha-particles; circles correspond to single exposure, squares to 2 equal exposures, separated by 12 hours. (Adapted from Barendsen GW. Annals, NYAS 114:96-114, 1964).

Figure 9

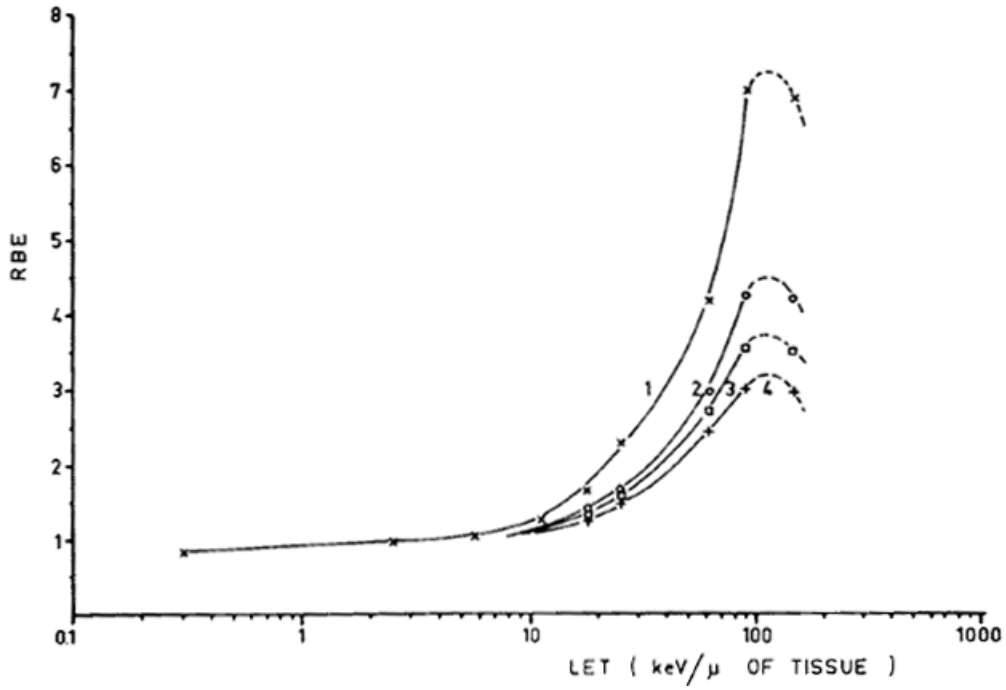

Figure 9 – LET-RBE relationship. RBE for surviving fractions of 1: 0.8, 2: 0.2, 3: 0.05, and 4: 0.005. Alpha-particles were used for LET 24.6-140 keV/μm; deuterons for LET 5.6-17.4 keV/μm; X-rays for LET 2.5 and 6 keV/μm; beta particles for LET = 0.3 keV/μm. Kidney cells of human origin (T_1) were used for all experiments. (Copied from Barendsen GW, et al. Rad Res 18:196-119, 1963.).

Figure 10

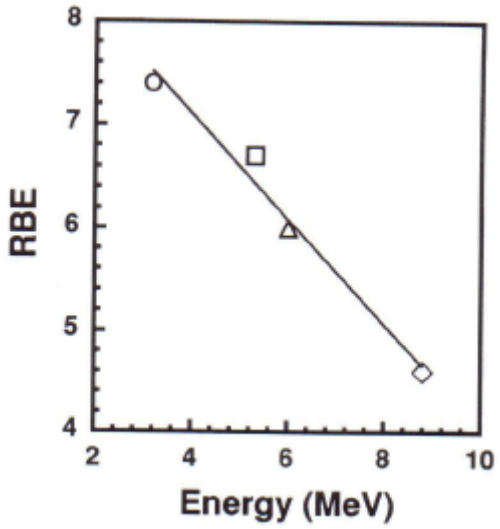

Figure 10. Relative biological effectiveness of alpha particles for killing of spermatogonial cells in mouse testes. The ordinate represents the initial energy of alpha particles emitted by radionuclides that were injected into the testes. (○) 3.2 MeV from ^{148}Gd, (□) 5.3 MeV from ^{210}Po, (Δ) 6.0 MeV from ^{213}Bi, (◊) 8.8 MeV from ^{212}Po . Reprinted from Reference (*125*).

Figure 11

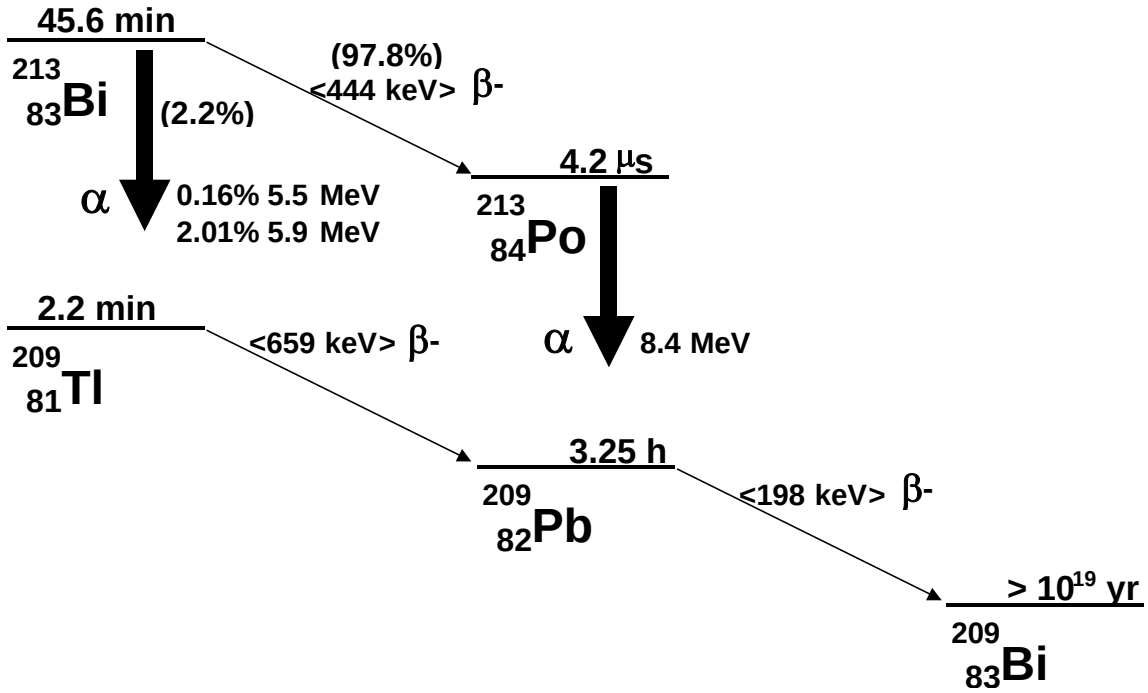

Figure 11. Decay scheme for ^{213}Bi